1-1-1999

Dynamics and structure of semicrystalline polymers as characterized by NMR, and their relationship to macroscopic properties.

Weiguo, Hu
University of Massachusetts Amherst

DYNAMICS AND STRUCTURE OF SEMICRYSTALLINE POLYMERS AS CHARACTERIZED BY NMR, AND THEIR RELATIONSHIP TO MACROSCOPIC PROPERTIES

A Dissertation Presented

by

WEIGUO HU

Submitted to the Graduate School of the
University of Massachusetts Amherst in partial fulfillment
of the requirements for the degree of

DOCTOR OF PHILOSOPHY

September 1999

Polymer Science & Engineering

DYNAMICS AND STRUCTURE OF SEMICRYSTALLINE POLYMERS AS CHARACTERIZED BY NMR, AND THEIR RELATIONSHIP TO MACROSCOPIC PROPERTIES

A Dissertation Presented

by

WEIGUO HU

Approved as to style and content by:

Klaus Schmidt-Rohr, Chair

Richard Stein, Member

Alan J. Lesser, Member

Richard J. Farris, Department Head
Polymer Science & Engineering

To Mom, Dad and Zhaohui.

ACKNOWLEDGMENTS

Many people have helped the work of this dissertation. The first person I should thank is Professor Klaus Schmidt-Rohr. It is a distinct pleasure to have him as my advisor because I have learned so much, in terms of science as well as life. He showed me what good science is, and how to be an honest, persistent and fun scientist. I thank the members of my committee, Professor Richard Stein and Professor Alan Lesser, for their help in the direction of my research and the innumerable valuable suggestions which greatly improved my understanding of polymer science.

I am also grateful to Dr. L. Charles Dickinson for his always timely and dedicated help whenever I encountered problems with the NMR spectrometers. Professor Mei Hong, Professor Jacques Penelle, and the late Professor Roger Porter have been greatly helpful with the many enlightening discussions throughout our collaborations. I am thankful to Dr. Alan Waddon, Dr. Andre Mel'cuk and Mrs. Eileen Besse for their kind assistance in the past years.

I would like to express my appreciation to all the members of the Schmidt-Rohr group: Professor Kristin Kumashiro, Professor Tito Bonagamba, Professor Hironori Kaji, Dr. Dick Sandstrom, Dr. Ioannis Polios, Mr. Matt Dunbar, Mr. Mikhail Gelfer, Mr. Doug Harris, Mr. Dan Mowery, Mr. Eduardo Azevedo, Mr. Fabio Becker-Guedes, Ms. Gabi Menges ... They have been fun to work with and made the lab hours a memorable experience. I thank my collaborators in the Plant and Soil Department, Professor Baoshan Xing and Mr. Jingdong Mao. They opened up a fascinating field to me and let me realize a new field of science.

Finally, I sincerely thank my wife Zhaohui for her enduring love and support throughout the years. It is always the time spent with her that reminds me that life is full of beauty. I am most indebted to my mom and dad who love me and miss me. Though they live on the other side of the planet, they always listen to me, talk to me, encourage me, and cheer over every bit of my progress.

ABSTRACT

DYNAMICS AND STRUCTURE OF SEMICRYSTALLINE POLYMERS AS CHARACTERIZED BY NMR, AND THEIR RELATIONSHIP TO MACROSCOPIC PROPERTIES

SEPTEMBER 1999

WEIGUO HU, B.S., TSINGHUA UNIVERSITY

M.S., TSINGHUA UNIVERSITY

M.S., UNIVERSITY OF MASSACHUSETTS AMHERST

PH.D., UNIVERSITY OF MASSACHUSETTS AMHERST

Directed by: Professor Klaus Schmidt-Rohr

In this dissertation the 180°-flip motion and morphology in polyethylene are studied by solid-state NMR. An explanation of the varying (ultra)drawability of semicrystalline polymers in terms of α_c-relaxation chain mobility is proposed. Crystalline domains composed of "polyethylene-like" chains in soil organic matter are detected and characterized.

In high-density polyethylene (HDPE) and in ultra-high molecular-weight polyethylene (UHMWPE) fibers, the 180° chain-flip motions are observed in terms of changes in the ^{13}C-^{13}C dipolar couplings. In the HDPE sample, the motion is observed directly via two-dimensional exchange spectroscopy, stimulated-echo decays, and 1D lineshape changes. The data yield an activation energy of 122±10 kJ/mol. In the fibers,

the narrowing of natural-abundance ^{13}C-^{13}C dipolar satellites indicates a flip rate of 1000/s at 360 K.

An explanation of the varying (ultra)drawability of semicrystalline polymers is proposed, based on NMR evidence of α_c-relaxation-associated helical jumps and chain diffusion through the crystallites of "α_c-mobile" polymers. The chain motions provide a mechanism by which these polymers can be ultradrawn to draw ratios >30, without melting. Other semicrystalline polymers that lack a crystalline α-relaxation only have draw ratios of < 14.

The structure of ultradrawn UHMWPE fibers is investigated by solid-state NMR. A crystallinity of (88±2)% was determined by traditional ^1H NMR and a new adaptation of the ^{13}C NMR direct-polarization method. ^1H spin diffusion yields amorphous domain sizes of 10±5 nm, and crystalline regions of 100±50 nm diameter. A second, highly mobile, amorphous phase, making up (0.8±0.2)% of the sample, was detected by ^1H NMR. The fraction of partially mobile, oriented interfacial material or tie-molecules in the fiber was found to be ~ 5%.

Crystalline domains composed of poly(methylene) chains have been unambiguously detected by solid-state NMR and wide angle X-ray scattering in several samples of soil organic matter, including surface soil (peat), humic acids from surface soil and young coal, and humins. The crystallite thickness is deduced from the NMR-detected melting range and ^1H spin diffusion experiments. The crystallites are expected to have long residence times in the soil and may be related to the formation of petroleum.

TABLE OF CONTENTS

LIST OF TABLES

LIST OF FIGURES

CHAPTER 1

INTRODUCTION

1.1 Overview of the Dissertation

A wide variety of polymer products are being produced in the world and more are being developed. So many different polymers are produced industrially because each material has certain property limitations. For example, high-density polyethylene (HDPE), a widely used strong and tough plastic, is not suitable for high temperature applications. Its low melting point is only part of the reason. Already 50°C below the melting point, at 80°C, the modulus of HDPE is only 1/10 of the room temperature value. Therefore, HDPE is not even a good candidate for hot drink cups. This phenomenon has been attributed to the crystalline α-relaxation in polyethylene.[1,2]

The α-relaxation in semicrystalline polymers[2] is related to important materials properties like creep,[3] annealing,[4] and crystallization[5]. It has also been suggested that it is related to the ability of semicrystalline polymers to be extruded in the solid state or drawn to high draw ratio (ultradrawability).[6-12] As an example, ultraoriented polyethylene fibers with draw ratios exceeding 100 can be produced that are extremely strong yet lightweight and are used, for instance, in bullet-proof vests.[13,14] However, such a relationship between the α_c-relaxation and ultradrawability has not been studied mechanistically, and other models of polymer deformation still prevail. At the same time, the molecular mechanism of the crystalline α-relaxation has not be examined systematically. Especially, although a model for the chain motion related to the α_c-relaxation in polyethylene has been

suggested[1,15,16] and indirectly confirmed by experiments[17-20], it has not been directly proven. Therefore, it is necessary to investigate the molecular mechanism of the α-relaxation in PE in detail, and to compare it with similar processes in other polymers, in order to achieve a fundamental understanding of the relationship between the crystalline α-relaxation and ultradrawability.

The extraordinary mechanical properties of ultradrawn polyethylene fibers originate from their special morphology. Various experimental evidences, such as high thermal conductivity and tensile modulus, suggest a continuous crystalline phase, which would be very different from that in HDPE. Therefore, investigation of this morphology is of both fundamental and practical significance, providing an excellent example of a unique microscopic structure that produces outstanding macroscopic properties.

While polyethylene is usually considered as one of the typical synthetic plastics, a "polyethylene-like" component has also been found in soil organic matter. It has a long residence time in soil and may be related to the formation of petroleum.[21-26] An investigation of the morphology and dynamics of this component is crucial to understand its physical properties and the long residence time in soil.

The objective of this dissertation is thus to achieve a detailed understanding of crystalline chain motion in PE, characterize the PE fiber morphology and understand how it influences the chain dynamics, and explore the relationship between these microscopic phenomena and macroscopic material properties. The "polyethylene"-like component in soil organic matter is investigated, and its semicrystalline nature is identified by NMR as well as wide-angle X-ray scattering.

1.2 Crystalline Chain Dynamics in Polymers

Many semicrystalline polymers have a crystalline dielectric and dynamic mechanical α-relaxation (α_c) which is related to many important material properties.[3-5,7] The underlying molecular mechanism of the α_c relaxation is large-amplitude chain translation and rotation. These motions have been elucidated by solid-state NMR in various semicrystalline polymers, including POM,[27-29] iPP,[28-30] and PEO.[29] In polyethylene, 180° chain flips have long been considered as the dominant mode of the α-relaxation in the crystalline regions.[1,15-17,20] However, to date these flips have not been observed directly, since the most accessible NMR interactions are invariant under the 180° flip. As a result, its relationship to dielectric and dynamic mechanical α_c relaxations, and how it is affected by morphology, have not been well understood.

In Chapter 3 we report the direct detection of 180°-flip motion of chains in the crystallites of ^{13}C-^{13}C labeled HDPE. Using two-dimensional (2D) exchange, one-dimensional (1D) lineshape change, and stimulated echo techniques, the temperature dependence, activation energy, and correlation function of the motion are determined. The crystalline chain dynamics in ultradrawn polyethylene fibers is examined by a dipolar satellite-narrowing experiment. The influence of morphology on chain dynamics is studied.

1.3 Understanding Semicrystalline Polymer Ultradrawability

Not in all semicrystalline polymers do the crystalline chains undergo large amplitude dynamics. In other words, the α_c relaxation may be absent. Will this difference in molecular dynamics result in differences in macroscopic properties?

It has been suggested that the α_c relaxation is related to the ability of semicrystalline polymers to be extruded in the solid state or drawn to high draw ratios (ultradrawability).[6-12] Tensile drawing of semicrystalline polymers, to draw ratios of greater than 20 ("ultradrawing"), up to several hundred,[31] produces fibers of excellent mechanical properties.[13,14] Therefore, the drawability of many industrial polymers has been investigated. It has been found to vary greatly, even for chemically similar polymers.[12,32,33] Despite serious efforts, no ultrastrong fibers have been produced from nylons,[34-37] semicrystalline poly(ethylene terephthalate) (PET),[38,39] syndiotactic polypropylene (sPP),[11,12] or isotactic poly(1-butene) (iPB1),[32,40] all of which draw poorly.

Explanation of the ultradrawability of semicrystalline polymers has been attempted by many models, which includes sliding of fibrils[41], local melting and recrystallization[42,43], solid-solid phase transition[44], etc. Nevertheless, the observed differences in drawability are not explained by these models.

With a detailed examination of crystalline α_c-relaxation chain dynamics and ultradrawability, we find a fundamental relationship between these two phenomena. Chapter 4 presents an explanation of the varying (ultra)drawability of semicrystalline polymers, based on NMR evidence of α_c-relaxation-associated helical jumps and chain diffusion through the crystallites of polyethylene and several similarly "α_c-mobile" polymers. The motion through the crystallites is thermally activated and the applied stress only biases the direction of the jumps; this explains the crucial role of temperature and rate in tensile drawing and solid-state extrusion processes. Various stages of drawing are distinguished and other models of ultradrawability are discussed critically.

1.4 Morphology of Ultradrawn Polyethylene Fibers

As the chain mobility-ultradrawability relationship indicates, the polymers which have α_c-relaxation chain mobility can be ultradrawn. PE is the most prominent example. Upon ultradrawing, ultraoriented, highly crystalline fibers can be produced, which exhibit excellent modulus, strength and impact resistance.[13,14] The morphology of ultradrawn polyethylene fibers has been studied by various techniques. However, many issues have not been clearly understood. A precise and model-independent measurement of crystallinity has not been obtained. The sizes of crystalline and amorphous domains need to be determined, since they are crucial for establishing a correct structural model for the fibers. It has been suggested that in drawn semicrystalline polymers, there are crystal-trapped rigid-gauche segments.[10] There have also been reports about the presence of a highly mobile component in the fibers[45,46]. However, its properties were not well characterized, and a convincing interpretation is lacking.

In chapter 5 we describe a close examination of the fiber morphology by solid-state NMR experiments and comparison with other techniques. The crystallinity is determined by traditional ^{1}H NMR lineshape decomposition, and by a new adaptation of ^{13}C NMR crystallinity determination for polyethylenes with extremely long crystalline T_1 relaxation times. The sizes of amorphous domains and crystalline regions are estimated by ^{1}H spin diffusion. ^{13}C spectra are examined for partially mobile, oriented interfacial material or tie-molecules and for proposed rigid gauche conformers. A detailed characterization of the highly mobile component is given and a possible association with voids is discussed. Based on these observations, a five-component structural model for ultradrawn PE fibers is proposed.

1.5 Crystalline Domains in Humic Substances

Soil organic matter (SOM) represents a major component of the world surface carbon reserves. The structures of individual SOM fractions regulate their reactivity, property, and functions, but are poorly understood. A better understanding of SOM structures, particularly humic substances, would help to determine their origin and genesis, reactivity, and roles in environmental processes.

So far, SOM was considered to be amorphous. In Chapter 6 the discovery of aliphatic crystalline domains in SOM is described. Thin crystallites composed of $(CH_2)_n$ ("polymethylene-like") chains are unambiguously detected by solid-state NMR and wide angle X-ray scattering (WAXS) in several samples of soil organic matter, including surface soil (peat), humic acids from surface soil and young coal, and humins. From the NMR-detected melting range and ^1H spin diffusion experiments, the crystallite thickness is deduced. The crystallites are expected to be resistant to environmental attack and thus have long residence times; they may be related to the formation of petroleum[21-26]. Their presence may affect many physical and chemical properties of soil organic matter.

1.6 References

(1) Boyd, R. H. *Polymer* **1985**, *26*, 323,1123.

(2) McCrum, N. G.; Read, B. E.; Williams, G. *Anelastic and Dielectric Effects in Polymeric Solids*; Dover Publications, Inc.: New York, 1991.

(3) Ward, I. M.; Wilding, M. A. *J. Polym. Sci.: Polym. Sci. Ed.* **1984**, *22*, 561-575.

(4) Reneker, D. H. *J. Polym. Sci.* **1962**, *59*, S39-S42.

(5) Strobl, G. *The Physics of Polymers*; Springer-Verlag: Berlin Heidelberg, 1996.

(6) Aharoni, S. M.; Sibilia, J. P. *Polym. Eng. Sci.* **1979**, *19*, 450-455.

(7) Aharoni, S. M.; Sibilia, J. P. *J. Appl. Polym. Sci.* **1979**, *23*, 133-140.

(8) Bigg, D. M. *Polym. Eng. Sci.* **1988**, *28*, 830-841.

(9) Gedde, U. W. *Polymer Physics*; Chapman & Hall: London, 1995.

(10) Clark, E. S.; Scott, L. S. *Polym. Eng. Sci.* **1974**, *14*, 682-686.

(11) Sakata, Y.; Unwin, A. P.; Ward, I. M. *J. Mater. Sci.* **1995**, *30*, 5841-5849.

(12) Uehara, H.; Yamazaki, Y.; Kanamoto, T. *Polymer* **1996**, *37*, 57-64.

(13) Lemstra, P. J.; Kirschbaum, R.; Ohta, T.; Yasuda, H. In *Developments in Oriented Polymers-2*, Ward, I. M., Ed.; Elsevier Applied Science: London and New York, 1987, pp 39-77.

(14) Porter, R. S.; Wang, L.-H. *J. Macromol. Sci.-Rev. Macromol. Chem. Phys., C* **1995**, *35*, 63-115.

(15) Hoffman, J. D.; Williams, G.; Passaglia, E. *J. Polym. Sci.: Part C* **1966**, *14*, 173-235.

(16) Mansfield, M.; Boyd, R. H. *J. Polym. Sci.: Polym. Phys. Ed.* **1978**, *16*, 1227-1252.

(17) Olf, H. G.; Peterlin, A. *J. Polym. Sci. Part A-2* **1970**, *8*, 753-770.

(18) Olf, H. G.; Peterlin, A. *J. Polym. Sci.: A-2* **1970**, *8*, 771-790.

(19) Olf, H. G.; Peterlin, A. *J. Polym. Sci.: A-2* **1970**, *8*, 791-797.

(20) Opella, S. J.; Waugh, J. S. *J. Chem. Phys.* **1977**, *66*, 4919-4924.

(21) Baldock, J. A.; Oades, J. M.; Waters, A. G.; Peng, X.; Vassallo, A. M.; Wilson, M. A. *Biogeochemistry* **1992**, *16*, 1-42.

(22) Hatcher, P. G.; Spiker, E. C.; Szeverenyi, N. M.; Maciel, G. E. *Nature* **1983**, *305*, 498-501.

(23) Kogel-Knabner, I.; Hatcher, P. G.; Tegelaar, E. W.; de Leeuw, J. W. *Sci. Tot. Environ.* **1992**, *113*, 89-106.

(24) Tegelaar, E. W.; de Leeuw, J. W.; Saiz-Jimenez, C. *Sci. Tot. Environ.* **1989**, *81/82*, 1-17.

(25) Tegelaar, E. W.; De Leeuw, J. W.; Derenne, S.; Largeau, C. *Geochim. Cosmochim. Acta* **1989**, *53*, 3103-3106.

(26) Tegelaar, E. W.; Kerp, H.; Visscher, H.; Schenck, P. A.; de Leeuw, J. W. *Paleobiology* **1991**, *17*, 133-144.

(27) Kentgens, A. P. M.; de Boer, E.; Veeman, W. S. *J. Chem. Phys.* **1987**, *87*, 6859-6866.

(28) Hagemeyer, A.; Schmidt-Rohr, K.; Spiess, H. W. *Adv. Magn. Reson.* **1989**, *13*, 85-130.

(29) Schmidt-Rohr, K.; Spiess, H. W. *Multidimensional Solid-State NMR and Polymers*; Academic Press: London, 1994.

(30) Schaefer, D.; Spiess, H. W.; Suter, U. W.; Fleming, W. W. *Macromolecules* **1990**, *23*, 3431-3439.

(31) Kanamoto, T.; Tsuruta, A.; Tanaka, K.; Takeda, M.; Porter, R. S. *Macromolecules* **1988**, *21*, 470-477.

(32) Ball, R.; Porter, R. S. *J. Polym. Sci.: Polym. Lett. Ed.* **1977**, *15*, 519-526.

(33) He, T.; Porter, R. S. *Polymer* **1987**, *28*, 946-950.

(34) Ito, M.; Morishita, Y.; Mizuochi, K.; Kanamoto, T. *J. Macromol. Sci. -Phys.* **1997**, *B36*, 367-380.

(35) Postema, A. R.; Smith, P.; English, A. D. *Polym. Commun.* **1990**, *31*, 444-447.

(36) Gogolewski, S.; Pennings, A. J. *Polymer* **1985**, *26*, 1394-1400.

(37) Kanamoto, T.; Zachariades, A. E.; Porter, R. S. *J. Polym. Sci., Polym. Phys. Ed.* **1982**, *20*, 1485-1496.

(38) Huang, B.; Ito, M.; Kanamoto, T. *Polymer* **1994**, *35*, 1329-1331.

(39) Ito, M.; Takahashi, K.; Kanamoto, T. *J. Appl. Polym. Sci.* **1990**, *40*, 1257-1263.

(40) Weynant, E.; Haudin, J. M.; G'Sell, C. *J. Mater. Sci.* **1980**, *15*, 2677-2692.

(41) Peterlin, A. *J. Mater. Sci.* **1971**, *6*, 490-508.

(42) Wu, W.; Wignall, G. D.; Mandelkern, L. *Polymer* **1992**, *33*, 4137-4140.

(43) Flory, P. J.; Yoon, D. Y. *Nature* **1978**, *272*, 226-229.

(44) Saraf, R. F.; Porter, R. S. *J. Polym. Sci.: Part B: Polym. Phys.* **1988**, *26*, 1049-1057.

(45) Kitamaru, R.; Horii, F. *Adv. Polym. Sci.* **1978**, *26*, 137-178.

(46) Smith, J. B.; Manuel, A. J.; Ward, I. M. *Polymer* **1975**, *16*, 57-65.

CHAPTER 2

NMR BACKGROUND

2.1 Nuclear Magnetic Interactions in Polymers

What NMR spectroscopy detects is various nuclear magnetic interactions[1], which in turn reflect the chemical structure and motion of the molecules[2,3]. In this section the commonly encountered ^{1}H and ^{13}C magnetic interactions will be discussed. These two nuclei are the most common NMR-relevant nuclear species in polymers.

2.1.1 ^{13}C Chemical Shift Anisotropy (CSA)

Chemical shift in the solid state is a tensor, which means that the resonance frequency is dependent on the relative orientation of the tensor and magnetic field. In static ^{13}C spectra of an isotropic sample, the signal has a distribution over a frequency range ("powder pattern") which is determined by the three principal values of the chemical shift tensor. For example, the powder pattern of PE spreads from 13 to 51 ppm, i.e., about 40 ppm wide.

The principal values of chemical shift tensor can be read off from a powder pattern. To determine the orientation of the tensor relative to the molecular structure, analysis of one or several of the following spectra may be needed: (1) 1D spectrum of an oriented sample; (2) 2D correlation spectrum, often C-H dipolar coupling/CSA correlation; (3) 1D spectrum reflecting both chemical shift and one other interaction, for example, C-C dipolar coupling (see Chapter 3).

Segment motion produces averaging effects on the chemical shift tensor, therefore, the change of powder pattern often reveals many details of molecular motion.[4] For materials with complex chemical structure, the powder patterns of the many different carbons overlap. To elucidate the chemical structure of solid material, it is usually desired to remove the overlap. Magic angle spinning (MAS) is widely used to remove the chemical

shift anisotropy so that sharp peaks reflecting isotropic chemical shifts are obtained (see Chapter 5 and 6).

2.1.2 ^{1}H-^{1}H Dipolar Coupling

In most polymers there are abundant hydrogen atoms. Because of their large gyromagnetic ratio and spatial proximity, ^{1}H-^{1}H dipolar coupling is very strong, usually > 30 kHz in rigid polymers. On the other hand, the ^{1}H chemical shift is on the order of ppm, which is only several kHz in modern superconducting spectrometers. Therefore, ^{1}H-^{1}H dipolar coupling usually dominates solid-state ^{1}H spectrum.

Since molecular motion produces an averaging effect on the ^{1}H-^{1}H dipolar coupling, the ^{1}H spectrum is a good indicator of molecular motion. In the extreme case, in solution because of the fast tumbling of the molecules, the dipolar coupling is completely averaged out and only the isotropic chemical shift remains.

^{1}H spectra can give detailed information about molecular motion. Fig. 2.1 shows ^{1}H spectra of 1,22-docosanediol before and after a solid-solid phase transition. The lineshape of the sample undergoes a dramatic change when heated past a phase transition. Calculation of the second moment of the spectra indicates that below the transition, chains are not undergoing fast 180°-flip motion[5]. Above the transition temperature, chains are rotating very fast, but there is no or very slow lateral diffusion and motion along the chain direction, i.e., the phase is solid-like[6-8]. This example illustrates the details of molecular dynamics one can obtain from ^{1}H spectra.

Strong ^{1}H-^{1}H dipolar coupling leads to fast ^{1}H spin diffusion (exchange of magnetization over distance). Spin diffusion can be detected and is often exploited to determine domain sizes of heterogeneous polymer systems, such as semicrystalline polymers, polymer blends and block copolymers. ^{1}H spin diffusion coefficient has been determined experimentally[9] and can be conveniently estimated by ^{1}H spectrum linewidth, which is a function of proton density and mobility.

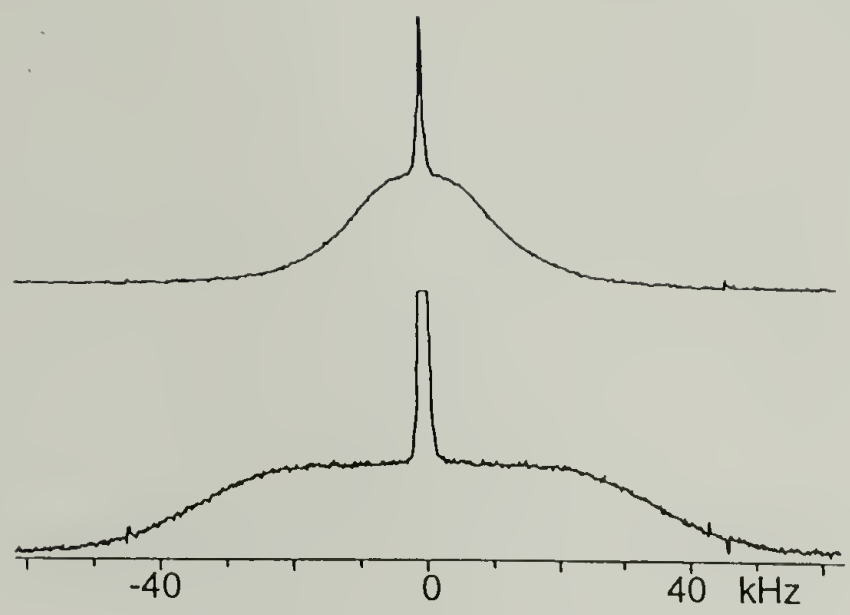

Fig. 2.1: ^{1}H spectra of 1,22-docosanediol below and above the solid-solid phase transition temperature. (a) 85°C. (b) 100°C. The very sharp peak in the middle shows the existence of a highly mobile phase.

2.1.3 ^{1}H-^{13}C Dipolar Coupling

^{1}H-^{13}C dipolar coupling is sensitive to C-H distance and segment mobility. The ^{1}H-^{13}C dipolar coupling constant for a rigid, directly bonded ^{1}H-^{13}C pair is ~ 20 kHz. ^{1}H-^{13}C dipolar coupling is often used to distinguish domains of different mobility in heterogeneous systems and to distinguish protonated and unprotonated carbons.

^{1}H-^{13}C dipolar coupling is widely exploited to achieve cross-polarization (CP), which is a transfer of magnetization from ^{1}H to ^{13}C in order to obtain a stronger polarization. Since ^{1}H-^{13}C dipolar coupling is determined by C-H distance and mobility, CP efficiency is often different for different chemical groups in the sample. For example, protonated ^{13}C builds up magnetization much more quickly in CP than unprotonated carbons. For the same chemical structure, segments in rigid domains have larger CP efficiency than those in soft domains. Therefore, CP spectrum is usually not a quantitative measurement of populations.

^{1}H-^{13}C dipolar coupling can also be used to achieve correlation between ^{1}H and ^{13}C magnetic properties. For example, 2D wideline separation (WISE) spectroscopy[10], which shows ^{1}H-^{1}H dipolar coupling in the first dimension and ^{13}C chemical shift in the second dimension, uses CP to relate ^{1}H and ^{13}C magnetization (see Chapter 6). A caution to be taken is that since ^{1}H spin diffusion is active during CP, the CP time should not be very long.

In most of the ^{13}C detection experiments, ^{1}H-^{13}C coupling is removed by continuous wave ^{1}H irradiation, with a field strength no less than the ^{1}H-^{13}C coupling strength. The decoupling may be interfered by segment motion, especially when the motion rate approaches the decoupling field strength. As a result, MAS signals are broadened.

2.1.4 ^{13}C-^{13}C Dipolar Coupling

In natural abundance sample, the average distance between ^{13}C nuclei is > 0.6 nm. As a result, the average ^{13}C-^{13}C dipolar coupling constant between neighboring ^{13}C nuclei is only a few Hz and thus often neglected. Nevertheless, in certain cases it can be useful. In PE, as a result of the chain translation through the crystallites, ^{13}C nuclei initially far apart may get closer and enhanced spin exchange is observed.[11] Despite the extremely small population of directly bonded ^{13}C-^{13}C pairs, they can be detected and the information about the chain motion is obtained (see Chapter 3).

To take full advantage of ^{13}C-^{13}C dipolar coupling, labeled sample are often prepared so that ^{13}C-^{13}C dipolar coupling can be observed more conveniently. In Chapter 3 a ^{13}C labeled polyethylene is used to determine the chain motion in crystallites.

2.2 Nuclear Magnetic Relaxation

Magnetic relaxation in polymers is usually caused by molecular motion which provides fluctuating nuclear magnetic interactions. Relaxation times exhibit minimum values when the correlation time of the motion approaches the resonance frequency.

2.2.1 ^{1}H T_1 Relaxation

^{1}H-^{1}H dipolar interaction is mainly responsible for ^{1}H T_1 relaxation. ^{1}H T_1 can be long for rigid materials due to the lack of fluctuating ^{1}H-^{1}H dipolar interaction. For example, it is > 100 s for 1,22-docosanediol at room temperature. Based on the similarity of chain mobility, it can be rationalized that the intrinsic ^{1}H T_1 of crystalline PE is similarly long at room temperature.

The fast ^{1}H spin diffusion usually plays an important role in ^{1}H T_1 relaxation in heterogeneous polymer systems. In PE, due to the chain mobility, the ^{1}H T_1 relaxation in the amorphous regions is < 1 s. The relaxed magnetization can quickly diffuse into the crystalline regions so that the T_1 in the crystalline region becomes much shorter, usually 1 ~ 5 seconds (see Chapter 5).

2.2.2 ^{1}H $T_{1\rho}$ Relaxation

The relaxation time $T_{1\rho,H}$ of spin-locked ^{1}H magnetization detects the modulation of H-H dipolar couplings. It exhibits a minimum when the jump rate $k = 1/2\tau_c = \gamma B_1$, where τ_c is the correlation time, γ is gyromagnetic ratio and B_1 is the spin-lock magnetic field strength. Since γB_1 is ~ 400 kHz, $T_{1\rho,H}$ is especially sensitive to slow molecular motion.

The experimental measurement of $T_{1\rho,H}$ is often complicated by spin diffusion in the spin-lock field, due to different $T_{1\rho,H}$ values in different regions (see Chapter 3). $T_{1\rho,H}$

relaxation occurs during CP, therefore, CP time should not be too long, especially for the domains which have short $T_{1\rho,H}$ relaxation time.

2.2.3 ^{13}C T_1 Relaxation

Intrinsically, ^{13}C T_1 is caused by the modulation of C-H dipolar coupling and ^{13}C chemical shift anisotropy as a result of motion. It is usually free of spin diffusion in natural abundance samples on a time scale of seconds. Therefore, it is a good indicator of local segmental dynamics. In amorphous PE at room temperature, the ^{13}C T_1 is less than 1 s because of the large amplitude motion, while in ultradrawn PE fibers, the ^{13}C T_1 of crystalline core segments is ~ 5000 s due to the lack of chain mobility (see Chapter 5).

Nevertheless, ^{13}C T_1 relaxation is sometimes not a totally local phenomenon. For example, there are (at least) four processes that may lead to ^{13}C T_1 relaxation in the crystallites of PE: (i) Chain flip motion (and other possible motion modes, see Chapter 3) induces relaxation intrinsically by contributing to the spectral density near the Larmor frequency. (ii) Chain oscillations[12] induce relaxation intrinsically by contributing to the spectral density near the Larmor frequency. (iii) Chain diffusion transports magnetization from the fast-relaxing amorphous regions into the crystallites.[13] (iv) ^{13}C spin diffusion, based on dipolar couplings between the ^{13}C spins, transfers ^{13}C magnetization from the fast-relaxing amorphous regions into the crystallites.

In addition to backbone motion, side group motion can also facilitate both ^{13}C T_1 and ^{1}H T_1 relaxation. Examples are methyl group rotation and phenyl ring flip. For example, as a result of methyl group rotation, the ^{1}H and ^{13}C T_1 relaxation in crystalline alanine is much faster than in glycine.

2.2.4 ^{1}H T_2* Relaxation

^{1}H T_2* is actually not an irreversible relaxation time, but the reversible ^{1}H-^{1}H dipolar dephasing time. Being the inverse of ^{1}H spectrum width, ^{1}H T_2* is usually a sensitive measure to segmental mobility in the >100 kHz range, as discussed in Section 2.1.2. A ^{1}H T_2* filter, which selectively preserves the magnetization in the mobile regions based on the difference in ^{1}H T_2*, is a useful component in spin diffusion experiments (see Chapter 5). The WISE experiment also utilizes the^{1}H T_2* dephasing in the evolution period. ^{1}H T_2* is less than 10 μs in rigid and proton-rich materials, such as polyethylene, and >20 μs for rubbery polymers.

2.3 References

(1) Abragam, A. *Principles of Nuclear Magnetism*; Oxford University Press: Oxford, 1961.

(2) Schmidt-Rohr, K.; Spiess, H. W. *Multidimensional Solid-State NMR and Polymers*; Academic Press: London, 1994.

(3) McBrierty, V. J.; Packer, K. J. *Nuclear Magnetic Resonance in Solid Polymers*; Cambridge University Press: London, 1993.

(4) Vega, A. J.; English, A. D. *Macromolecules* **1980**, *13*, 1635-1647.

(5) Ewen, B.; Fischer, E. W.; Piesczek, W.; Strobl, G. *J. Chem. Phys.* **1974**, *61*, 5265-5272.

(6) Olf, H. G.; Peterlin, A. *J. Polym. Sci. Part A-2* **1970**, *8*, 753-770.

(7) Olf, H. G.; Peterlin, A. *J. Polym. Sci.: A-2* **1970**, *8*, 771-790.

(8) Olf, H. G.; Peterlin, A. *J. Polym. Sci.: A-2* **1970**, *8*, 791-797.

(9) Clauss, J.; Schmidt-Rohr, K.; Spiess, H. W. *Acta Polymer.* **1993**, *44*, 1.

(10) Schmidt-Rohr, K.; Clauss, J.; Spiess, H. W. *Macromolecules* **1992**, *25*, 3273-3277.

(11) VanderHart, D. L. *J. Magn. Reson.* **1987**, *72*, 13-47.

(12) Hentschel, D.; Sillescu, H.; Spiess, H. W. *Makromol. Chem.* **1979**, *180*, 241-249.

(13) Schmidt-Rohr, K.; Spiess, H. W. *Macromolecules* **1991**, *24*, 5288-5293.

CHAPTER 3

CHAIN FLIPS IN POLYETHYLENE CRYSTALLITES AND FIBERS

3.1 Introduction

The α-relaxation in semicrystalline polymers[1] is related to important materials properties like creep,[2] annealing,[3] crystallization,[4] extrudability,[5] and drawability (see Chapter 4). The underlying microscopic chain motions in the crystallites[6] have been elucidated by solid-state NMR in various semicrystalline polymers, including poly(oxymethylene),[7-9] isotactic polypropylene,[8-10] and poly(ethylene oxide).[9] Helical jumps, which are surprising large-amplitude chain rotations, requiring concomitant translations by full chemical repeat units, are directly detected by two-dimensional exchange NMR[9] in terms of changes of the angle-dependent ^{13}C chemical shift or ^{2}H quadrupolar coupling. In poly(tetrafluoroethylene),[11,12] translational disorder and in poly(vinylidene fluoride)[13], trans-polybutadiene[14], and possibly in form-II of isotactic poly(1-butene),[15] dynamic conformational disorder of similarly large amplitudes has been observed.

In polyethylene, 180° chain flips have long been considered as the dominant mode of the α-relaxation in the crystalline regions.[6,16-19] However, to date these flips have not been observed directly, since the most accessible NMR interactions are invariant under the 180° flip. Chemical shift, geminal H-H dipolar, C-H dipolar[17] and ^{2}H

quadrupolar tensors[20] are exactly inverted by the chain flip, which therefore leaves the corresponding NMR frequencies unchanged. In NMR, the α-relaxation has been studied by observing that the ^{1}H spin-lattice relaxation time in the rotating frame ($T_{1\rho}$), which reflects the modulation of long-range H-H couplings, strongly decreases with increasing temperature for segments in the crystallites.[21] However, most of the available NMR data do not strictly exclude other possible explanations for the α-relaxation in PE. For instance, straight displacement of the chain without rotation would account for most of the available NMR data, including chain diffusion.[22] The ^{13}C-^{13}C satellite narrowing observed by VanderHart[23] in oriented PE is the only good NMR indication of chain rotation in PE. Dielectric relaxation observes reorientation of C=O defects in the chains, with a strong direction dependence in oriented samples, which indicates chain rotation in the crystallites.[24] However, most of the defects may be located near the interface and rotations of limited amplitude around the chain axis might also account for the dielectric data. Recently, NMR line broadening has been interpreted as evidence that more than half of the chains in the crystallites of various high- and low-density polyethylenes undergo 180° flips in the kHz range at ambient temperature.[25] Quantitative interpretation of NMR, dielectric, and dynamic-mechanical relaxation measurements is not straightforward and model dependent.

In this chapter, we present direct observation of the 180° flips in terms of the reorientation of ^{13}C-^{13}C internuclear vectors in the crystallites of PE. As indicated in Fig. 3.1 (a), these C-C bonds reorient by the large bond angle of ~ 112°, observed in terms of

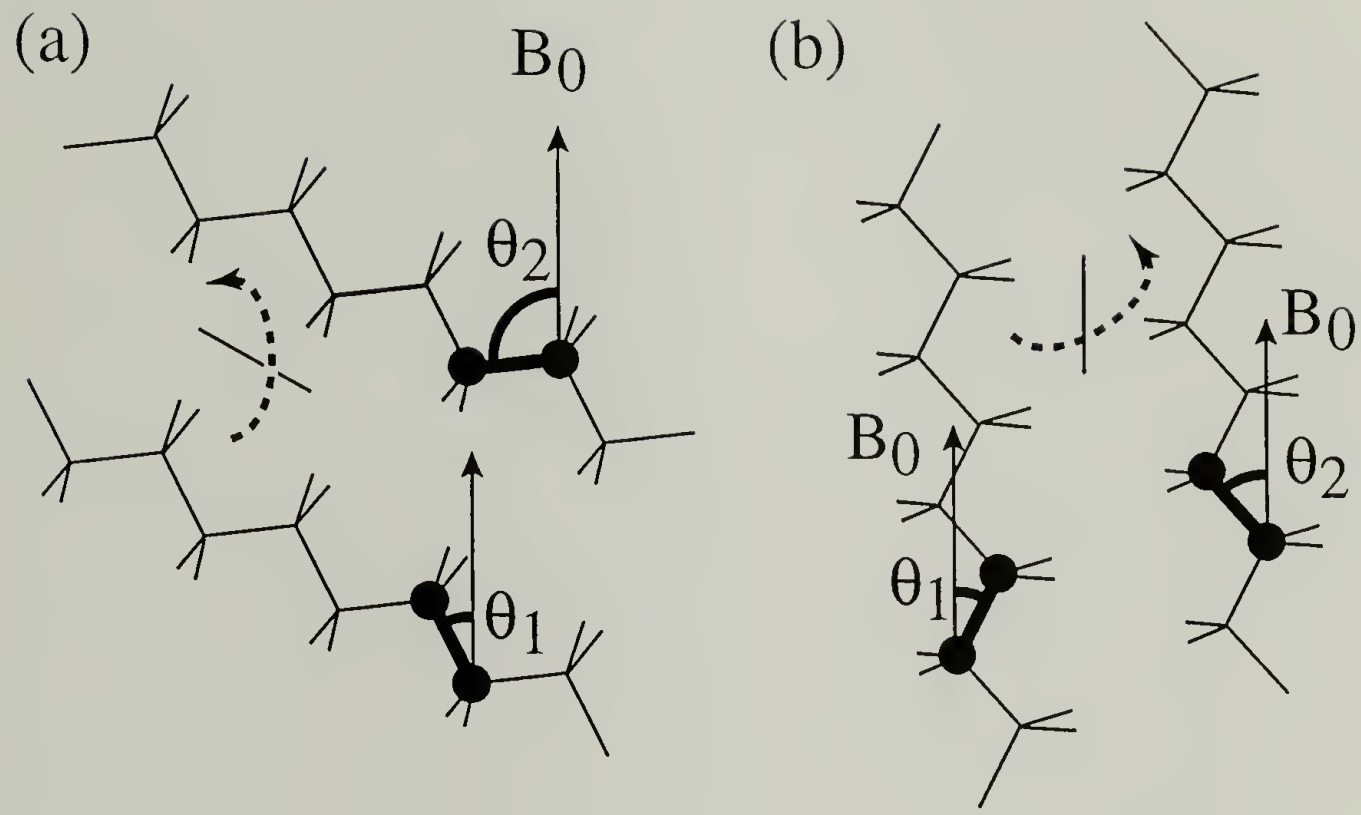

Fig. 3.1: Effects of 180° chain flips on ^{13}C-^{13}C bonds in polyethylene. The external field B_0 is along the vertical direction. (a) General case of a 180°-flip in an unoriented sample, producing a great change in the ^{13}C-^{13}C bond orientation, from θ_1 to θ_2. Consequently, the orientation-dependent frequency $\omega(\theta)$ will also be changed drastically. (b) Effect of a chain flip in a chain in a slightly misaligned fiber that is part of a fiber bundle oriented along the external field B_0. The average angle of θ_1 and θ_2 will be similar for different degrees of slight misalignment.

changes of the ^{13}C-^{13}C dipolar couplings in a specially prepared HDPE containing ^{13}C-^{13}C spin pairs. The correlation function of the chain reorientation is measured directly in terms of the mixing time dependence of stimulated echoes of the dipolar coupling. Combining these measurements with the analysis of line-shape changes at higher temperatures, the activation energy of the motional process is obtained.

We also report the occurrence of chain flips in highly drawn ultra-high-molecular-weight polyethylene (UHMWPE) fibers. These are engineering fibers with excellent mechanical properties,[26] which can be produced by tensile drawing of solid-state extruded reactor powder to a final draw ratio of > 80. These fibers are ca. 90 % crystalline[27] and believed to contain continuous crystals over micrometer length scales.[28] This makes it doubtful whether chain flips, which require mobility and "slack" of chains in the amorphous regions, are possible. On the other hand, under large stress, the applicability of the fibers is limited mostly by creep[29] which is related to the dynamic-mechanical α-relaxation in the crystalline regions.[30] Dielectric studies of the unoxidized and unchlorinated fibers would be challenging. It is our goal to elucidate by NMR whether and how the microscopic chain flips occur in the highly crystalline fibers. When the fibers are aligned with the magnetic field (B_0) direction, dynamics of the ^{13}C-^{13}C bond can be observed in terms of the narrowing of the dipolar satellites produced by natural-abundance ^{13}C spin pairs.[23] The relation of the microscopic dynamics and the macroscopic mechanical behavior such as creep and the dynamic-mechanical relaxation will be discussed.

3.2 Experimental

Samples. The melt-crystallized high-density polyethylene labeled with dilute ^{13}C-^{13}C spin pairs was prepared by copolymerizing ~95% natural abundance and ~5% doubly ^{13}C-labeled ethylene, using a titanium catalyst. 100 mg (3.4 mmol) of ^{13}C-labeled ethylene were transferred into an evacuated 2-liter flask containing the catalyst in toluene, and then the remaining volume was quickly filled to atmospheric pressure with 85 mmol of unlabeled ethylene gas. The flask was sealed and then stirred for 24 hours, producing a slurry of the polymer- and catalyst in toluene which was poured into an excess of isopropyl alcohol.

The actual ratio of directly-bonded and isolated ^{13}C nuclei was determined to be close to 4.4 : 1.1 in the analysis of the experimental ^{13}C spectra shown below. The sample was melted in a glass tube with 4-mm inner diameter and cooled in air. Two heating cycles (up to 360 K for 2 hours) were applied before the variable temperature $T_{1\rho,H}$ measurements. The sample before and after this thermal treatment is termed HDPE-b and HDPE-a, respectively. A commercial random copolymer of ethylene and hexene, produced by a Ziegler-Natta catalyst, was used to measure the minimum value of $T_{1\rho,H}$. The mole fraction of hexene in the sample was 4.4%.

The ultradrawn UHMWPE polyethylene fibers (in a tape of a cross section of 0.1 mm × 1.8 mm) were kindly provided by the late Prof. R. S. Porter. The molecular weight (viscosity average) is about 4×10^6. To produce the fibers, films of compacted Himont

Hifax 1900 reactor powder were solid-state extruded at 110°C to a draw ratio of 5, followed by tensile drawing at 135°C resulting in a fibrous tape. The final draw ratio achieved is 82-85, with a tensile modulus of up to 130 GPa. No isotope labeling was used. A uniaxially oriented sample for the NMR experiments was produced by aligning many layers of the tape parallel to each other and wrapping the bundle with Teflon® tape, which is invisible in ^{1}H-^{13}C cross-polarization experiments. Two sections of 6-mm length were cut out and aligned in the NMR radio-frequency coil of 8-mm diameter. The NMR spectra show that the fibers in the bundle are on average parallel within ±4°.

NMR Experiments. The NMR experiments were performed on a Bruker MSL-300 spectrometer at a ^{13}C frequency of 75.48 MHz and a ^{1}H frequency of 300.13 MHz. Various NMR techniques were used to obtain a more comprehensive understanding of the material:

(1) ^{13}C-^{13}C dipolar coupling 2D exchange experiment. As in the related 2D dipolar DECODER experiment by Utz *et al*,[31] the pure C-C dipolar coupling was detected in both dimensions. An illustration of the pulse sequence is shown in Fig. 3.2, with the main trace shown for the cosine dataset. For the sine data set, the two 90° pulses before and after t_m are replaced by $45°_{x}$ and $45°_{-x}$, respectively, as shown at the bottom of the figure. A double-quantum filter before the 2D exchange sequence was used to remove the contribution from isolated ^{13}C sites, which otherwise produces a very high peak in the center of the spectrum, with concomitant baseline distortions. To minimize the non-uniform excitation effect from the double-quantum filter, data with double quantum

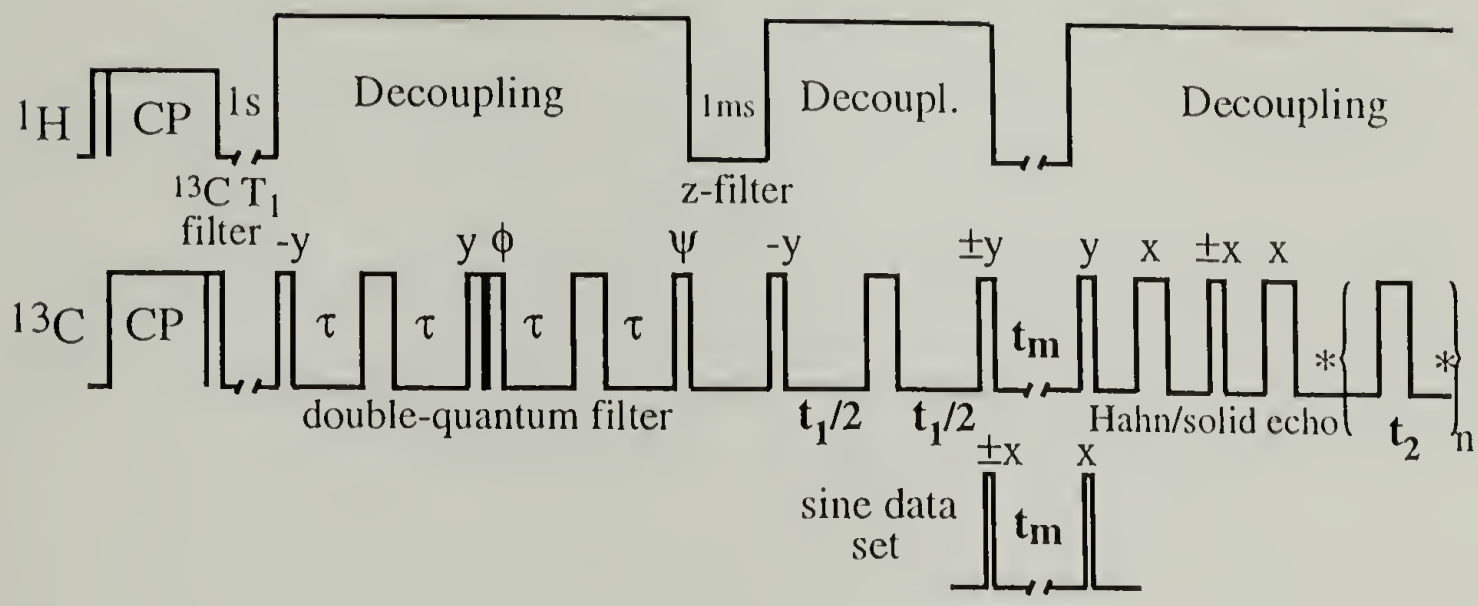

Fig. 3.2: 2D pulse sequence to detect reorientations of ^{13}C-^{13}C dipolar tensors. After a T_1 filter to suppress the amorphous-phase signal, a double-quantum filter removes the signal of isolated ^{13}C spins (with ϕ = x, y, -x, -y and ψ = x, -y, -x, y). During the evolution time t_1, a single 180° pulse refocuses the chemical shift, retaining the pure ^{13}C-^{13}C dipolar coupling. During the long mixing time t_m, segmental reorientations may occur, which are detected in terms of the changed ^{13}C-^{13}C dipolar frequency. A Hahn-solid-Hahn echo before detection allows for dead-time-free detection. During t_2, a train of 180° pulses with phases [a, a, -a, -a] perpendicular to the initial magnetization constantly refocuses the chemical shift while points are acquired at the times denoted by "*". The sequence shown in the middle, with 90° pulses flanking the mixing time t_m, produces the cosine data set, while the 45° pulses indicated at the bottom yield the sine data set.

exeitation / reeonversion times of 140, 280, 420, 560, 700, and 840 μs were added up. Before the start of deteetion, the dead-time problem was overeome by a Hahn-solid-Hahn eeho whieh refoeuses both the ehemieal shift and the ^{13}C-^{13}C dipolar eoupling.[32] The experiment was performed at ambient temperature. The mixing time was 100 ms. The signal of the amorphous regions was suppressed by a $T_{1,C}$ filter of 0.4 second. 48 data points were aequired in the first dimension, for both sine and eosine data sets, with an inerement of 48 μs. The ^{1}H deeoupling field strength was $(\gamma B_1/2\pi) > 120$ kHz in a coil of 5-mm diameter.

(2) Stimulated echo deeay measurement,[9,33] using the pulse sequenee of Fig. 3.2 (eosine data set) with $t_2 = t_1 = 1.25$ ms. The intensity of the ^{13}C-^{13}C dipolar stimulated eeho produeed at $t_2 = t_1$ was measured as a funetion of the mixing time t_m. A $T_{1,C}$-filter of 1.5 seeonds and a double-quantum filter were applied to remove the signal eontributions of the amorphous phase and isolated ^{13}C sites. The reeyele delay was 3 s.

(3) 1D ^{13}C lineshape of the erystalline regions at various temperatures. A $T_{1,C}$-filter of 1.5 to 3 s was applied to remove the signal of the amorphous regions. It reduees the signal of the all-trans segments by less than 10%. The reeyele delay was 3 to 4 s. Longer filter and reeyele delays were used at higher temperatures. The deeoupling field strength was >120 kHz. Before deteetion, a Hahn-solid-Hahn eeho[32] with a total pre-echo delay of 90 μs was applied at 310 K and below. A Hahn spin eeho with a total pre-eeho delay of 32 μs was used at higher temperatures.

(4) Narrowing of the ^{13}C-^{13}C dipolar satellites at elevated temperature (360 K) in UHMWPE fibers aligned along the B_0 field. The pulse sequence was cross polarization (CP) with ^{1}H decoupled ^{13}C detection. The decoupling field strength ($\gamma B_1/2\pi$) was 55 kHz. For each spectrum, approximately 20 000 scans were averaged, with a recycle delay of 7 s.

(5) Crystalline $T_{1\rho,H}$ at various temperatures and sample orientations with respect to the B_0 field. The spin lock field ($\gamma B_1/2\pi$) was 55 kHz. The pulse sequence consisted of a variable ^{1}H spin-lock, cross polarization to ^{13}C, a 0.6-s phase-cycled z-filter to suppress the signal of the noncrystalline regions based on their short $T_{1,C}$, and ^{1}H-decoupled ^{13}C detection. The cross polarization time was 0.1 ms. Hardware consideration limited the radio-frequency irradiation for the spin-lock to less than 30 ms.

3.3 NMR Techniques and Results

In the following sections, the principles and results of the various NMR techniques applied to ^{13}C-^{13}C labeled HDPE and unlabeled UHMWPE fibers will be presented.

3.3.1 2D Exchange Spectrum

As an alternative to the treatment in ref. [31] where a similar experiment, but with sample flip in the mixing time, was applied to polycarbonate, we describe the evolution of the density operator in terms of simple Cartesian product operators. In the following

derivations, S and L stand for two directly bonded ^{13}C nuclear spins. We consider the strong-coupling limit of the homonuclear dipolar coupling, where the difference of the chemical-shift frequencies between S and L is always zero, as appropriate for the all-trans conformation of crystalline polyethylene. Using Pauli matrices to represent the spin operators of the spin-1/2 nuclei,[9] one obtains the following simple dipolar evolution

$$\rho(t) = (S_x + L_x)\cos(\omega_{d,1}\, t_1) + 2(S_y L_z + S_z L_y)\sin(\omega_{d,1}\, t_1) \qquad (3.1)$$

where the dipolar-coupling frequency is

$$\omega_{d,1} = -\frac{3}{2}\frac{\mu_0}{4\pi}\hbar\frac{\gamma^2}{r_{cc}^3}\frac{1}{2}(3\cos^2(\theta_1)-1)$$

θ_1 is the angle between the magnetic field and the C-C bond before the mixing time, and r_{CC} is the distance between the two ^{13}C nuclei. To obtain spectra with the maximum possible quadrature information, two data sets were combined. As indicated in Fig. 3.2, the "cosine" data set is obtained from the cosine-modulated magnetization by the standard phase cycle of $\pm z$ storage, 90° readout pulse of phase α, and $\pm(\alpha+90^\circ)$ detection phases, which yields a signal $\langle\cos(\omega_{d,1}\, t_1)\cos(\omega_{d,2}\, t_2)\rangle$.

The sine data sets require more careful consideration. The necessary modification of the pulse sequence is shown at the bottom of Fig. 3.2. By a 45°_{-x} storage pulse at the end of the t_1 period, the density operator is converted to

$$(S_x + L_x)\cos(\omega_{d,1}t_1) + 2\left[\frac{1}{\sqrt{2}}(S_y + S_z)\frac{1}{\sqrt{2}}(L_z - L_y) + \frac{1}{\sqrt{2}}(S_z - S_y)\frac{1}{\sqrt{2}}(L_y + L_z)\right]\sin(\omega_{d,1}t_1) \qquad (3.2)$$

of which $2\ S_z\ L_z\ \sin(\omega_{d,1}\ t_1)$ survives after T_2-relaxation of the transverse terms. By a 45°_x read-out pulse, this is converted to $2(1/\sqrt{2}\,S_z + 1/\sqrt{2}\,S_y)\ (1/\sqrt{2}\,L_z + 1/\sqrt{2}\,L_y)$ $\sin(\omega_{d,1}\ t_1)$, of which $(S_zL_y + S_yL_z)\ \sin(\omega_{d,1}\ t_1)$ becomes observable magnetization under the action of the dipolar coupling, according to

$$(S_zL_y + S_y\,L_z)\ \sin\ \omega_{d,1}t_1 \longrightarrow$$

$$(S_zL_y + S_yL_z)\ \sin(\omega_{d,1}\ t_1)\ \cos(\omega_{d,2}\ t_2)\ -\ 1/2\ (S_x\ + L_x)\ \sin(\omega_{d,1}\ t_1)\ \sin(\omega_{d,2}\ t_2) \qquad (3.3)$$

The observed signal is thus $1/2\ \langle\sin(\omega_{d,1}\ t_1)\ \sin(\omega_{d,2}\ t_2)\rangle$. The factor of 1/2 must be compensated by scaling the sine data set up by a factor of two. Acquiring the sine data with twice the number of scans relative to the cosine data set is a convenient alternative that yields a slightly better signal-to-noise ratio per unit time. This approach was adopted here. The data were measured and combined in t_1 according to the TPPI scheme and processed accordingly on the MSL spectrometer. To remove residual signal along the antidiagonal which may be due to pulse imperfections, the sine data set was scaled by a

factor of 1.1 before combination with the cosine data set. The experiment was performed on sample HDPE-b and the spectrum shown in Fig. 3.3(a) was obtained in two days of signal averaging. It exhibits intensity far from the diagonal, which indicates large changes in frequency and orientation due to the motion in the 100-ms mixing time. The elliptical ridges observed in the spectral intensity patterns are well known from ^2H exchange NMR.[34,10] They have an ratio of half-axis lengths of $b/a = (2.5 \pm 0.5)$. According to $|tan\ \beta| = b/a$,[34,10] this yields a reorientation angle β of $(112 \pm 5)^\circ$ or $(68 \pm 5)^\circ$.

A simulation of the above exchange experiment is shown in Fig. 3.3(b). It is based on a reorientation of the C-C bond by $\beta = 112^\circ$ before and after the 180° rotation around the chain axis. A C-C bond length of 1.56 Å (±0.01)Å and a C-C-C bond angle of 112° (±2)° were used in the simulation. Spectra with different double quantum evolution times, as described in section 3.2, were added up. The experimental and simulated spectra are slightly asymmetric due to the double quantum filtering. The jump rate used in the simulation was 15 /s, which was determined by a stimulated echo measurement applied to the same sample (HDPE-b) at the same temperature.

3.3.2 Dipolar Coupling Stimulated Echo Experiments

The intensity of the stimulated echo[9,33] generated by the ^{13}C-^{13}C dipolar coupling was recorded as a function of the mixing time to measure the correlation function of the 180°-flip motion. The stimulated echo is due to the ^{13}C sites that have the same frequency before and after the mixing time. For a two-site jump process such as the 180°-

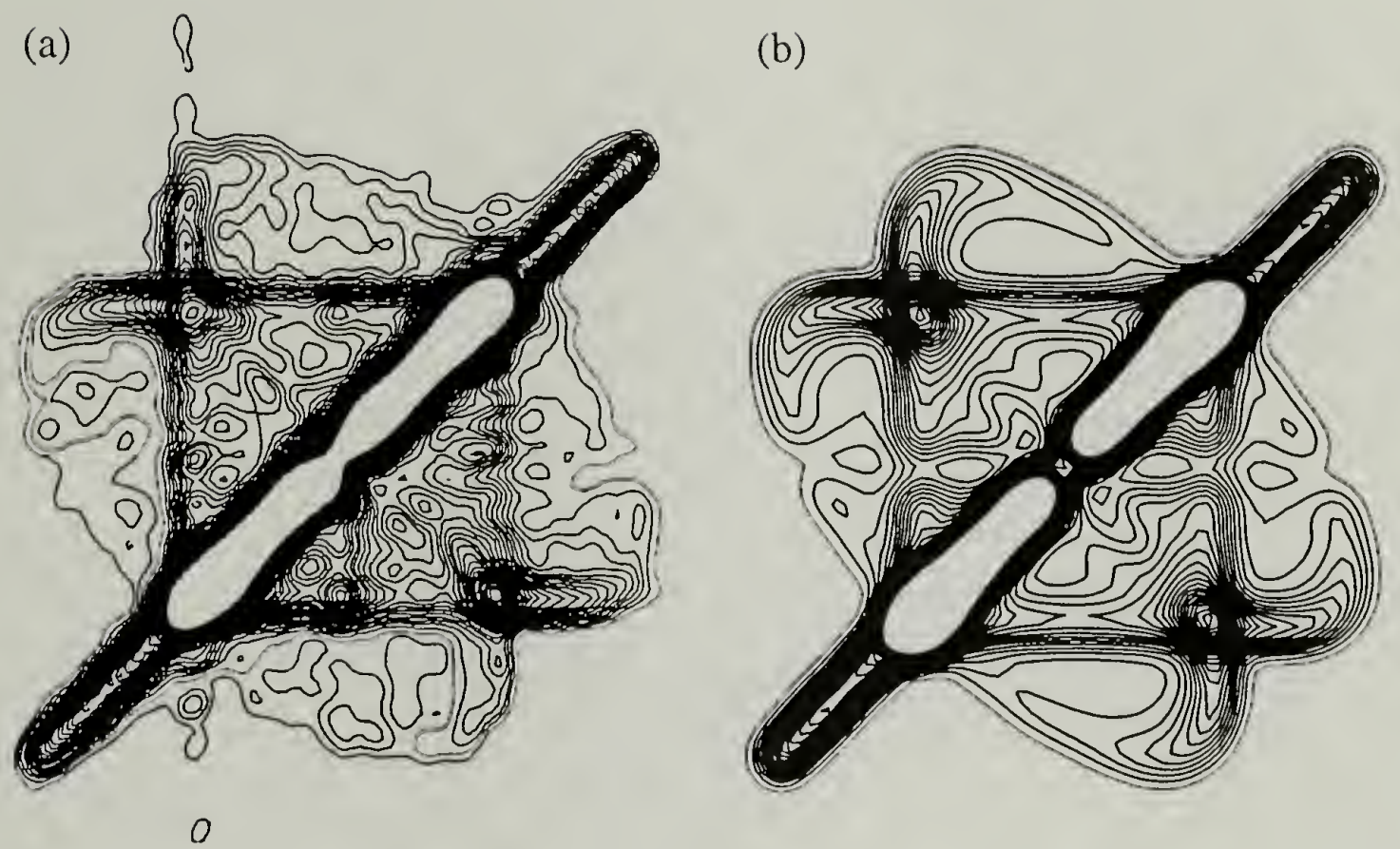

Fig. 3.3: 2D exchange spectrum of the ^{13}C-^{13}C dipolar coupling in ^{13}C-^{13}C pair labeled HDPE. (a) Experimental spectrum, T = 293 K, t_m = 100 ms. (b) Corresponding simulation for 180° flips. 30 contour lines are plotted between 0.8% and 20% of the maximum intensity. The slight asymmetry of the spectrum is due to the double-quantum filter, which does not excite equally the signals for all ^{13}C-^{13}C orientations. Integral projections onto the ω_2 axis are shown at the top.

flip motion, ideally the echo height after complete loss of correlation after long mixing time is 1/2 of the original value at short t_m. Actually, spin diffusion between ^{13}C nuclei on different chains further reduces the echo height at long mixing time. This restricts the correlation-time measurements at low temperatures. The limitation at high temperatures is the requirement of the slow-motion regime ($\tau_c > 2\ t_1$), which means that during the dephasing period t_1 and refocusing period $t_2 = t_1$ no reorientation of the ^{13}C-^{13}C pair occurs. Therefore, we limited our measurement to temperatures ≤ 310 K ($\tau_c > 20$ ms).

Fig. 3.4 shows the echo height decay as a function of the mixing time at 280 K and 310 K. At 310 K, a constant value of ~ 1/2 is observed between 0.1 s and 0.5 s. At $t_m \geq$ 1 s, the echo height decays to <1/2 due to spin diffusion. At 280 K, where the motion is slower, the echo decay due to reorientation and spin diffusion occurs on similar timescales.

Fig. 3.5 (a) shows the correlation function in sample HDPE-a at various temperatures as a function of reduced mixing time, t_m/τ_c, where τ_c is obtained by best fit with a single exponential function. The fit with a stretched exponential $\exp(-(t_m/\tau_c)^\beta)$ for $\beta = 0.8\ (\pm 0.1)$ is shown in Fig. 3.5(b); here, τ_c is obtained by best fit with the stretched-exponential function. The stretched exponential is found to fit the experimental data significantly better.

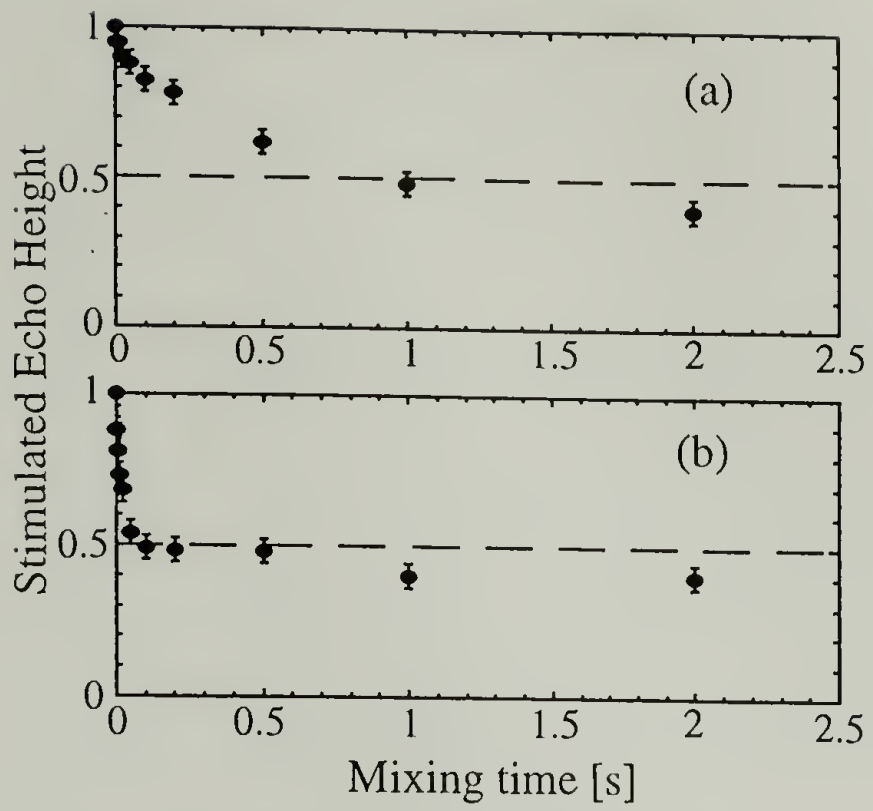

Fig. 3.4: ^{13}C-^{13}C dipolar stimulated echo height as a function of mixing time at (a) 280 K and (b) 310 K. At $t_m < 0.5$ s, the decay is due to reorientations of the ^{13}C-^{13}C vectors; at $t_m > 0.5$ s, there is a significant effect of spin diffusion between chains of different orientation.

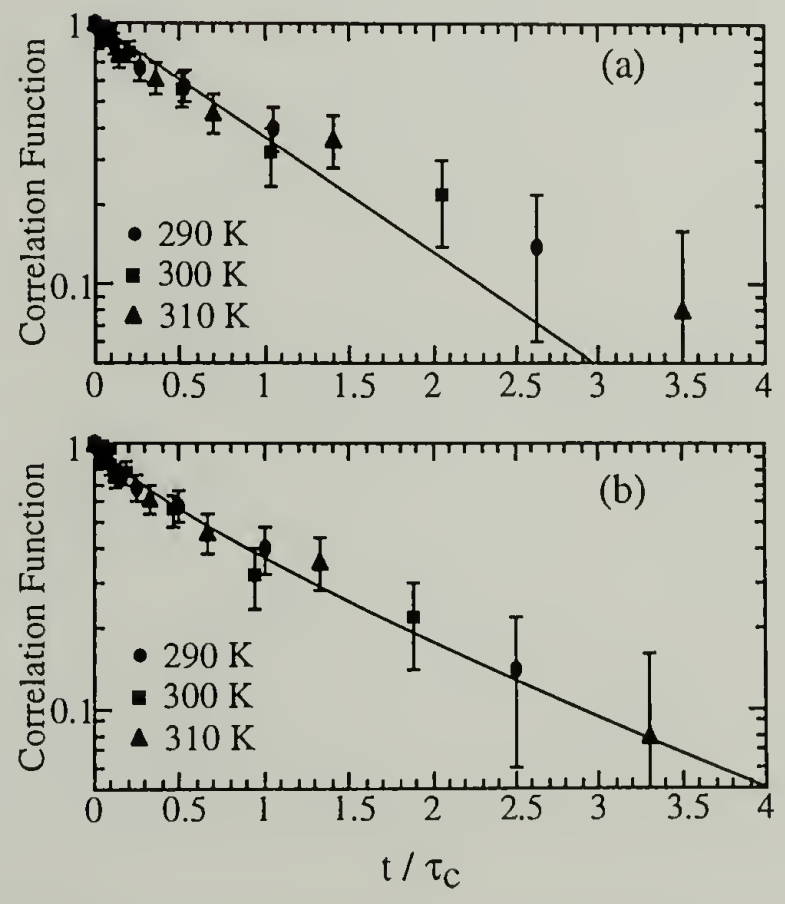

Fig. 3.5: Correlation function from stimulated-echo decays vs. reduced mixing time t/τ_c at 290, 300 and 310 K. (a) single exponential fit. (b) stretched-exponential $\exp(-(t/\tau_c)^{0.8})$ fit.

3.3.3 Motional Rates from ^{13}C-Lineshape Changes

The 1D lineshape reflecting ^{13}C-^{13}C dipolar coupling and chemical shift depends on the motional rate, which can be quantified by comparison with simulated spectra. According to Abragam[35], the lineshape of a single segment which undergoes jumps between two sites with average frequency $\overline{\omega}$ and splitting 2δ is given by

$$I(\omega) \propto \frac{4\delta^2 k}{(\omega-\overline{\omega})^4 + 2(\omega-\overline{\omega})^2(2k^2-\delta^2)+\delta^4} \qquad (3.4)$$

where k is the flip rate $k = 1/2\tau_c$. For $k << \delta$ (slow limit), two sharp lines at $\omega = \overline{\omega} \pm \delta$ are observed. For $k >> \delta$ (fast limit), only one sharp line at $\omega = \overline{\omega}$ is observed due to motional averaging.

In the case of interest here, the frequencies $\overline{\omega}+\delta$ and $\overline{\omega}-\delta$ are produced by the simultaneous action of ^{13}C-^{13}C dipolar couplings and ^{13}C chemical-shift anisotropies. For a flip between two given $^{13}CH_2$-$^{13}CH_2$ segment orientations, the average frequency $\overline{\omega}$ depends on both the (invariant) chemical-shift anisotropy and the average dipolar coupling, while the splitting δ reflects the difference between the dipolar couplings for the two ^{13}C-^{13}C vector orientations. The calculation is performed most conveniently in the principal-axes system of the $^{13}CH_2$ chemical-shift tensor.[36] Here, the orientations of the ^{13}C-^{13}C internuclear vectors before and after the flip are fixed and well-defined, so that the dipolar frequencies can be calculated easily from the angle between the B_0 field and the

^{13}C-^{13}C internuclear vector.[9] The powder spectrum is obtained by summing up spectra calculated according to eq.(3.4) for all orientations of the $\mathbf{B}_0$ field, with the polar coordinates (β, α) incremented by 0.5° and 1°, respectively. The parameters used in the simulations are: a bond length and a bond angle of 1.56 Å and 112°, respectively, as in the 2D exchange simulations; chemical shift principal values of 50, 35 and 13 ppm;[37] ^{13}C-^{13}C spin pairs and isolated ^{13}C population in a ratio of 4:1.

Fig. 3.6(a) shows the 1D spectra of HDPE-a at various temperatures. The lineshape changes at elevated temperatures as a result of the chain motion. Figure 3.6(b) shows the corresponding simulations based on 180°-flip motion, in which the chemical shift is invariant while ^{13}C-^{13}C dipolar coupling tensor changes. As seen from the figure, the motion can be well described by this flip motion. The determination of the flip rate from the one-dimensional lineshape is reliable in a window of rates between 100/s and 10^5/s. Outside the window, the system is in the fast- or slow-motion limit and the lineshape is not sensitive to the motional rate.

The best fits for 2D exchange (with pure dipolar coupling) and 1D lineshape (with both dipolar coupling and chemical shift) yield a C-C bond length of (1.56 ± 0.01) Å and C-C-C bond angle of (112 ± 2)°. The bond length result agrees well with neutron scattering data but the lattice constant c predicted by the simulations is (2.59 ± 0.02) Å, which is bigger than the published value of 2.54 Å from scattering[38]. The conflict is even more remarkable if the satellites positions in the UHMWPE fiber spectrum are applied to calculate the *c* value. Our best fit for R_1 and R_2 peak positions (1740 and 620 Hz,

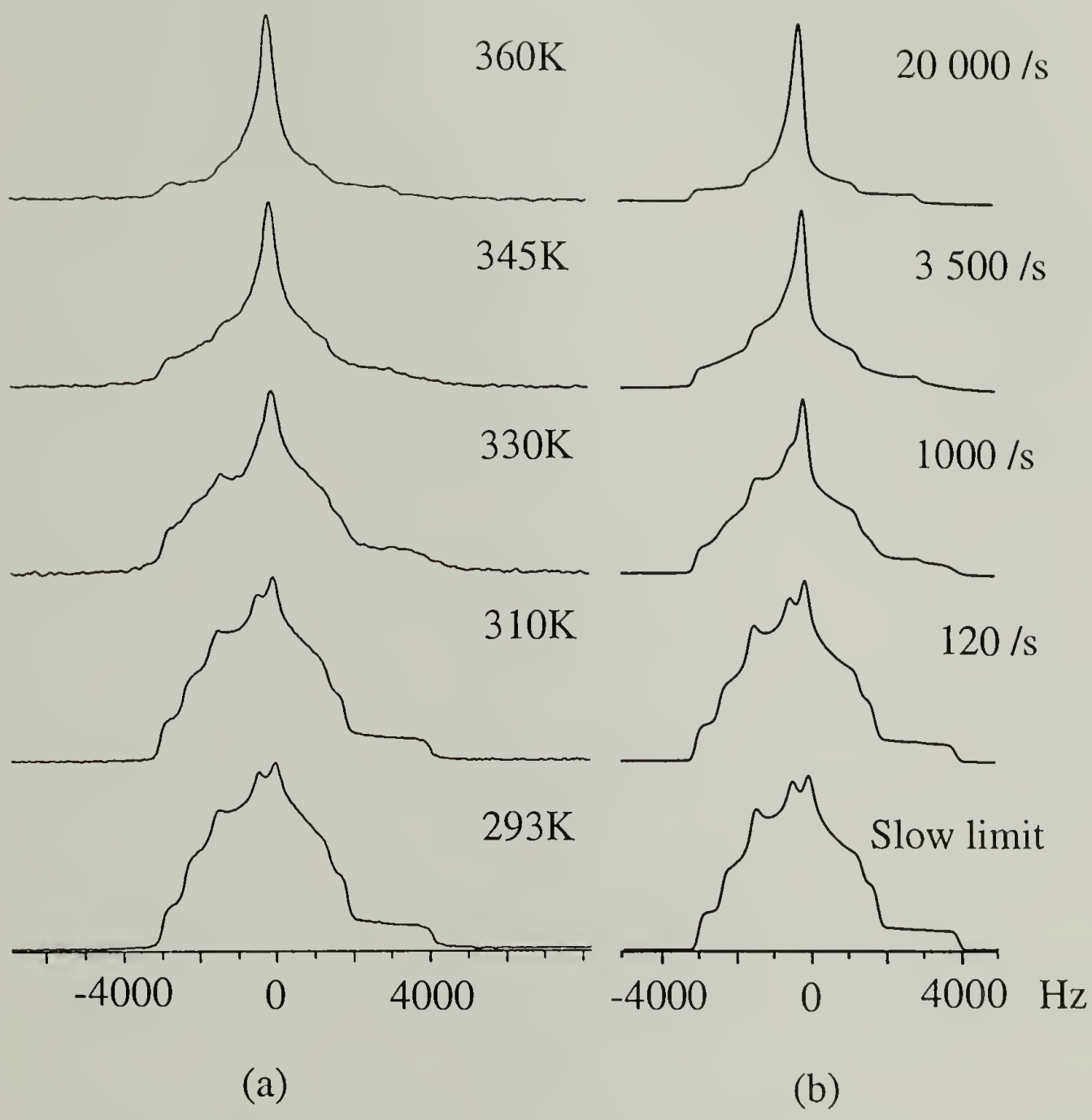

Fig. 3.6: 1D ^{13}C NMR lineshapes of the crystalline regions, reflecting dipolar coupling and chemical shift. (a) Experimental spectra as a function of temperature. (b) Corresponding simulations, with the indicated jump rates.

respectively, which agree with experimental values within the error limit) yields a bond length of (1.56 ± 0.01) Å and a bond angle of (116 ± 2)°. The R_2 peak position of 620 Hz directly gives a lattice constant *c* of (2.65 ± 0.02) Å, much higher than the published value from scattering measurements. This agrees with the NMR results of VanderHart[23], who noticed that the position of R_2, 600 Hz from the center, deviates from the value of 700 Hz calculated based on the dipolar coupling strength with c = 2.54 Å from X-ray scattering. He considered many potential reasons for the reduction of the coupling, but the deviation was not fully explained. Our experiment was performed at a much higher B_0 field strength and nevertheless found that the R_2 position remains the same (590 Hz). This shows that the deviation is intrinsic, not related to the magnetic field strength.

3.3.4 Flip Rates in UHMWPE fibers from Narrowing of Dipolar Satellites

Studying the motion in unenriched PE by reorientation of ^{13}C-^{13}C pairs is much more difficult because these spin pairs represent only an extremely small fraction (2.2/10000) of all carbon sites. Still, in highly oriented polyethylene fibers aligned with the B_0 field the ^{13}C-^{13}C spin pairs produce observable dipolar satellites.[23] A slight distribution in chain orientations leads to a broadening of the satellite. If the motional rate exceeds the width of the satellite, it narrows because the average dipolar frequencies for slightly misaligned chains are all similar, see Fig. 3.1 (b) (pg. 20).

Various arrangements of ^{13}C nuclei occur statistically and can be distinguished based on their ^{13}C-^{13}C dipolar couplings: (a) isolated ^{13}C sites (C); (b) directly bonded

^{13}C pairs (R_1) and (c) ^{13}C pairs (^{13}C-C-^{13}C) separated by two bonds (R_2). The spectrum of site C reflects only the chemical shift, while sites R_1 and R_2 experience chemical shift as well as different dipolar couplings. When the fiber axis is aligned parallel to B_0, the resonance frequency of site C does not have a strong angle dependence because one of the principal axes of the chemical shift tensor is parallel to B_0. The angle dependence of the R_2 dipolar coupling is $\omega(\theta) = -2\pi \cdot 620 \text{ Hz } (3\cos^2\theta - 1)/2$, where θ is the angle between the internuclear ^{13}C-^{13}C vector and the B_0 field. For R_2, $\theta \approx 0$ and the angle dependence of the frequency is small due to $d\omega/d\theta|_0 = 0$. On the other hand, the dipolar coupling of the R_1 pair, which is $\omega(\theta) = -2\pi \cdot 3.0 \text{ kHz } (3\cos^2\theta - 1)/2$ with an average θ angle of 34°, has a strong angle dependence, $d\omega/d\theta|_{34} = -2\pi \cdot 70 \text{ Hz}/^\circ$. Since the chain axes are not perfectly aligned along the magnetic field, in the absence of significant chain motion the R_1 peak is much broader than those of C and R_2.

As proven for unoriented HDPE above, the crystalline chain motion in PE is a 180° chain-flip motion during which the chain flips by 180° and translates by one CH_2 unit so that chain after the flip still fits the crystal lattice. In oriented PE, the flip motion leaves the ^{13}C chemical shift tensor invariant but the R_1 dipolar coupling changes before and after the flip for chains that are not perfectly aligned along B_0 (see Fig. 3.1b).[23] Thus, the 180° flip motion in the crystalline region will cause motional averaging of the R_1 signal due to the ^{13}C-^{13}C bond reorientation. As a result, if the motional rate is high enough, i.e. comparable to the low-temperature linewidth of the R_1 peaks, we will see narrowing of the R_1 satellites.

Figure 3.7(a) shows the room temperature spectrum with two different vertical scales, as well as corresponding simulations. The high and sharp central peak at 13 ppm is due to isolated ^{13}C spins. The broad and small peak (R_1), at ~1790 Hz from the central peak, is one of the two dipolar satellites (indicated by arrows in the figure) of the directly bonded ^{13}C-^{13}C pairs. The dipolar satellite at about 590 Hz from the central peak is generated by ^{13}C-C-^{13}C pairs (R_2). The full widths at half height of the central and R_1 peaks are 160 Hz and 650 Hz, respectively. The R_2 peak overlaps with the tail of the central peak, but it can be seen that it is sharper than the R_1 peak. From the single-site signal shape it is clear that besides a major highly oriented component (~80%) that contributes to the narrow part of the peak, there is a considerable amount of less oriented segments in the sample (~20%) that contribute to the low and wide shoulder on the left.

Simulations were performed to fit the R_1 peak at room temperature and at 360 K. The orientation distribution used in the simulation was composed of two parts with Gaussian angular distributions: $\sigma = 4°$ (80%) and 23° (20%). Parameters used in the simulation are the C-C bond length of 1.56 Å and the C-C-C bond angle of 116°. Gaussian line broadening of 100 Hz was applied. The overall order parameter S_2 can be estimated from the simulation parameters to be 0.92 ± 0.02. Since the CP spectrum underestimates the amorphous phase contribution, the actual S_2 should be slightly lower than this value.

The experimental spectrum at 360 K is shown in Figure 3.7(b). The R_2 peak is almost invisible due to additional broadening of the central peak. The width of the R_1 peak is ~350 Hz, showing significant line narrowing compared to the room-temperature

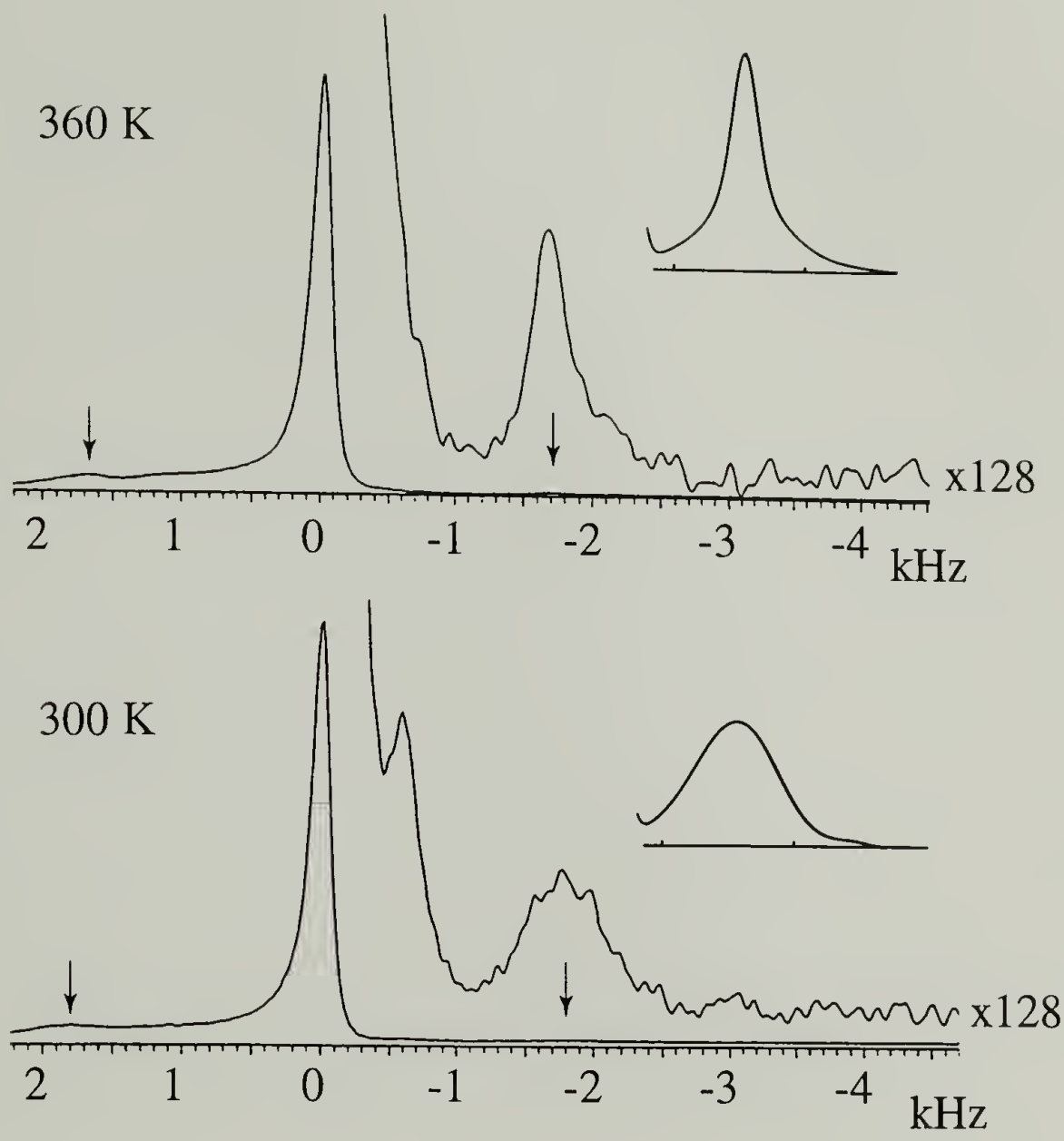

Fig. 3.7: ^{13}C spectra of UHMWPE fibers with fiber axis parallel to B_0, demonstrating motional narrowing of a ^{13}C-^{13}C dipolar satellite. The positions of the satellites are indicated by the two vertical arrows. (a) Experimental spectrum at room temperature (~300 K) and simulation (inset) of the dipolar satellite for a flip rate of $k < 10$ /s. The upper trace of the experimental spectrum was expanded vertically by a factor of 128. 100-Hz line-broadening was applied. (b) Experimental spectrum at 360 K, and simulation (inset) for a flip rate of $k = 1000$ /s. Narrowing of the dipolar satellite is observed clearly.

width of ~650 Hz. This demonstrates that 180° flip motion does occur in the highly crystalline UHMWPE fibers. A simulation of the satellite line shape, based on formula (4), is shown as an inset in Fig. 3.7(b). It gives a flip rate of (1000 ± 300) Hz at 360 K. Significant narrowing was not observed below 340 K. Besides the narrowing, the distance of R_1 from the center peak decreases from 1790 Hz at room temperature to 1690 Hz at 360 K, consistent with VanderHart's observation in a different oriented polyethylene.[23]

3.3.5 Motional Rates and $T_{1\rho,H}$ Relaxation

The relaxation time $T_{1\rho,H}$ of spin-locked ^1H magnetization in crystalline PE is sensitive to the chain-flip motion. $T_{1\rho,H}$ detects the modulation of H-H dipolar couplings. It exhibits a minimum when the jump rate $k = 1/2\tau_c = \gamma B_1$. In our measurements, $\gamma B_1 =$ 350 kHz. Under the 180° chain flips of PE, the strongest dipolar interactions, the geminal H-H dipolar couplings, are invariant. However, the long-range couplings to most other protons do change due to the flip.

Fig. 3.8 (pg. 45) shows $T_{1\rho,H}$ of the crystallites in HDPE-a, and in UHMWPE fibers at two different orientations, as a function of temperature. Our measurements cover only the slow-motion regime of $T_{1\rho,H}$, in which $T_{1\rho,H}$ decreases with increasing temperature, toward its minimum of $T_{1\rho\,H,min} \approx (0.9\pm0.3)$ ms, which was measured on the crystalline CH_2 units in the ethylene-hexene copolymer sample at a similar B_1 field (indicated by a dashed line). Because of the invariance of the strongest coupling, the

depth of the $T_{1\rho,H}$ minimum in PE[21] is less pronounced than, for instance, in the helical jumps of the 7_2 helix[9] of poly(ethylene oxide).[39]

At low temperatures, the sensitivity of $T_{1\rho,H}$ to the chain flips is compromised by ^1H spin diffusion to the amorphous regions. Due to the higher mobility, ^1H magnetization in the amorphous regions relaxes faster. Therefore, these regions act as "sinks" for magnetization in the crystallites, with the coupling between the domains provided by ^1H spin diffusion. In the UHMWPE fibers, spin diffusion occurs on a time scale of 15 ms (see Chapter 4), but it should be noted that under the spin lock during the $T_{1\rho}$ measurement, ^1H-^1H dipolar couplings and spin diffusion are reduced by a factor of 0.5. Thus, spin diffusion requires ca. 30 ms of spin lock to affect the magnetization in the crystallites. Even more importantly, the small (~15%) (see Chapter 4) amorphous and interfacial components in the fibers relax the crystalline regions only very inefficiently on a time scale during which the exchange in a Goldman-Shen experiment is incomplete. Therefore, the crystalline $T_{1\rho}$ of 23 ms ($c//B_0$) at 360 K is reduced little by spin diffusion and reflects the intrinsic relaxation time in the crystallites to a good approximation.

Since relaxation cannot occur faster than the loss of correlation in the underlying dynamic process, for the true rotating-frame relaxation without spin diffusion, $T_{1\rho} > \tau_c$. Thus, we conclude that the motional rate at 360 K must exceed $(23\ ms)^{-1}/2 = 20$ Hz. This lower limit is consistent with the flip rate of ~ 1000 Hz estimated from the satellite narrowing.

The combination of intrinsic $T_{1\rho}$ relaxation and spin diffusion at lower temperatures can lead to a complex behavior.[40] However, it is certain that the apparent $T_{1\rho}$ values for the crystallites are shorter than the true ones, since they are partially equilibrated with the shorter $T_{1\rho}$ in the amorphous regions. This reduces the apparent activation energy, to 43 kJ/mol in our system.

It is interesting to note that $T_{1\rho,H}$ of the crystallites in the fiber aligned with B_0 is twice as long as that of fibers perpendicular to B_0, at all temperatures measured. This shows directly that the relaxation process originates in oriented regions in the sample. A similar effect in the dielectric relaxation in highly oriented extruded polyethylene was taken as evidence that the α-relaxation occurs in the crystallites.[24]

3.4 Discussion

3.4.1 Geometry of the Chain Motion in the Crystallites

The two-dimensional exchange NMR spectrum of Fig. 3.3 and the decay of the stimulated echo height to 1/2 in Fig. 3.4(b) provide the most direct proof available to date for exact 180° jumps in the α-relaxation of polyethylene. The off-diagonal intensity pattern in the 2D spectrum depends sensitively and exclusively on the reorientation angle of the ^{13}C-^{13}C internuclear vector. As required for the 180° rotation of the chain, the reorientation angle matches the C-C-C bond angle of 112°. There is no sign of a significant distribution of reorientation angles; the spectrum is only consistent with a width of less than ±7° around 112°.

While the off-diagonal pattern reflects the reorientation geometry, the relative intensity of off-diagonal and on-diagonal signals yields information on the number of sites involved in the motion and the occupancy of these sites. This information is obtained in a more easily quantifiable manner from the stimulated-echo height, which reflects the fraction of the intensity along the diagonal in the 2D spectrum. The final echo height of 1/2 observed in Fig. 3.4(b) at 0.1 s < t_m < 0.5 s, i.e. before spin-diffusion sets in, shows that at long times, the probability of a ^{13}C-^{13}C bond being parallel to its original orientation is 1/2. This confirms the 180° flips, which involve exactly two bond orientations.

Both the well-defined geometry and parallelity of bonds contradict Wunderlich's simulations that predict major disorder in polyethylene crystallites at ~300 K.[41] ^{2}H NMR by Hentschel et al. shows that the C-H bonds in HDPE undergo fast librations with a root-means-square amplitude of only 4° at 295 K.[20] This is consistent with the observation of little motional averaging of the ^{13}C-^{13}C dipolar couplings in the one-dimensional spectrum obtained at 300 K, see Fig. 3.6 bottom.

3.4.2 Correlation Function

The stimulated-echo decay measures the occupancy of ^{13}C-^{13}C bond orientations parallel to the initial orientation, as a function of the mixing time t_m. Thus, it maps out the correlation function of the motion. For a jump motion between two equally probable bond orientations, this correlation function is given by $p_0(t) = \exp(-t_m/\tau_c)$. The correlation

time τ_c is related to the jump rate k between the two sites according to $\tau_c = 1/2k$ The data displayed in Fig. 3.5 show that a stretched exponential $\exp(-(t_m/\tau_c)^{\beta})$ with $\beta = 0.8$ gives a significantly better fit than a mono-exponential function. This indicates the superposition of correlation functions with different relaxation times. The β value of 0.8 corresponds to a width of the relaxation time spectrum of about 0.5 decades,[42] which is close to the result obtained for the dielectric α-relaxation[43] while significantly narrower than that of the dynamic-mechanical α-relaxation.[44]

The decay of the correlation functions to a final value of 1/2 indicates that the chain energies before and after the jump are similar. This is in agreement with 3D exchange NMR observations on POM, where little preference for return jumps was found.[9] A difference could arise due to the change of the length and torsion of the chain segments in the amorphous phase on either end of the chain stem in the crystal.

3.4.3 Motional Rate of Chain Flips in HDPE

The temperature dependence of the motional rates of the 180°-flip motion, as obtained from the lineshape analysis of Fig. 3.6 and from stimulated-echo measurements, is shown in the Arrhenius plot of Fig. 3.9. Data points at $T \geq 290$ K fall on a straight line. The points at the lowest rates and temperatures have higher apparent rates, due to temperature-independent spin diffusion (see Fig. 3.4) which contributes to the stimulated-echo decay. Therefore, they were excluded from the determination of the

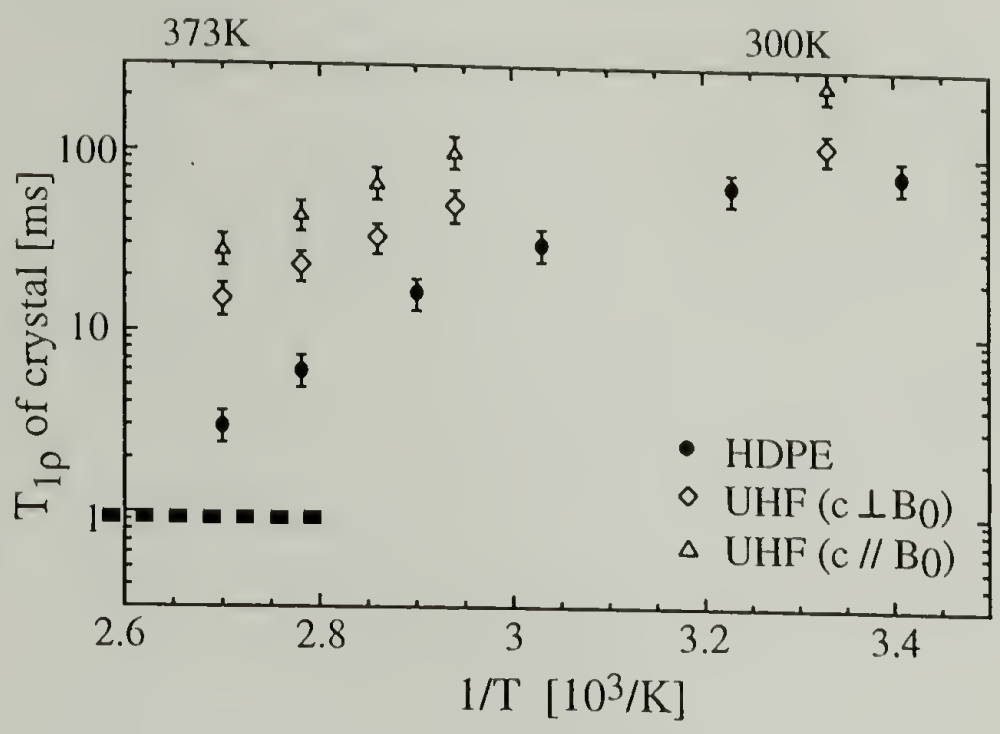

Fig. 3.8: $T_{1\rho,H}$ data at various temperatures: (o) HDPE; (<>) UHMWPE fibers with fiber axis perpendicular to B_0; (Δ) fiber axis parallel to B_0. The level of the $T_{1\rho,H}$ minimum at 0.9 ms is indicated by the dashed line.

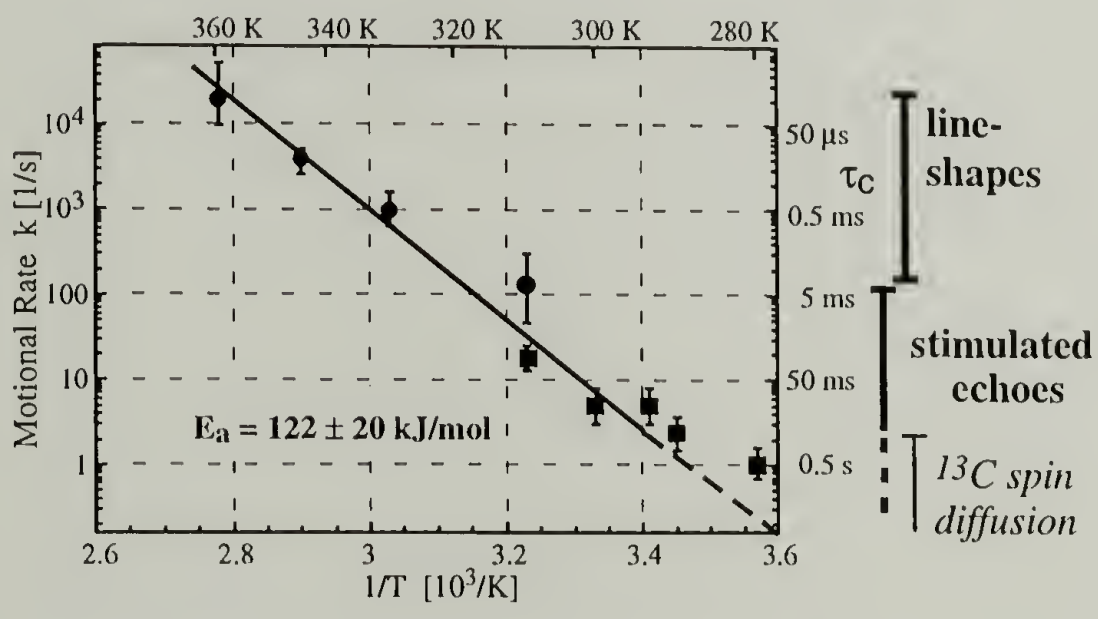

Fig. 3.9: Arrhenius plot of the correlation times of the 180°-flip motion in the crystallites obtained from the stimulated-echo decays ([]) and the 1D lineshape changes (o), see Fig. 6. The slope of the line yields an activation energy of (122 ± 10) kJ/mol. Points at the lowest temperatures were excluded from the fit since spin diffusion increases the rate of exchange artificially.

activation energy. The activation energy of the motion obtained from the slope of the line is E_a = (122±10) kJ/mol. This result is close to dielectric relaxation results of E_a = 99 kJ/mol in lightly chlorinated[43] and E_a = 106 kJ/mol in lightly oxidized high-density polyethylene.[45,1] For various polyethylenes, values of 100-120 kJ/mol are quoted for the dielectric and dynamic mechanical crystalline α-relaxations.[6]

Recently, it was proposed that 60 - 90% of chains in both high and low-density polyethylenes undergo fast 180° flips in the kHz range at ambient temperature.[25] This conclusion was based on a bimodal lineshape and cross-polarization-inversion of the crystalline signal in magic-angle-spinning (MAS) NMR spectra of various polyethylenes. However, this bimodal lineshape is not observed in MAS spectra of similar PEs obtained by other groups.[46] The measurement of ^{13}C-^{13}C bond reorientations in one- and two-dimensional spectra presented in the present work allows for a much more direct observation of the chain dynamics. The spectral lineshapes and $T_{1\rho}$ relaxation times shown above contain no signs of fast flipping units at ambient temperature. They directly preclude that more than ~20% of the crystalline segments in HDPE undergo fast 180° flips at 300 K.

The lineshape measurements described in this work depend on motional averaging of orientation-dependent frequencies before and after the 180°-flip. Certain other possible motional modes in the crystalline regions such as translation of chain without flipping or 360° rotation with translation would not produce lineshape changes, but reduce $T_{1\rho,H}$ due to the modulation of the resulting long-range H-H couplings. No

indications of such motions are seen here or in chain-diffusion measurements,[22] and their calculated activation energies are higher than those for the chain flips.[47]

3.4.4 Dependence of $T_{1\rho,H}$ on τ_c

From the ^{13}C lineshape and $T_{1\rho,H}$ measurements on the same sample at various temperatures, a relation between $T_{1\rho,H}$ and the correlation time of the 180°-flip motion can be obtained. It is plotted in Fig. 3.10, which can be used as a calibration curve to estimate the 180°-flip motion rate in a PE material from its $T_{1\rho,H}$, provided $T_{1\rho,H} < 30$ ms. Such a curve should prove useful since $T_{1\rho,H}$ can be measured very quickly and easily on any polyethylene sample. The data points for the HDPE and the fiber fall in the same region, which confirms that the same motional rates will lead to similar $T_{1\rho,H}$ for different polyethylene materials. When the motion is too slow ($\tau_c > 50$ ms), we find $T_{1\rho,H} < \tau_c$. Since the relaxation cannot be faster than the underlying motion, in this range the relaxation must be dominated by spin diffusion from the amorphous regions, where $T_{1\rho,H}$ is short. Therefore, the upper limit below which the plot provides a reliable estimate of the motional rate is $T_{1\rho,H} < 30$ ms.

3.4.5 Chain Flips in UHMWPE Fibers

The ^{13}C dipolar lineshape and ^{1}H $T_{1\rho}$ data consistently show that the 180°- flip rate in the UHMWPE fibers at 360 K is by a factor of 1/20 slower than in HDPE. This

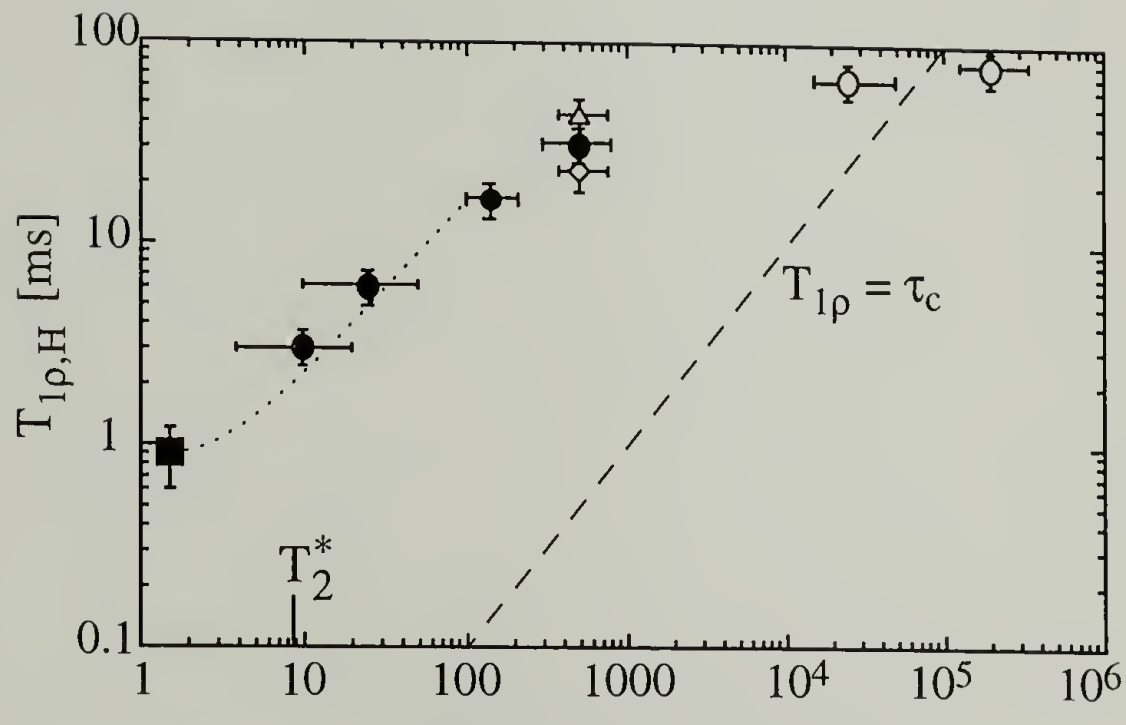

Fig. 3.10: $T_{1\rho,H}$ as a function of correlation time τ_c for (o) HDPE, (<>) UHMWPE fibers with fiber axis perpendicular to B_0, and (Δ) UHMWPE fibers with fiber axis parallel to B_0. The $T_{1\rho}$ minimum at $\tau_c = 1/2\gamma B_1$ ([]) was measured on the ethylene-hexene copolymer sample. The dashed line indicates where $\tau_c = T_{1\rho,H}$. For $T_{1\rho,H} >$ 30 ms, effects of spin diffusion become significant. In that range, the τ_c dependence of $T_{1\rho,H}$ plotted here cannot be expected to be valid for other PE samples.

slow-down is most likely due to the larger erystallite thiekness in the highly erystalline fibers. Aeeording to the empirieal relation between erystallite thiekness and the frequeney of the dieleetrie loss maximum,[19] the erystallite thiekness in the UHMWPE fibers is an order of magnitude larger than in the HDPE sample; the erystallite thiekness estimated on this basis would be 200 ± 100 nm. The erystal-thiekness dependenee of the motional rate, eombined with erystallite thiekening at elevated temperature, is probably also the eause for the differenee between the motional rate in the HDPE sample before (HDPE-b) and after (HDPE-a) annealing.

In the literature, the α-relaxation is sometimes termed α-transition and the temperature T_α is treated as a transition temperature below whieh no motion takes plaee. The eontinuous temperature dependenee of the motional eorrelation time and the $T_{1\rho,H}$ relaxation time eonfirm that the motion does not set in abruptly at a speeifie "transition temperature", as eoneluded on isotropie samples already a long time ago.[18]

3.4.6 Comparison with Dynamie-Meehanieal and Creep Measurements

The 180°-flips observed direetly in this study oeeur in the erystalline regions. At the same time, they must ehange the length of the ehain segments in the amorphous regions. The ehain flips oeeur between energetieally equivalent states of the erystalline part of the ehain and therefore do not eontribute to the meehanieal relaxation. In eontrast, the length and assoeiated eonformation ehanges in the amorphous regions ean lead to energy dissipation, whieh results in a meehanieal relaxation. This is fully eonsistent with

the earlier observation that the mechanical α-relaxation originates in the amorphous regions but requires the participation of motion in the crystallites.[6]

The excellent mechanical properties of UHMWPE fibers at ambient temperature are due to its high degree of parallel chain orientation and crystallinity, which in turn is a result of its high drawability in the solid state. In Chapter 4, we present strong evidence that solid-state ultradrawability of polyethylene and other semicrystalline polymers is based on the chain translation associated with the crystalline α-relaxation whose elementary step we have studied here for polyethylenes. The 20-fold slow-down of the flip motion compared to an isotropic sample is the likely origin of gradual strain hardening during the high-temperature draw.[26,48] The significant creep that occurs in UHMWPE fibers at elevated temperatures is a direct manifestation of the α-relaxation. In this regard, the reduction of the motional rate is expected to reduce creep at ambient temperature.

The 20-fold reduction of the chain flip rate in the UHMWPE fibers compared to isotropic HDPE is particularly interesting in view of the observation that the temperature of the maximum mechanical loss modulus E" or G" at 1 Hz is similar for both types of materials (60°C) [30,44], as reported specifically by Ward and coworkers.[49] In fact, the flip rate that we have found in the UHMWPE fibers is close to the dynamic-mechanical relaxation rate for ultra-high-modulus PE fibers obtained from data measured by Ohta et al. (ca. 100 Hz at 360 K).[30] In contrast, in common PE materials the macroscopic mechanical relaxation rates and the microscopic flip rates found by dielectric relaxation or NMR are different by about two orders of magnitude; at a temperature around 100°C the

dynamical mechanical relaxation rate is ~ 100/s while dielectric and NMR rates are ~ 10^4/s.[1,6] The closer agreement of the rates of the two processes in the UHMWPE fibers indicates that in the fibers, the 180° chain flip motion is more closely related to the mechanical α-relaxation and creep. The 180°-flips occur in the crystallites, while the mechanical α-relaxation is believed to originate in the amorphous regions.[6] Since the chains in UHMWPE fibers are much more extended, it is possible that the two phases are more strongly coupled in their dynamic properties. Ohta *et al* also observed that by incorporating small amounts of CH_3 side groups into the main chain, creep of UHMWPE fibers is effectively hindered.[30] This corroborates that the chain flips in the crystallites are indeed closely related to creep.

3.5 Summary

The 180°-flip motion of chains in the crystallites of ^{13}C-^{13}C labeled HDPE was directly confirmed using 2D exchange NMR spectroscopy. The temperature dependence of the motional rate was determined based on 1D lineshape changes and stimulated-echo decays. An activation energy of (122 ± 10) kJ/mol was obtained, which is close to that of the dielectric and dynamic-mechanical α-relaxations. A non-exponential correlation function of the motion was observed in the stimulated echo experiments, indicating a width of the relaxation-time spectrum of ~0.5 decades. The relation between the $T_{1\rho,H}$ relaxation time in the crystallites and the correlation time of the 180°-flip motion was directly determined. In ultradrawn polyethylene fibers, dipolar satellite narrowing has

shown that the crystalline chain segments undergo 180° flips with a reduced rate of ~1000 jumps/s at 360 K. This coincides relatively well with the dynamic-mechanical relaxation rate, indicating a closer relation between the chain flips and creep in the fibers than in isotropic polyethylene where the rates differ by two orders of magnitude.

3.6 References

(1) McCrum, N. G.; Read, B. E.; Williams, G. *Anelastic and Dielectric Effects in Polymeric Solids*; Dover Publications, Inc.: New York, 1991.

(2) Ward, I. M.; Wilding, M. A. *J. Polym. Sci.: Polym. Sci. Ed.* **1984**, *22*, 561-575.

(3) Reneker, D. H. *J. Polym. Sci.* **1962**, *59*, S39-S42.

(4) Strobl, G. *The Physics of Polymers*; Springer-Verlag: Berlin Heidelberg, 1996.

(5) Aharoni, S. M.; Sibilia, J. P. *Polym. Eng. Sci.* **1979**, *19*, 450-455.

(6) Boyd, R. H. *Polymer* **1985**, *26*, 323,1123.

(7) Kentgens, A. P. M.; de Boer, E.; Veeman, W. S. *J. Chem. Phys.* **1987**, *87*, 6859-6866.

(8) Hagemeyer, A.; Schmidt-Rohr, K.; Spiess, H. W. *Adv. Magn. Reson.* **1989**, *13*, 85-130.

(9) Schmidt-Rohr, K.; Spiess, H. W. *Multidimensional Solid-State NMR and Polymers*; Academic Press: London, 1994.

(10) Schaefer, D.; Spiess, H. W.; Suter, U. W.; Fleming, W. W. *Macromolecules* **1990**, *23*, 3431-3439.

(11) Vega, A. J.; English, A. D. *Macromolecules* **1980**, *13*, 1635-1647.

(12) McCall, D. W.; Douglass, D. C.; Falcone, D. R. *J. Phys. Chem.* **1967**, *71*, 998-1004.

(13) Hirschinger, J.; Schaefer, D.; Spiess, H. W.; Lovinger, A. J. *Macromolecules* **1991**, *24*, 2428-2433.

(14) Schilling, F. C.; Gomez, M. A.; Tonelli, A. E.; Bovey, F. A.; Woodward, A. E. *Macromolecules* **1987**, *20*, 2954-2957.

(15) Beckham, H. W.; Schmidt-Rohr, K.; Spiess, H. W. In *Multidimensional Spectroscopy of Polymers*, Urban, M. W.; Provder, T., Ed.; American Chemical Society: Washington DC, 1995; Vol. 598, pp 243-253.

(16) Olf, H. G.; Peterlin, A. *J. Polym. Sci. Part A-2* **1970**, *8*, 753.

(17) Opella, S. J.; Waugh, J. S. *J. Chem. Phys.* **1977**, *66*, 4919-4924.

(18) Hoffman, J. D.; Williams, G.; Passaglia, E. *J. Polym. Sci.: Part C* **1966**, *14*, 173-235.

(19) Mansfield, M.; Boyd, R. H. *J. Polym. Sci.: Polym. Phys. Ed.* **1978**, *16*, 1227-1252.

(20) Hentschel, D.; Sillescu, H.; Spiess, H. W. *Makromol. Chem.* **1979**, *180*, 241-249.

(21) McCall, D. W.; Douglass, D. C. *Appl. Phys. Lett.* **1965**, *7*, 12-14.

(22) Schmidt-Rohr, K.; Spiess, H. W. *Macromolecules* **1991**, *24*, 5288-5293.

(23) VanderHart, D. L. *J. Magn. Reson.* **1976**, *24*, 467-470.

(24) Boyd, R. H.; Yemni, T. *Polym. Eng. Sci.* **1979**, *19*, 1023-1028.

(25) Hillebrand, L.; Schmidt, A.; Bolz, A.; Hess, M.; Veeman, W. *Macromolecules* **1998**, *31*, 5010-5021.

(26) Porter, R. S.; Wang, L.-H. *J. Macromol. Sci.-Rev. Macromol. Chem. Phys., C* **1995**, *35*, 63-115.

(27) Furuhata, K.; Yokokawa, T.; Seoul, C.; Miyasaka, K. *J. Polym. Sci.: Polym. Phys. Ed.* **1986**, *24*, 59-67.

(28) Brady, J. M.; Thomas, E. L. *Polymer* **1989**, *30*, 1615-1622.

(29) Ohta, Y.; Sugiyama, H.; Yasuda, H. *J. Polym. Sci.: Part B: Polym. Phys.* **1994**, *32*, 261-269.

(30) Ohta, Y.; Yasuda, H. *J. Polym. Sci.: Part B: Polym. Phys.* **1994**, *32*, 2241-2249.

(31) Utz, M.; Eisenegger, J.; Suter, U. W.; Ernst, R. R. *J. Magn. Reson.* **1997**, *128*, 217-227.

(32) Schmidt-Rohr, K. *J. Magn. Reson.* **1998**, *131*, 209-217.

(33) Roessler, E. *Chem. Phys. Lett.* **1986**, *128*, 330-334.

(34) Schmidt, C.; Wefing, S.; Blumich, B.; Spiess, H. W. *Chem. Phys. Lett.* **1986**, *130*, 84.

(35) Abragam, A. *Principles of Nuclear Magnetism*; Oxford University Press: Oxford, 1961.

(36) VanderHart, D. L. *J. Chem. Phys.* **1976**, *64*, 830-834.

(37) Tzou, D. L.; Schmidt-Rohr, K.; Spiess, H. W. *Polymer* **1994**, *35*, 4728-4733.

(38) Brandrup, J.; Immergut, E. H.*Polymer Handbook*; 3rd ed.; John Wiley & Sons, 1989.

(39) Johansson, A.; Wendsjo, A.; Tegenfeldt, J. *Electrochimica Acta* **1992**, *37*, 1487-1489.

(40) Packer, K. J.; Pope, J. M.; Yeung, R. R.; Cudby, M. E. A. *J. Polym. Sci.: Polym. Phys. Ed.* **1984**, *22*, 589-616.

(41) Noid, D. W.; Sumpter, B. G.; Wunderlich, B. *Macromolecules* **1991**, *24*, 4148-4151.

(42) Lindsey, C. P.; Patterson, G. D. *J. Chem. Phys.* **1980**, *73*, 3348-3357.

(43) Ashcraft, C. R.; Boyd, R. H. *J. Polym. Sci.: Polym. Phys. Ed.* **1976**, *14*, 2153-2193.

(44) Boyd, R. H. *Macromolecules* **1984**, *17*, 903-911.

(45) Reddish, W.; Barrie, J. T. *I. U. P. A. C. Symp. uber Macromol*, Wiesbaden, Kurzmitteilung I.A.3, 1959.

(46) Kuwabara, K.; Kaji, H.; Horii, F.; Bassett, D. C.; Olley, R. H. *Macromol.* **1997**, *30*, 7516-7521.

(47) Syi, J.-L.; Mansfield, M. L. *Polymer* **1988**, *29*, 987-997.

(48) Lemstra, P. J.; Kirschbaum, R.; Ohta, T.; Yasuda, H. In *Developments in Oriented Polymers-2*, Ward, I. M., Ed.; Elsevier Applied Science: London and New York, 1987, pp 39-77.

(49) Gibson, A. G.; Davies, G. R.; Ward, I. M. *Polymer* **1978**, *19*, 683-693.

CHAPTER 4

POLYMER ULTRADRAWABILITY: THE CRUCIAL ROLE OF α-RELAXATION CHAIN MOBILITY IN THE CRYSTALLITES

4.1 Introduction

Tensile drawing of polyethylene[1-6] and several other semicrystalline polymers, such as isotactic polypropylene (iPP)[7-13], poly(oxymethylene) (POM)[14-16] or poly(tetrafluoroethylene) (PTFE)[17], to draw ratios of greater than 20 ("ultradrawing"), up to several hundred,[6] produces fibers of excellent mechanical properties.[18,19] Therefore, the drawability of many industrial polymers has been investigated, in particular by Porter et al., Ward et al., and Kanamoto et al.[16,18,20-26]. It has been found to vary greatly, even for chemically similar polymers.[20,22,27] Despite serious efforts, no ultrastrong fibers have been produced from nylons,[28-31] semicrystalline poly(ethylene terephthalate) (PET),[21,32] syndiotactic polypropylene (sPP),[20,33] or isotactic poly(1-butene) (iPB1),[22,34] all of which draw poorly.

The observed differences in drawability are not explained by classical models of polymer drawing,[35,36] which have often focused on the transformation from the spherulitic to a fibrous morphology at small draw ratios and low temperatures. It has been proposed that (ultra)drawability requires sliding of microfibrils,[35,37] or local melting[38,39], which should occur similarly for similar polymers such as iPP, sPP, and

iPB1, while in fact these systems show strikingly different ultradrawing behavior.[20,22,27] Discussions of ultradrawability that focus on low levels on entanglements[40-43], on intermolecular forces[44], on crystal-crystal transitions[45], or on crystal slip[46-48] also do not account for the differences between these structurally similar polymers with weak interchain interactions.

In this chapter, we present a systematic classification of semicrystalline polymers into two classes. They are termed "α_c-mobile" and "crystal-fixed", depending on the presence or absence, respectively, of a crystalline α-relaxation that provides mobility of chains in and through the crystallites. We first review recent experimental evidence, in particular direct observation by two-dimensional NMR, of the chain motions giving rise to the α_c-relaxation in various semicrystalline polymers. Then we summarize the salient features of the various stages of the drawing process. Two requirements for ultradrawability, namely α_c-mobility and a low degree of entanglement, are identified.

This work extends an empirical correlation of polymer extrudability and the crystalline α-relaxation by Aharoni and Sibilia[49,50]. On the basis of Aharoni's work, Bigg[51] and Gedde[52] have also stated that the α_c-relaxation is important for ultradeformation in general, however without detailed justification or a critical discussion of alternative models. In addition, there are scattered suggestions of the importance of the α_c-relaxation for the ultradrawability of specific polymers.[14,20,33,53,54] That this view has not found wide acceptance is demonstrated by the lack of a discussion of the relation

between the α_c-relaxation and ultradrawability in many modern textbooks and reviews that discuss these topics individually[18,37,42,43,47,55,56]. The literature on (ultra)drawing of polymers, which is in fact so vast and diverse that we can quote it only selectively, shows clearly that the other explanations of ultradrawability mentioned above are still more widely held[12,18,19,37,38,44,45,47,57-60]. Now, the NMR characterization provides more detailed knowledge about the specific large-amplitude chain motions associated with the α_c-relaxation and makes it easy to understand how those chain motions result in polymer ultradrawability. We will show that the absence of such motion prevents ultradeformation, even in polymers with weak intermolecular forces, such as sPP or iPB1 (form I). The implications for molecular details of the drawing process, such as chain pull-out, will be addressed. Finally, a critical discussion of various other explanations of ultradrawability will be given.

4.2 Review of NMR-Observation of α_c-Relaxation Chain Mobility

The presence of distinct relaxation processes in semicrystalline polymers, labeled α-, β-, γ-relaxations from high to low temperature, was revealed first by dielectric and dynamic-mechanical relaxation measurements. The results of these classical techniques have been discussed in several extensive reviews.[56,61] In this section, we will focus on the results of nuclear magnetic resonance (NMR) techniques, which have revealed the characteristics of the molecular motions in solid polymers in unprecedented detail.[62]

In the NMR experiments, the dependence of the NMR frequencies on the segmental orientation is exploited. The quadrupolar coupling of ^2H and the anisotropic chemical shift of ^{13}C have been used most extensively. In the two-dimensional exchange experiment, changes in segmental orientation during a mixing time t_m of 1 ms to 10 s are observed in detail by measuring the orientation-dependent frequency ω_1 before t_m and ω_2 afterwards for each segment.[62] Plotting the intensity as a function of these two frequencies ω_1 and ω_2, segments that do not reorient during the mixing time have $\omega_1 = \omega_2$ and therefore produce signal along the diagonal. Intensity far off the diagonal indicates large frequency and angle changes, while small-amplitude motions produce a broadening of the ridge that is observed along the diagonal.

If the change in segmental orientation occurs faster than the range of the angle-dependent NMR frequency, which is 3 - 20 kHz for the chemical shift, and 125 kHz for the quadrupolar coupling, motionally averaged NMR frequencies are observed. These result in narrowing and shape changes of the one-dimensional spectrum. This has long been exploited in ^1H wideline NMR,[63] where the up to 60-kHz wide spectrum reflects the dipolar couplings between the protons, and in ^2H NMR,[64] where the quadrupolar coupling of up to $\pm$ 130 kHz indicates the (re)orientation of the C-^2H bond.[62]

4.2.1 Helical Jumps

Effects of large-amplitude dynamics in the crystallites of polyethylene (PE), PTFE, and POM were detected early on by ^1H NMR in terms of the reduction of the

second moment of the ^{1}H (or ^{19}F) wideline spectrum[63] and $T_{1\rho}$ relaxation time as the temperature is increased.[63,65,66] The first detailed description of large-amplitude reorientations in the crystallites in terms of helical jumps was given by Kentgens et al. for POM by 2D magic-angle-spinning exchange ^{13}C NMR.[67] Investigations of POM by 2D exchange NMR without sample rotation confirmed the picture in detail.[68] The geometry and activation energy of the motion has been determined in these experiments.[67,68]

In the helical jump process, the helical polymer chain in the crystallites is rotated and translated in such a way that the chain before and after the jump is in equivalent, crystallographically allowed orientations and positions, which is required unless the crystal is disordered. For an N_m helix, where N monomer units on m turns form one repeat unit of the helix, a rotation by 360° m/N together with a translation by one repeat unit fulfills this requirement, see Fig. 4.1. The most convincing proof of the helical jumps is provided by 2D and 3D exchange spectra in highly oriented POM, $[\text{-O-CH}_2\text{-}]_n$ [68] (produced by solid-state extrusion made possible by the helical-jump process itself, see below). Since the chains in all crystallites are parallel to within ±4°, the only degree of freedom is the rotation of chains around the coincident microscopic chain and macroscopic sample axes. Therefore, the 2D exchange NMR patterns have a unique relation with the rotation angle around the chain axis. In particular, the experimental spectrum of POM shows patterns for two and three successive jumps in the same direction, which proves that the helical-jump process involves not just a flip-flop between two adjacent orientations but can lead to long-range diffusion. Three-

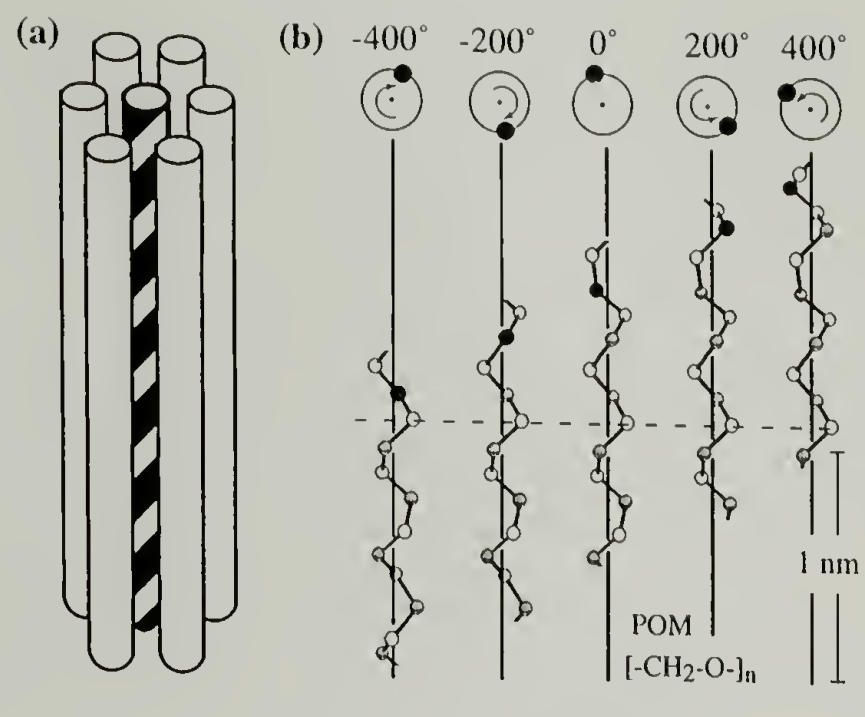

Fig. 4.1: Helical jumps in the crystallites of semicrystalline polymers. (a) Sketch of a given helical chain, in the channel formed by the neighboring chains. Translation along the chain axis, following the contour of the helix, is much easier than lateral diffusion. (b) Several steps of the helical jump motion in POM, $[\text{-O-CH}_2\text{-}]_n$. For this 9_5-helical structure, a rotation by $360^\circ \cdot 5/9 = 200^\circ$ together with a translation by one monomer unit moves the chain into an energetically equivalent position and orientation in the crystallite (as indicated by the dashed line). While the crystalline section of the chain before and after such a helical jump seems unchanged, the individual segment observed by NMR has rotated and translated as a result of the jump. In addition, the chain length in the amorphous regions has been decreased by one repeat unit on one side of the crystallite and increased by the same length on the other. Many such jumps lead to significant chain diffusion through the crystal.

dimensional exchange spectra have confirmed that the probability of return jumps is not significantly enhanced.[62] Clear indications of the chain diffusion resulting from a large number of jumps were detected by magic-angle-spinning NMR on polyethylene[69-71]. ^{13}C exchange NMR also proved helical jumps in isotactic polypropylene,[68] which were soon after confirmed in detail by ^{2}H exchange NMR.[72] 2D exchange spectrum of oriented iPP shows strong off-diagonal intensity for the signals of the CH_2, CH, and CH_3 groups. In contrast, in oriented sPP no off-diagonal exchange intensity is observed in the 2D ^{13}C exchange spectrum, obtained at T = 355 K ($\approx T_m$ - 100 K) and t_m = 2 s. This is fully consistent with the absence of a crystalline α-relaxation in sPP.[20,33]

In PEO, $[-O-CH_2-CH_2-]_n$, the ^{13}C 2D exchange spectrum shows strong exchange by helical jumps much faster than 10/s at 240 K ($\approx T_m$ - 100 K).[62] The cross-section parallel to the ω_2-axis at the indicated ω_1-frequency shows a 6:1 ($\pm$1) ratio of off- to on-diagonal intensity. This shows that the jumps occur between more than six sites; in the 7_2 helix of PEO, there are indeed seven sites with distinguishable orientations. Again, the NMR data prove that the α_c-motion is not just a flip—flop process. In PEO, the dynamics occur so close to the glass transition that the dielectric and dynamic-mechanical crystalline α-relaxation is not well resolved from the relaxation in the amorphous regions. At ambient temperature, ^{1}H $T_{1\rho}$ relaxation and the large width of the ^{13}C signal under magic-angle spinning confirm that the rate reaches ~ 50,000 jumps/s at 300 K.[73] In PEO,

PE, iPP, and POM, the ratios of off- and on-diagonal intensity in the NMR spectra prove that all of the crystalline chain stems are involved in the jump motion.

In PE, $[-CH_2-]_n$, it was proposed early on that chain flip-flops, each accompanied by a displacement of the chain stem in the crystallite by one CH_2 unit, give rise to the dielectric α_c-relaxation.[74-76] Due to the high symmetry of the planar all-trans chain, direct observation of the 180° flips by 2D exchange NMR has been achieved only recently by detecting the change in the orientation-dependent ^{13}C-^{13}C dipolar-coupling frequency.[77] The activation energy for the chain flips was determined as 122 ± 20 kJ/mol.[77] This value, as well as the flip rates measured, are consistent with the results obtained for the dielectric α_c-relaxation in lightly oxidized HDPE.

At 100°C, the rate of chain flips in HDPE reaches a value near 30 000 jumps/s[77], and even higher values in LDPE. This is expected to result in displacements of chain segments by tens of Ångströms within a few seconds. In particular, chain diffusion of segments between amorphous and crystalline regions will occur, which can be observed by NMR[69] since the different conformational environments lead to different isotropic chemical shifts observed under magic-angle spinning. In addition to cross-peaks in 2D exchange NMR spectra at high temperatures, the diffusive rather than exponential ^{13}C T_1 relaxation[69,78] with its strong crystallite-thickness dependence[78] are strong indications that this chain-diffusion process indeed occurs.

4.2.2 More Complex Dynamics

In PTFE, $[-CF_2-]_n$, the α_c-relaxation must be identified with the β-relaxation,[61] which involves chain rotation in the crystallites, as proven by the lineshape of ^{19}F chemical-shift powder spectra obtained under multiple-pulse decoupling.[79] In addition, ^{19}F wideline spectra show a small width reduction around 100°C, which has been taken as an indication of fast chain translation that leads to a reduction of long-range ^{19}F-^{19}F dipolar couplings. This might be the origin of the α-relaxation in PTFE. Otherwise, the NMR study by Vega and English indicates that the geometry of rotations of the segments in the crystallites remain nearly unchanged up to the melting point, while the amplitude of the motions in amorphous regions seems to increase continuously.[79] A detailed scattering and vibrational-spectroscopy study shows dynamic helix reversals, probably occurring in twin defects, and conformational defects, but also residual long-range order.[80]

In poly(vinylidene fluoride), PVDF, $[-CH_2-CF_2-]_n$, the α-relaxation involves trans—gauche isomerizations between different inequivalent chain conformations in a disordered crystal structure, as was shown in a beautiful ^2H 2D exchange-NMR study[81].

In poly(acrylonitrile), PAN, the α-relaxation near 100°C has traditionally been considered as a glass transition. ^1H and ^2H NMR, however, show that all segments, not just the amorphous parts, undergo similar anisotropic rotations of large amplitude.[82,83] A crankshaft-type rotation in a partially disordered paracrystalline structure has been suggested as the motional mechanism.

In *trans* polybutadiene, t-PBD, $[-CH_2-CH=CH-CH_2-]_n$, chain mobility in the crystallites sets in at an order-disorder phase transition near 70°C.[84,85] Blurring of all non-equatorial wide-angle X-ray reflections proves translational disorder in the high-temperature phase. ^2H and ^{13}C NMR without sample rotation show fast ($>10^5$/s) rotational motions. Significant changes in the isotropic ^{13}C chemical shifts strongly suggest conformational changes. Though little effect on the dynamics is observed when the translation is inhibited by rigid chain folds,[85] sliding motion of the freely rotating chains in the crystallites is certainly easy in form-II.

Poly(para-hydroxy benzoic acid), PpHBA, is an example of a relatively rigid polymer that becomes liquid crystalline at high temperatures.[85] As expected, the ^{13}C NMR lineshape of the carbonyl group of PpHBA indicates 180° flips or free chain rotation above the phase transition.[86]

4.2.3 Comparison of α_c-Processes

As this brief review has indicated, various sub-types of α_c-mobility can be distinguished. Regular helical jumps occur in PE,[77] POM, and iPP.[72] Helical jumps are also observed in PEO, but some conformational disorder is present. In PTFE, translational disorder is observed above 31°C, which means that the discrete helical jumps can change to a more or less continuous rotation and translation. In PVDF,[81] PAN, and t-PBD,[85] conformational disorder is present in the crystallites and the α_c-relaxation dynamics involves major conformational changes. Thus, these three polymers fulfill the

conditions of Wunderlich's concept of dynamical conformational disorder (condis phase)[87]. In t-PBD, fast rotational motions are also present. For these systems, it is not clear whether translational motion occurs. However, since good extrudability and workability is observed in the α_c-relaxation region,[49] it seems likely that translational chain motions in the crystallites are also facile (see below).

In the case of helical jumps, the displacement of the chain by each jump is the larger the longer the repeat unit. In POM and iPP, the atoms in the backbone are displaced by 2.5 Å along the chain contour, and in PEO by as much as 4 Å. In t-PBD, which has a chemical repeat unit with a contour length of nearly 6 Å, the chain motion occurs in a disordered phase, which avoids the necessity of translational jumps by full repeat units.

It seems to be a necessary condition for the occurrence of helical jumps that the amorphous regions are mobile. This means that helical jumps can only occur above the T_g of the amorphous layers, which produces a β or γ relaxation. Obviously, this is not a sufficient condition: iPP, sPP, and iPB1 have similar T_g values (near 265 K) but only iPP is α_c-mobile. Similarly, POM and PEO have $T_g \sim 200$ K, but the helical-jump rate at 300 K is ~1/s in POM and $> 10^4$ in PEO. In PEO, helical jumps set in so close to the glass-transition temperature that the Arrhenius line of the crystalline α-relaxation must be "bent down" by the WLF curve near T_g. This effect still awaits a detailed experimental investigation.

We would like to mention that NMR, by unequivocally demonstrating the occurrence of helical jumps or similar large-amplitude motions, disproves the suggestion by Aharoni and Sibilia[49] that small-angle torsional motions were responsible for the α_c-relaxation. A shallow minimum in the intra-molecular energy, as implicated by Aharoni and Sibilia, may be necessary to allow for the distortions occurring in the traveling defect that rotates the chain, but cases like iPS show that the barrier height in the intermolecular energies is similarly important.[88]

4.2.4 Models of the α_c-Dynamical Defects

2D exchange NMR observes the relative orientation of the chain segments before and after a helical jump during the mixing time. The detailed process of chain rotation is too fast to be observed. Some indirect information is provided by the activation energy and its dependence on chain structure and crystallite thickness. These can be compared to predictions of model calculations. Since the activation energy of rigid-rod chain rotation increases linearly with the number of segments in a given crystalline stem, rotation of the chain by a traveling defects with a twist and a translational mismatch localized within about two dozen backbone atoms has a lower activation energy. The older but widely known Reneker model with only 2 ~ 3 CH_2 groups involved in the defect[74] has a relatively high energy.[75] Mansfield and Boyd, and Mansfield et al.[75,88] have proposed a more extended defect that traverses the crystallite with a speed of 1 nm/ps (1 km/s). In PE, it involves a rotational mismatch over 12 CH_2 units and an

adjaeent region of translational mismateh, with one CH_2 unit more or less, over a similar length.[75] For a variety of semierystalline polymers, these ealeulations are quite sueeessful at predieting the aetivation energies of α_c ehain motions. In partieular, the absenee of an α_c-relaxation in sPP[20,33] and iPS is explained on this basis. Generally, the α_c-mobility is suppressed by large sidegroups. For helieal jumps, the aetivation energy inereases with the length of the repeat units.[88] However, a transition into a disordered phase allows mobility even in the ease of long repeat units. Interestingly, the α_c-mobility in poly(vinyl aleohol) at $T > 160^{\circ}C$ shows that even elosely spaeed OH-groups with the potential for H-bonding do not neeessarily prevent ehain rotation and translation at high temperatures.

Other possible defeets that have been eonsidered are disloeations, involving translations without rotation along the e axis, whieh would be invisible to exehange NMR.[47,89] In polyethylene, sueh disloeations are energetieally favorable[89] and may be responsible for axis shear observed by several groups.[90-92] However, in other polymers sueh as 9_5-helieal POM, or 7_2-helieal PEO, the periodieity of the erystal strueture along the e-axis is as long as 15-20 Å, making any ehain translation without rotation highly improbable. In nylon 12, the length of the ehemieal repeat unit is too long for any ehain translations, with or without rotation.

4.2.5 Crystal-Fixed Polymers

There are many semicrystalline polymers which do not exhibit a detectable α_c-relaxation. These "crystal-fixed" polymers include nylons, PET, PBT, sPP, iPS, iPMMA, and others, as listed in Table 4.1(b). As already mentioned, sPP shows no exchange intensity in 2D exchange NMR spectra at T_m - 60K; the same holds for iPB1 in the thermodynamically stable form I.

Some researchers have assumed that all semicrystalline polymers, including in particular nylons, PET, and iPS, exhibit an α_c-relaxation.[93] For nylons and PET, this claim is based mostly on the observation of crystal thickening. Such a process, however, can be due to (re)crystallization above T_g, e.g. in PET, or may require the presence of residual solvent, as was shown in the case of nylons[94]. For nylons, ^2H NMR work by English et al. has shown convincingly that the N-^2H bonds remain essentially static up to the melting point, excluding large-amplitude chain rotations and translations[29,95]. Data for sPP[20,33] are clear in showing no α_c-relaxation peak below T_m in the 3 - 10 Hz region. They only exhibit a slight up-turn in tanδ near T_m, which is associated with a strong decrease in both the storage and the loss modulus. This behavior is also observed for other polymers, e.g. for PVDF far above the α_c-relaxation[61], and is most likely due to premelting. Thus, for the polymers listed in Table 4.1(b), the evidence against an α_c-relaxation is strong.

Table 4.1: Drawability and α_c-relaxation dynamies of various semierystalline polymers. Reported maximum draw ratios λ_{max} (tensile or in extrusion) are given for melt-crystallized ("melt-eryst.") materials and for samples prepared from initial states of low entanglement ("low entg.") sueh as dilute solution, gel, or reaetor powder. Listed are the moleeular nature of the α_c-proeess as determined by NMR, motional rates measured at speeifie temperatures, and approximate melting points for referenee. LC: liquid erystalline. (a) Properties of ultradrawable and α_c-mobile polymers. Rates of α_c-relaxations in materials not yet investigated by NMR are given in braekets. Note that in several cases, melt-cyrstallized samples have been ultradrawn or solid-state extruded. (b) Crystal-fixed polymers. Various other polymers are probably erystal-fixed, but sinee their drawabilities are so disappointingly low, few data are reported in the literature.

Polymer	λ_{max} melt cryst	λ_{max} low entg.	Nature of α_c-process	Jump rate at T_{exp}	T_m	Refs.
(a) α_c-Mobile Polymers						
PE, $[-CH_2-]_n$	36	350	180° flips	~10^4/s at 100°C	136°C	6,77
iPP, $[-CH_2-CH(CH_3)-]_n$	>14	80	Helical jumps	>10/s at 100°C	160°C	12,13
iP4MP $[-CH_2-CH\{CH_2CH(CH_3)_2\}-]_n$	>14	>30	(dyn.-mech.)		231°C	27,72
POM, $[-O-CH_2-]_n$	>30		Helical jumps	>10/s at 100°C	180°C	14,67,68
PEO, $[-O-CH_2-CH_2-]_n$	>30		Helical jumps	>10^4/s at 30° C	67°C	62,105
PTFE, $[-CF_2-]_n$	>14	60	Chain rotation [β-relaxation]	phase transition, > 10^4/s at 50°C	327°C	17,79
PVDF, $[-CH_2-CF_2-]_n$	>14		trans-gauche	10/s at 90°C	231°C	26,81
P(E-c-TFCE) $[-(CH_2)_2-CFCl-CF_2-]_n$	>14		(dielectric, dyn.-mech.)	> 10/s at 130°C	242°C	49,125
PVA, $[-CH_2-CHOH-]_n$		38	(dyn.-mech.)	200/s at 200°C	258°C	18,53
PAN $[-CH_2-CH(C\equiv N)-]_n$		110	crankshaft jumps (?)	$7\cdot10^5$/s at 150°C	>300°C	83,126
t-PBD $[-CH_2-CH=CH-CH_2-]_n$	>14		rotation & condis	phase transition, > 10^5/s at 75°C	136°C	25,85
PpHBA $[-C_6H_4-COO-]_n$	>14		LC at > 350°C	> 10^4/s at 357°C	>450°C	49,86
PPO $[-C_6H_2(CH_3)_2-O-]_n$	>14		(dielectric)	>10/s at 240°C	264°C	49
(b) Crystal-Fixed Polymers						
sPP $[-CH_2-CH(CH_3)-]_n$	14		no exchange at 355 K	--	150°C	20,33
iPB1(form I) $[-CH_2-CH\{CH_2CH_3\}-]_n$	(not extrudable)		no exchange at 360 K	--	135°C	49,127
Nylons	5	12		--	~260°	28-30, 49, 107
PET $[OOC-C_6H_4-COO-CH_2-CH_2-]_n$	4.5	16		--	258°C	21,49
PBT $[OOC-C_6H_4-COO-\{CH_2\}_4]_n$	(not extrud-able)			--	223°C	49
iPS $[-CH_2-CH(C_6H_5)-]_n$	4			--	240°C	88,98
Other crystal-fixed polymers: $[-(CH_2)_2-(CF_2)_2-]_n$ [49], iPMMA.						

It should be noted that at very low temperatures, all polymers are "crystal fixed". However, we mostly use the term to denote polymers that are crystal fixed at all temperatures below the melting point. In these polymers, the activation energy of longitudinal chain motions is apparently comparable to or higher than the free energy required for achieving isotropic mobility, i.e. melting.

4.3 Drawing of Semicrystalline Polymers

A considerable variety of structural features observed when semicrystalline polymers are drawn have been described in the literature. Following Peterlin[35], three stages of tensile drawing can often be distinguished: (i) The elastic and plastic deformation of the spherulites at small draw ratios λ; (ii) the nearly discontinuous transformation of the spherulitic into a fibrillar structure where the chains in the crystalline regions are oriented parallel to the draw direction; this process often leads to necking; and (iii) the plastic deformation of the fibrillar structure, which is required for ultradrawing to $\lambda > 15$ (see Fig. 4.2). In our analysis of ultradrawing, we will be concerned mainly with the presence or absence of a significant stage (iii). Details of the spherulite deformation,[47] stage (i), seem to be rather unimportant for the formation of the fibrillar structure, since highly oriented semicrystalline fibers are also obtained from a variety of other initial states, such as solution-crystallized crystal lamellae,[6] as-polymerized reactor powder,[96] polymer gel,[4] and amorphous fibers. To provide a perspective, in the following we will briefly summarize the structural features associated with stages (ii) and (iii), as observed

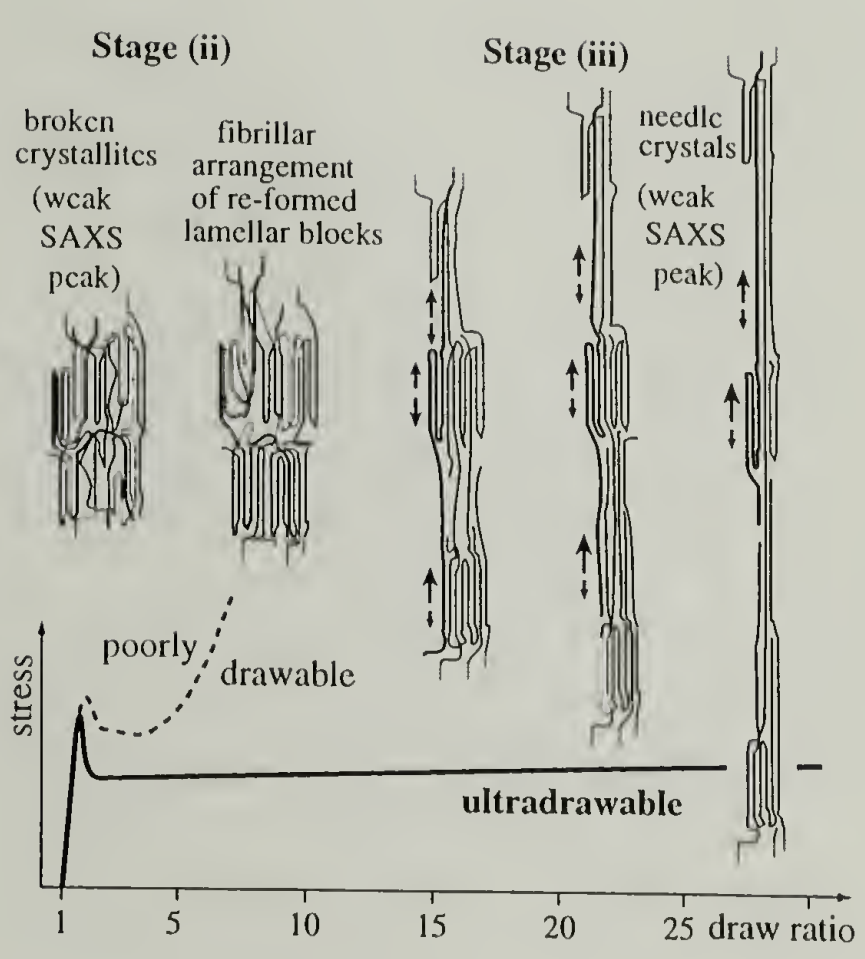

Fig. 4.2: Sketch of the probable evolution of the local morphology during tensile drawing. After necking, the lamellar crystallites are broken but the chains are aligned with the draw direction. After some reformation of lamellar crystal blocks, thermally activated chain translation in α_c-mobile polymers, indicated here by arrows for the highlighted chain, permits further deformation of the already aligned lamellar blocks into needle-shaped crystals, which arise by crystallization of tie molecules into crystalline bridges. In crystal-fixed, poorly drawable polymers, after the possible reformation of the lamellar blocks, which act as physical cross-links, only limited and mostly reversible deformation of the amorphous regions is possible.

by several groups[35,97]. The boundaries between stages (i) and (ii), and between stages (ii) and (iii) are sometimes diffuse, particularly in hot drawing. Nevertheless, there is always a clear difference between stage (i) and stage (iii). Unfortunately, this distinction has often been disregarded in the literature, which has resulted in rather unclear descriptions of the drawing process and relatively little regard to the special features of the ultradrawing process, stage (iii), for polymers other than polyethylene.

4.3.1 Formation of the Fibrillar Structure [Stage (ii)]

Traditional cold drawing (i.e. near ambient temperature for PE) in stage (ii) leads to necking, at a draw ratio of 1.1 to 2. There is strong evidence from SAXS, electron microscopy, and neutron scattering that existing lamellar crystallites are more or less destroyed[38,98-100] by the shear forces and then re-form with a different thickness (depending on the temperature of draw)[36], decreased lateral dimensions and reduced perfection[57]. To what extent this athermal decrystallization, which has been observed down to 77 K,[98] and the subsequent formation of aligned crystal blocks constitutes melting and recrystallization remains a matter of debate.[35,38,39,57,97,99]

Electron microscopy evidences show that the necking region for a PE single crystal can be as narrow as ~ 2 nm, or 4 to 5 layers of crystalline stems.[98] This suggests that during necking the chains are "peeled off" from the crystal and quickly recrystallize. Such a "peeling-off" is a very local phenomenon and occurs when the α_c chain mobility is not sufficiently high. Necking becomes less important at higher temperature, where α_c

chain mobility becomes higher and most of the chains simultaneously contribute to the deformation process.

The morphology in the necked region consists of small aligned lamellar blocks, which are connected by stretched non-crystalline tie molecules or crystalline bridges.[14,35] The draw ratio of the strain-hardened necked region is referred to as the "natural draw ratio",[35] which is typically < 7.[14] At these small draw ratios, the chains must still be folded[37]: Whether one starts from a regularly chain-folded lamella or from a frozen-in random coil, the end-to-end distance of a chain of MW = 10^5, which has a fully extended length of ~ 1000 nm, projected on the draw direction is ~ 25 nm, see Figure 4.3.[101] Thus, the minimum macroscopic draw ratio at which the chain is fully extended is 1000 nm/ 25 nm = 40.[101,102]

4.3.2 Fibril Extension and Ultradrawing [Stage (iii)]

All semicrystalline polymers can be drawn to draw ratios of $\lambda \geq 3$ after the fibrillar structure was first formed in stage (ii). Further (hot) drawing to $\lambda > 15$ is only possible for polymers with an α_c-relaxation and sufficiently low level of entanglements (see below). It produces highly extended fibers at only slowly increasing apparent stress. The disappearance of the SAXS peak[103] and analysis of electron micrographs show that very long needle-like crystals (protofibrils)[104] are formed, in which the chains must be highly extended. The modulus of the fiber at room temperature increases with the draw

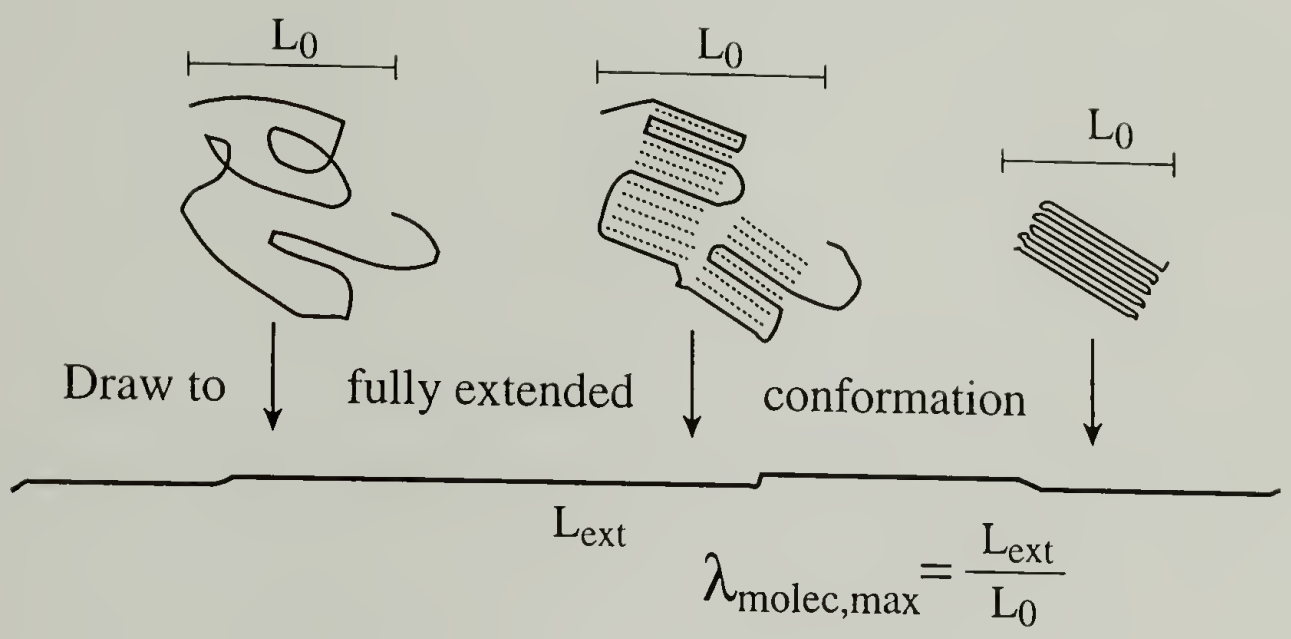

Fig. 4.3: Schematic representation of the maximum molecular draw ratio obtainable by full extension of a random polymer coil, a quench-crystallized polymer coil, and a chain in a crystal with perfect adjacent reentry. For clarity, only a relatively short chain is shown. If the crystal thickness indicated is 10 nm, its molecular weight would be ~15,000, giving a maximum molecular draw ratio of $L_{ext}/L_0 \sim 5$ to 10. The figure can also be taken to indicate the minimum macroscopic draw ratio that is necessary to fully extend a typical molecule of the given molecular weight.

ratio, up to draw ratios of ~ 100 where it starts to level off.[6] The increase in modulus must be directly proportional to the density of load-bearing chains per cross-section area. For this quantity to increase, the degree of chain folding must slowly decrease and the chains become more stretched out, as sketched in Fig. 4.2 (pg. 72).

Why ultrahigh molecular weight polymers are required in order to reach draw ratios > 50 is indicated in Fig. 4.3 (pg. 75):[101,102] Chains of MW ~ 10^5 become highly extended at these draw ratio, so that further strain only involves sliding of chains past each other, which does not produce a stronger fiber and eventually results in ductile failure. In this argument, it is assumed that the macroscopic and microscopic draw ratios are similar. Neutron scattering[57] indicates that this assumption applies in PE at T_m - 50 K, but that at higher temperatures the molecular draw ratio starts to lag significantly behind the macroscopic λ.

High nominal draw ratios can be achieved by drawing or extrusion in the melt. However, this procedure does not produce materials of high chain orientation or modulus, except in the case of liquid-crystalline melts. [17]

4.4 Ultradrawability and the α_c-Relaxation

Summarizing the literature data on ultradrawability from our viewpoint, we conclude that two classes of polymers need to be distinguished and differ fundamentally in terms of the presence or absence of an α_c-relaxation:

4.4.1 Ultradrawable Polymers

PE is the prime representative of the class of ultradrawable semicrystalline polymers, which also include PTFE,[17] PEO,[105,106] POM,[14] iPP,[12,13,18] and iP4MP,[27] (see Table 4.1 for a more comprehensive list). In these systems, hot drawing ($T > 50^{\circ}C$ for PE) or extrusion, stage (iii), can yield draw ratios in excess of 30 at only slowly increasing stress levels, if the degree of entanglement is sufficiently low; this applies for gel-spun[19] or solution-crystallized[6] material, reactor powder which has never been melted,[96] or low-to-medium-molecular-weight material.[14] Many authors agree that in this ultradrawing process, chains are moved through and out of the crystals due to some process of high chain mobility.[18,33,35,39,45] We argue that this process is the chain translation associated with the α_c-relaxation as described above.

4.4.2 Poorly Drawable Polymers

In the second class of semicrystalline polymers, no significant plastic deformation of the fibrillar structure, stage (iii), can be achieved. Nylons,[29,107] PET,[21,32,108] iPS,[109,110] iPMMA,[109] P(E/TFE) copolymer,[49] iPB1 (form 1),[22] and sPP[20,33] cannot be ultradrawn, even when prepared with few entanglements,[18] and cannot be solid-state extruded.[49]

While fibrillar structures formed by destruction and re-formation of crystallites (stage (ii) of drawing) have also been observed for the poorly drawable polymers,[107] the natural draw ratios of these polymers tend to be smaller than those of the drawable polymers,[20,33] in particular when the crystallinity is considerable. Contrary to casual statements in some reviews, there is no evidence of significant chain pull-out in these poorly drawable polymers. When reviewing the data for these systems, it should be noted that a limited amount of drawing can be achieved without chain pull-out, by extending the amorphous phase after fragmentation of the lamellar crystals and formation of small mosaic blocks up to $\lambda = 3$.[97] Porter has suggested that the natural draw in nylons is actually determined by the limit of the amorphous extension process.[18] This deformation is at least partly reversible by heating above T_g.

In PET[21,32], iPMMA, iPS, and to a lesser extent in nylons and sPP,[20] low initial crystallinity and crystallization during drawing can be exploited to circumvent the cross-linking effect of the crystallites and thus to achieve draw ratios > 5. In PET, the highest moduli and draw ratios, around 16, were reached for initially amorphous fibers in a three-stage drawing process.[21]

4.4.3 Ultradrawable = α_c-Mobile; Poorly Drawable = Crystal-Fixed

From the data collected in Table 4.1, it becomes obvious that ultradrawable polymers are α_c-mobile. In addition, it is apparent that the NMR-proven jump motion of the chains in the crystallites provides a molecular mechanism for the required major

extension of thc fibrils during ultradrawing. This will be diseusscd in more dctail below. By the samc token, crystal-fixed polymers are poorly drawable, see Tablc 4.1(b). Here, the crystallites present effeetive eross-links which fix thc ehains. It is interesting to note that large-amplitude mobility is found to be a unifying feature of rigid-backbonc liquid-erystalline [39] and flcxible α_c-mobile polymers, i.e. of thc two types of polymers that ean be oriented to yield fibcrs of extremely high moduli.

Some of thc observations and interpretations conecrning thc importance of an activated process like the α_c-relaxation for drawability were diseussed in 1974 by Clark and Scott who drew commcrcial-gradc POM to high draw ratios.[14] However, their work was mostly disregardcd[39] and in spite of their often lucid discussion, Clark and Scott suggested that nylons could bc ultradrawn, cven though they lack a erystalline α-relaxation. Convincing data on the molecular nature of the α_c-relaxation proccss has become available only recently with the advent of modern solid-state NMR, as reviewcd above. Ward's and Kanamoto's groups reeently suggested corrcctly that the α_c-relaxation affcets the drawability in polypropylenes[20,33]; however, in ref.[20], the α_c-relaxation is confuscd with a reversiblc erystal—crystal transition, whieh is inappropriate for polypropylenes and many other α_c-mobile polymers. In investigating the drawability of PVA, Garrett and Grubb also concluded that the α_c-relaxation was important, sincc its amplitudc corrclates with the drawability.[53]

Aharoni and Sibilia[49,50] presented an exeellent empirical eorrelation between solid-state extrudability and the occurrenee of a erystalline α-relaxation in a large number of semicrystalline polymers (PE, iPP, POM, PEO, iP4MP, PVDF, PVF, PTFE, t-PBD, and others). However, the authors of that study were not aware of the translations and large-angle rotations occurring in these systems, whieh were only later proved convincingly by NMR. Instead, they sought an explanation in terms of broad intramolecular potential minima. However, the proven ability of the chains to migrate through the crystal represents a mueh more eonvineing moleeular proeess for ehain extension in extrusion or drawing. In a review, Bigg[51] correctly generalized the findings of Aharoni and Sibilia, but his terminology of "alpha erystallization temperature" and "secondary transition" are not appropriate for deseribing the α_c-relaxation. In his reeent polymer-physics textbook, Gedde correctly eonnected ultradeformation and the α_c-relaxation, but did not discuss the experimental evidence and the many competing models of ultradrawability[52].

A seemingly similar proposal on the effect of the α_c-relaxation on deformation properties (among many others) was made by Rault[93]. However, in that paper it is assumed incorrectly that all semicrystalline polymers, including in partieular nylons, PET, and iPS, exhibit an α_c-relaxation. In addition, the drastieally different ultradrawability of α_c-mobile and crystal-fixed polymers was not properly reeognizcd.

4.4.4 Effects of Temperature

When reviewing the literature, it is important to note that temperature is a crucial parameter in drawing of polymers. In many treatments of the subject, the classical descriptions of cold drawing, stage (ii), are not distinguished from the more recently introduced ultradrawing and solid-state extrusion processes, stage (iii), which are always performed at high temperatures, i.e. close to the melting point, or, more pertinently, above the temperature where the rate of the crystalline α-relaxation is > 10^3/s. Drawing at room temperature is traditional cold drawing for PE, where the amorphous regions are mobile, but it must be considered hot drawing for PEO, which is highly α_c-mobile at 290 K. It is true cold drawing for PET or dry nylons, whose amorphous regions are rather rigid since $T_g > 300$ K.

Table 4.2 presents an attempt to categorize the drawing conditions in terms of chain mobility. It lists the draw ratios that can be reached, the features observed in small-angle X-ray scattering, and a few examples for each case. As indicated in category (1), the limiting draw ratios of $\lambda \leq 3$ found for nylons and PET of high crystallinities define the limit of drawability achievable by deformation of the sub-T_g amorphous regions with the crystallites serving as cross-links in which the chains are fixed. Heating above T_g while leaving the chains fixed in the crystallites, case (3), increases the drawability only slightly. The excess drawability of α_c-mobile polymers, in particular in categories (6) — (7), is due to chain motion through the crystallites that also generates the α_c-relaxation. Other processes, such as the break-up of lamellae, may also be facilitated by the low barriers to

Table 4.2: Classification of conditions of polymer drawing processes, according to drawing temperature T_{Draw}, α_c-mobility, and entanglement level. UHMW = ultra-high molecular weight. In the third column, it is indicated whether entanglement (E) or the crystal-fixed structure (C) limits the drawability; brackets indicate that the limitation is a minor effect. The draw ratios given in the fourth column should be considered typical; with special techniques, such as two-step processing, somewhat larger values may be achieved. The features of the SAXS peak after drawing, given in the fifth column, indicate the structure of the drawn material. Specific examples for the different cases are given in the last column.

T_{Draw}	Materials Characteristic	Draw Limit	Draw Ratio	SAXS Peak	Examples
truc cold drawing $T < T_g$	(1) Crystal-fixed (any polymer)	C (E)	$\lambda < 4$	weak	Dry nylon, T=20°C PE, T < -120°C
traditional cold drawing of PE & iPP	(2) Slowly α_c-mobile, entangled; natural draw ratio is limit	C (E)	$\lambda < 14$	weak	PE, T = 20°C
hot drawing $T > T_g$	(3) Crystal-fixed, >30% crystalline; natural draw ratio is limit	C	$\lambda < 14$	weak	Nylon, T > 100°C sPP, T > 50° C
	(4) Initially amorphous, crystallizing during drawing into crystal-fixed structure.	E, C	$\lambda<16$	intensity increases	Initially amorphous PET above T_g
hot drawing, $T>T\alpha(10^3/s)$	(5) α_c-mobile, but UHMW & melt-crystallized (highly entangled)	E	$\lambda < 7$	strong, position T-depend.	UHMWPE, 90°C
Ultradrawing	(6) α_c-mobile with high rate, intermediate MW (little entangled)	((E))	$\lambda<50$	disappears	PEO, T > 30°C POM, T > 90°C PE, T > 120°C
Ultradrawing	(7) α_c-mobile with high rate, UHMW, solution crystallized or reactor powder (unentangled)	--	$\lambda<400$	absent	UHMWPE>90°C iPP, T > 100°C PTFE, T > 45°C

chain displacement along the c-axis for which α_c-relaxation chain translation is an indication. The limit to drawability, the natural draw ratio, seems to be dominated by chain entanglements. For highly entangled systems in categories (2) and (5), α_c-mobility increases drawability only to a small extent. It has mostly a local effect on the phase structure, as reflected by the dependence of the SAXS peak position on the drawing temperature. But it is always a necessary condition for reaching high draw ratios as in categories (6) - (7), and can even override the effect of some entanglements, case (6).

4.4.5 Effect of Draw Rate

In addition to temperature, the speed of drawing is another important parameter. Often, high draw ratios can be reached only at low enough strain rates.[111] The temperature and rate dependence [112] strongly indicates that an activated process, which we have identified as being the α_c-relaxation chain diffusion, is responsible for drawability. An activation energy of the extensional viscosity of *ca.* 120 kJ/mol is obtained according to ref.[54] and of *ca.* 100 kJ/mol from Fig. 7 of ref.[112], which matches the activation energy of the α_c-relaxation.[56,77]

If melting was crucial for ultradrawability, an increase in the strain rate and the resulting reduction in the heat dissipation would be expected to improve the drawability, contrary to the experimental observations.

4.4.6 Tensile Drawing and Solid-State Extrusion

In addition to tensile drawing, solid-state extrusion and solid-state coextrusion have been used to produce drawn semicrystalline polymers.[18] Even though these processes are related, they differ in their details, involving tensile and compressive deformation, respectively. The limiting mechanism in tensile drawing is rupture, which does not occur in solid-state extrusion of the pure polymer (but can occur in coextrusion). On the other hand, solid-state extrusion is impossible for crystal-fixed polymers,[49] while some tensile drawing or solid-state coextrusion can always be achieved due to deformation of the amorphous regions. Solid-state coextrusion, where the polymer of interest is embedded into an envelope of ductile polymer,[18] is intermediate between tensile drawing and extrusion. Here, rupture can occur, but not as easily as in tensile drawing. The difference between tensile and extrusion drawing is demonstrated by polymers with extremely high chain mobilities in the crystallites, such as t-PBD above 70°C. For these materials, extrusion works very well, while the high plasticity leads to early rupture in tensile drawing.[25]

4.4.7 Microscopic Picture of Chain Motion and Drawability

The solid state draw or extrusion to the highest draw ratios is generally performed at temperatures just below the melting point.[18] At this temperature, the chain translation rates of α_c-mobile polymers are high enough for efficient crystallite deformation. Several researchers [14,18,35,39,49] realized that (often unexplained) dynamical processes are

crucial to drawability. The α_c-mobility actually fulfills the established requirements very well. For instance, it explains the activation energy of the extensional viscosity during ultradeformation in terms of the activation energy of the microscopic chain-flip and translation process.

The consequence of crystalline chain motion is random diffusion of chains into and out of crystallites if there is no external force, but it can become a directed motion under force and facilitate the crystallite deformation and rearrangement. This corresponds to the classical Eyring model of cold flow in glasses, which is based on stress-aided thermally activated mobility.[113,114] There is good evidence that tie molecules between crystallites play an important role in the plastic deformation of semicrystalline polymers (see Fig. 4.2).[35,37,58] For polymers with a crystalline α-relaxation, there will be no permanent taut tie molecules since chains can translate through the crystallites. Therefore, crystallites can be deformed on sufficiently long time scales. In other words, the crystalline α-relaxation leads to a reorganization of the amorphous regions, which redistributes the force burden among tie molecules and prevents the premature breaking of taut tie chains so that high drawability is achieved.

The chain-diffusion process along the chain contour changes the topology when a chain end slips through a crystallite, in which case the crystallite shrinks laterally and the draw ratio increases (see Fig. 4.2). Thus, the draw rate is expected to increase with the number of chain ends, or decrease with increasing molecular weight.

In the case of ultra-high molecular-weight polyethylene (UHMWPE), creep experiments strongly suggested[54,115-117], and our recent experiments have directly shown, that chain flips occur even in highly drawn fibers.[77] The chain 180°-flip rate is ~1000/s at 90°C. With an activation energy of ~120 kJ/mol, the rate will be > 10^4/s at 130°C. The less crystalline material before drawing should have an even higher rate. This is sufficient for the crystallite deformation and reorganization in solid-state drawing. The chain translation becomes slower as the crystal thickness along the chain direction increases during drawing. Once the rate is too slow, the sample will not be drawable any more and the maximum draw ratio is reached. This self-hardening process may affect the maximum draw ratio that can be attained at a given temperature and draw rate.

Another factor that can limit the maximum draw ratio is the molecular weight. As shown in the context of Fig. 4.3, at a molecular draw ratio > 50, chains of MW ~ 10^5 become fully extended and the modulus cannot increase further. Additional strain only involves sliding of chains past each other and eventually leads to ductile failure.

4.4.8 Isotactic Polypropylene vs. Syndiotactic Polypropylene

The difference in the ultradrawability of isotactic and syndiotactic polypropylene[20,33] provides an excellent example for the relations between microscopic structure, mesoscopic dynamics, and macroscopic properties. The slightly higher heat of fusion and melting temperature of iPP indicate that the interchain interactions of iPP are slightly stronger than, or at least similar to, those of sPP. Therefore, differences in these

interactions cannot at all explain the observed ultradrawability of iPP and poor drawability of sPP. The presence or absence of the α_c-relaxation, however, can be attributed to the structure of the repeat unit, which in sPP is twice as long as in iPP,[88] making a displacement of the chain by one repeat unit correspondingly more difficult. Syi and Mansfield have theoretically predicted a high activation energy of 210 kJ/mol for sPP. In summary, in iPP and sPP the microscopic structure of the repeat unit determines the presence or absence of the α_c-relaxation chain dynamics, which in turn dictates the presence or absence of macroscopic ultradrawability.

4.4.9 Role of Entanglements

The α_c-mobility stressed in this paper is one necessary condition for good drawability. The other, which has long been recognized[18,19,41-43], is a sufficiently low entanglement density. Melt-crystallized ultra-high-molecular weight polymers, even if in principle α_c-mobile, can only be drawn to a natural draw ratio of 3 to 5. When the same polymers are processed out of sufficiently dilute solution,[6] or from reactor powder that was never melted,[96] they strain-harden only very slowly and can be drawn to draw ratios > 50. This is a practical proof of the importance of entanglements, even though a direct characterization of the entanglement density has remained mostly elusive.

At the same time, it should be noted that polymers of medium molecular weight, even when melt-crystallized, can be drawn or extruded to draw ratios > 20 at temperatures where the chains are highly α_c-mobile. Examples include industrial grades

of POM,[14] PEO,[105] and iP4MP.[27] However, the moduli of the medium-moleeular-weight materials and maximum aehievable draw ratios are inferior to those of the ultra-high molceular weight fibers, due to extensive stretching of the chains (sce Fig. 4.3, pg. 75) and subsequent slip. As a result, the high-moleeular-weight systems have gained more industrial importance, in spite of the more eomplicated proccssing that they require.

4.4.10 Effeet of Side Branches

For polyethylene, materials with varying concentrations of short side branches, typieally 1 to 6 earbons long, are available. Materials with 2.8 mol % or more C_6H_{13}-braneh es have been shown to exhibit poor drawability, even though a meehanical α_c-relaxation is observed.[111] From the chain-diffusion standpoint, it is clear that the side braneh es inhibit the long-range displaeements through the crystallites that are rcquired for the ultradrawing proeess. Ohta et al.[115,116] observed that a small number of CH_3 side groups in UHMWPE greatly redueed both the creep rate and the maximum draw ratio. This indicates that even these relatively small side groups hinder the chain translation through the crystallites.

Thus, the effects of side branches and chain entanglements underline that thc presence of an α_c-relaxation is not a suffieient eondition for ultradrawability; however, it is a neeessary condition, aeeording to all the available data.

4.5 Critical Discussion of Other Explanations of Ultradrawability

The explanation of polymer ultradrawability and solid-state extrudability in terms of the chain translation of the α_c-relaxation should be discussed in light of several classical models of drawability: (I) Melting and recrystallization.[38,39] (II) Sliding of microfibrils past each other in stage (iii) of drawing.[37,118] (III) Direct chain pull-out, often assumed more or less implicitly.[58] (IV) Deformation-induced crystal-to-crystal transformation.[45] (V) Slip on crystal planes. [46,47,90-92] Of these, only model (IV) makes an attempt to explain or predict which polymers are drawable and which are not. Models I - V were motivated by important insights concerning the ultradrawing process. We will address these in the following and discuss further below how the thermally activated α_c-mobility of chains in the crystallites can account - at least qualitatively - for most of these observations.

Other mechanisms of deformation, such as stack rotation, sliding of lamellae, and twinning, [35] are relevant in stages (i) and (ii) of deformation, but not during ultradrawing. Unfortunately, the necessary distinction of the different stages of drawing has often been lacking in the literature.

(I) Melting and Recrystallization. The local melting and recrystallization hypothesis[39] was proposed, based on chain-topological arguments, to explain the drawability of polymers in general, without specific regard to ultradrawability. It states that due to the complex interconnections of different crystallites by many chains,

deformation of the phase structure is possible only if the crystallites are destroyed and reformed at some point. While there is evidence for[57,97,98] and against[35,99,119] decrystallization or melting during necking, indications of melting and recrystallization during ultradrawing are absent. According to Sadler and Barham[57], neutron scattering shows no indications of melting during the deformation of the already formed fibrillar structure (stage (iii) of drawing).

Secondly, there is no obvious reason why melting should not occur equally well in polymers which are not ultradrawable. In particular, the comparison of poorly drawable sPP[20,33] or iPB1[22] with ultradrawable iPP[11] or iP4MP[27] shows the shortcomings of the melting hypothesis. sPP and iPB1 should melt, and according to the melting hypothesis also be ultradrawable, more easily than iPP or iP4MP, which have higher melting points. That sPP and iPB1 are not ultradrawable or solid-state extrudable demonstrates the inability of the melting hypothesis to account for the experimental data.

The dependence of drawability on the draw rate is also telling: Melting should occur more easily at high draw rates, where the heat produced by the drawing process has less time to dissipate. In fact, however, the highest draw ratios are achieved at low draw rates.[6] The mechanism of longitudinal chain motion with an intrinsic rate provides a natural explanation for this observation.

Experiments on nylon 6[28] and sPP[20] indicate that local melting and recrystallization may occur when drawing is performed very close to the melting temperature. However, for significantly crystalline materials these processes result in

poorer drawability, i.e. lower moduli and smaller maximum tensile draw ratios, near the melting point.[20,28]

In some sense, on a very local scale, the α_c-relaxation does bear some similarity to melting and recrystallization, since the translational mobility moves individual segments from the crystalline into the amorphous phase and vice versa. However, the process is not possible in all polymers below T_m; in crystal-fixed systems, the activation energy for the sliding of the chains is too high.

(II) Sliding of Microfibrils. Mechanism (II) was proposed by Peterlin for stage (iii) of drawing: "longitudinal sliding of microfibrils past each other" was described as the main process in the plastic deformation of the fiber structure[35,37]. Drawing of sPP and other crystal-fixed polymers suggests that such a process may occur for draw ratios < 14[20,32,107]. However, this large-scale model does not provide the required relation between chemical structure and polymer ultradrawability to much higher draw ratios. Again, the comparison of poorly drawable sPP or iPB1 and ultradrawable iPP or iP4MP is instructive. For these four similar polymers, the friction forces between microfibrils should be quite similar. In fact, sPP has been shown to be prone to large-scale defects in its crystallites[120]; nevertheless, its microfibrils cannot slide well enough to produce draw ratios > 14. Similarly, branched polyethylenes are not ultradrawable, even though their crystallites are thinner and should slide more easily than those of unbranched

polyethylene, which is ultradrawable.[111] Thus, the model of microfibril sliding does not account for the experimental ultradrawability data.

It should be mentioned that in a brief description of hot drawing, Peterlin did suggest "increased mobility in the amorphous and crystalline regions", without further discussing in which polymers these does or does not occur.[35] Interestingly, in the explanation of necking, stage (ii), the same paper also suggests a "highly mobilised and aligned pseudomelt",[35] while in fact the main necking process is athermal and occurs even in the absence of an α_c-relaxation,[98,107] which only seems to reduce the yield stress[6]. This example shows that one must guard against identifying all suggestions of high chain mobility with the α_c-relaxation.

(III) Chain or Loop Pull-Out. The examples of sPP, PET, iPB1, and other crystal-fixed polymers prove that in the absence of α_c-mobility, pulling a chain through or out of a crystallite is not sufficiently facile to permit ultradrawing. For iPP, PEO, and many other helical polymers, this process can be compared to trying to pull a screw straight out of its hole, which has a prohibitively high activation energy. Only for PE with its compact all-trans chain, such a direct pull-out process may be conceivable. Even in this case, a high energy of 270 kJ/mol is required for pulling a chain out of the crystal, according to a calculation by Kausch and Langbein.[121] In α_c-mobile polymers, the necessary sliding of the chains occurs by thermal activation of helical jumps or related

motions along a path of lower activation energy that involves chain rotation, and is biased by the applied stress, reminiscent of Eyring's model[43,113,114] for cold flow of glasses.

The distinction between pulling chains through crystallites and biased helical jumps is real and testable. Straight pulling would not produce the rotation that can be observed in the helical jumps by NMR (see Section 4.2). This criterion could be useful in the analysis of chain translations found in computer simulations of the drawing process.

The comparison of iPP and sPP, which have similar intermolecular interactions, indicates that the α_c-relaxation is not just a reflection of the intermolecular forces that counteract chain puli-out. Rather, the ease with which the chain can achieve re-integration into the crystal lattice after a displacement also plays a significant role (see Section 4.2). Chain pull-out is also a crucial element of Takayanagi's tie-molecule model[58], which, however, fails to account for the differences in the forces needed to pull chains out of the crystallites.

Pull-out of two connected adjacent crystalline stems linked by a loop is a related process that appears attractive when considering how drawing affects the path of the chains[37]. Again, the poor drawability of the crystal-fixed polymers shows that such loop pull-out does not occur easily enough to permit ultradrawing.

(IV) Crystal-to-Crystal Transformations occur in many polymers.[45] In some cases, for instance orthorhombic/monoclinic PE or the α/β forms of iPP, the different modifications exhibit different packing modes of the chains without changing the helical

structure. In other cases, the chain structure is also modified, for instance in the different phases of PTFE or the various forms of iPB1. In a few systems such as PTFE, t-PBD, or liquid-crystalline polymers, an order—dynamic-disorder phase transition is known to be related to the crystalline α-relaxation and thus to drawability. On the other hand, several polymers do not exhibit good drawability even though they can occur in different modifications or even undergo crystal-to-crystal transformations.[122] Examples include iPB1 [22] with its several crystalline modifications but poor drawability and extrudability, sPP with its forms I-III [20], some nylons which undergo crystal—crystal transitions (α → γ) but draw poorly[28,29,107] as well as PBT which under stress changes from the α- to the β-modification[123]. In addition, there are drawable and α_c-mobile polymers such as poly(vinyl alcohol) for which no crystal-to-crystal transformations have been reported. Thus, it seems that crystal-to-crystal transformations have a relation to drawability only when they involve a transition into a dynamically disordered phase.

(V) Slip on Crystal Planes. In non-polymeric crystals, deformation under a shear force occurs by collective translation of large sections of the crystal, which involves sliding along certain crystal planes. This process is facilitated by the motion of dislocations.[89] Several research groups have interpreted the deformation of PE (in stages (ii)[91] and (iii)[46] of drawing) as such a sliding on crystal planes parallel to the [001] chain direction.[47,92] This process has been termed "chain slip". However, it must be noted

that such a collective motion of many chains is distinct from the thermally activated chain diffusion of individual chains that is characteristic of the α_c-relaxation. On the other hand, the overall effect of the individual chains moving, thermally activated, along their axes in the shear field can be similar to the collective sliding. Thus, the chain-diffusion process resulting from chain rotation-translation as described in this work, while distinct from crystal-plane chain slip of refs.[46,91], should be able to account for most of the reported observations.

For helical polymers such as POM and PEO, the repeat unit along the chain direction is more than 1.5 nm long. Thus, straight complete slip of adjacent crystal planes would require a prohibitively large displacement. At the same time, the rotation that circumvents this barrier in the helical jumps of individual chains would be required of all helices on one side of the slide plane. Such a speculative major reorganization of the crystals of POM and PEO is harder to conceive than the experimentally documented motion of individual chains. Partial fine slip[47], which avoids the large displacement, would lead to disorder in the crystals.

Straight translation on crystal planes may be relevant in PE in stages (i) and (ii) of drawing. In stage (iii), the agreement of the activation energy of the extensional viscosity with that of α_c-relaxation 180°-flip motion strongly suggests that in PE, the individual-chain motion is responsible for ultradeformation. In addition, the lack of ultradrawability in sPP and iPB1 (form I) shows that the sliding on crystal planes is not efficient enough to permit ultradrawing, even in polymers with weak intermolecular interactions.

Concluding Remarks and Outlook. In summary, there is excellent evidence that the thermally activated chain translation through the crystallites in the α_c-relaxation is the fundamental microscopic process that permits solid-state drawability and extrudability of semicrystalline polymers. The commonly found vague allusions to molecular dynamics during ultradeformation are now made specific based on the independent experimental characterization of the microscopic chain motions by NMR. The absence of such motions in many polymers, even in some with weak intermolecular forces, is recognized as an insurmountable barrier to ultradeformation.

The α_c-mobility combines, in a specific way, the crucial features of the other models discussed above: (I) As realized by Yoon and Flory,[39] the deformation process must be independent of the details of the reentry pattern of chain folds; this was their argument against crystal-plane sliding and prompted them to support the melting hypothesis. The α_c-dynamics, with its independent motion of chains, fulfills the requirement. (II & V) The α_c-mobile chains slide along the c-direction, which will account for many features attributed to microfibril sliding or chain slip. (III) By the bias imposed on the thermally mobile chains, these are effectively pulled through the crystal. (IV) Solid-solid transitions are in some systems associated with the α_c-mobility.

However, where the models differ, α_c-mobility provides the more consistent and comprehensive description of the ultradeformation process. In particular, it explains why certain polymers can or cannot be extruded or drawn to high draw ratios. On this basis,

from NMR mobility measurements or simply from dieleetric and dynamic-mechanieal relaxation data, ultradrawability, or its impossibility, can be predicted.

It is expected that the presence or absence of the α_c-relaxation will also affeet other deformation properties of semicrystalline polymers, as studied, for instance, for polyethylene, an α_c-mobile polymer, by Ward and his eoworkers[114,124]. However, sinee other proeesses sueh as deformation of the amorphous regions or erystalline lamellae also play a role here,[35] comparative studies of α_c-mobile and erystal-fixed polymers are needed.

4.6 Summary

The ultradrawability of semierystalline polymers has been shown to depend crueially on the —now experimentally well-eharacterized — large-amplitude ehain motions in the erystallites that are assoeiated with the α_c-relaxation. Semierystalline polymers lacking an α_c-relaxation are fixed by the erystallites and eannot be drawn to draw ratios in exeess of 14. Helieal jumps and related large-amplitude motions involving ehain rotation and translation, as proved by NMR in several important α_c-mobile polymers, provide a clear meehanism for the major rearrangement of ehains that is required for achieving large draw ratios. Rather than pulling ehains through the erystallites direetly, the meehanical stress biases the thermally aetivated jumps of the chains in the erystallites. This explains the erueial role of temperature and draw/extrusion rates. Loeal melting and straight ehain pull-out are seen to play no role in ultradrawing.

Considerations of both α_c-mobility and chain entanglements allow for the first time to explain and predict which polymers are highly drawable under what conditions.

4.7 References

(1) Statton, W. O. *J. Appl. Phys.* **1967**, *38*, 4149-4151.

(2) Ishikawa, K.; Miyasaka, K.; Maeda, M. *Rept. Progr. Polym. Phys. Japan* **1968**, *11*, 185.

(3) Capaccio, G.; Ward, I. M. *Nature Phys. Sci.* **1973**, *243*, 143.

(4) Smith, P.; Lemstra, P. J. *J. Mater. Sci.* **1980**, *15*, 505-514.

(5) Zwijnenburg, A.; Pennings, A. J. *J. Polym. Sci., Polym. Lett. Ed.* **1976**, *14*, 339-346.

(6) Kanamoto, T.; Tsuruta, A.; Tanaka, K.; Takeda, M.; Porter, R. S. *Macromolecules* **1988**, *21*, 470-477.

(7) Noether, H. D.; Singleton, R. W., U.S. Patent 3,161,709 (Dec. 15, 1964).

(8) Sheehan, W. C.; Cole, T. B. *J. Appl. Polym. Sci.* **1964**, *8*, 2359.

(9) Desper, C. R. *J. Macromol. Sci., Phys. Ed.* **1973**, *B7*, 105.

(10) Cansfield, D. L. M.; Capaccio, G.; Ward, I. M. *Polym. Eng. Sci.* **1976**, *16*, 721.

(11) Taylor, W. N.; Clark, E. S. *Polym. Eng. Sci.* **1978**, *18*, 518-526.

(12) Peguy, A.; Manley, R. S. J. *Polym. Commun.* **1984**, *25*, 39-42.

(13) Kanamoto, T.; Tsuruta, A.; Tanaka, K.; Takeda, M. *Polym. J.* **1984**, *16*, 75-79.

(14) Clark, E. S.; Scott, L. S. *Polym. Eng. Sci.* **1974**, *14*, 682-686.

(15) Brew, B.; Ward, I. M. *Polymer* **1978**, *19*, 1338.

(16) Hope, P. S.; Richardson, A.; Ward, I. M. *J. Appl. Polym. Sci.* **1981**, *26*, 2879-2896.

(17) Uehara, H.; Jounai, K.; Endo, R.; Okuyama, H.; Kanamoto, T.; Porter, R. S. *Polym. J.* **1997**, *29*, 198-200.

(18) Porter, R. S.; Wang, L.-H. *J. Macromol. Sci.-Rev. Macromol. Chem. Phys., C* **1995**, *35*, 63-115.

(19) Lemstra, P. J.; Kirschbaum, R.; Ohta, T.; Yasuda, H. In *Developments in Oriented Polymers-2*, Ward, I. M., Ed.; Elsevier Applied Science: London and New York, 1987, pp 39-77.

(20) Uehara, H.; Yamazaki, Y.; Kanamoto, T. *Polymer* **1996**, *37*, 57-64.

(21) Huang, B.; Ito, M.; Kanamoto, T. *Polymer* **1994**, *35*, 1329-1331.

(22) Ball, R.; Porter, R. S. *J. Polym. Sci.: Polym. Lett. Ed.* **1977**, *15*, 519-526.

(23) Richardson, A.; Ward, I. M. *Polym. Commun.* **1987**, *28*, 272-275.

(24) Schellekens, R.; Bastiaansen, C. *J. Appl. Polym. Sci.* **1991**, *43*, 2311-2315.

(25) van Aerle, N. A. J. M.; Lemstra, P. J.; Kanamoto, T.; Bastiaansen, C. W. M. *Polymer* **1991**, *32*, 34-38.

(26) Humphreys, J.; Ward, I. M.; Nix, E. L.; Mcgrath, J. C.; Emi, T. *J. Appl. Polym. Sci.* **1985**, *30*, 4069-4079.

(27) He, T.; Porter, R. S. *Polymer* **1987**, *28*, 946-950.

(28) Ito, M.; Morishita, Y.; Mizuochi, K.; Kanamoto, T. *J. Macromol. Sci. -Phys.* **1997**, *B36*, 367-380.

(29) Postema, A. R.; Smith, P.; English, A. D. *Polym. Commun.* **1990**, *31*, 444-447.

(30) Gogolewski, S.; Pennings, A. J. *Polymer* **1985**, *26*, 1394-1400.

(31) Kanamoto, T.; Zachariades, A. E.; Porter, R. S. *J. Polym. Sci., Polym. Phys. Ed.* **1982**, *20*, 1485-1496.

(32) Ito, M.; Takahashi, K.; Kanamoto, T. *J. Appl. Polym. Sci.* **1990**, *40*, 1257-1263.

(33) Sakata, Y.; Unwin, A. P.; Ward, I. M. *J. Mater. Sci.* **1995**, *30*, 5841-5849.

(34) Weynant, E.; Haudin, J. M.; G'Sell, C. *J. Mater. Sci.* **1980**, *15*, 2677-2692.

(35) Peterlin, A. *J. Mater. Sci.* **1971**, *6*, 490-508.

(36) Balta-Calleja, F. J.; Peterlin, A. *J. Macromol. Sci.-Phys.* **1970**, *B4*, 519-540.

(37) Peterlin, A. *Coll. Polym. Sci.* **1987**, *265*, 357-382.

(38) Wu, W.; Wignall, G. D.; Mandelkern, L. *Polymer* **1992**, *33*, 4137-4140.

(39) Flory, P. J.; Yoon, D. Y. *Nature* **1978**, *272*, 226-229.

(40) Smith, P.; Lemstra, P. J.; Pijpers, J. P. L.; Kiel, A. M. *Coll. Polym. Sci.* **1981**, *259*, 1070-1080.

(41) Ohta, T. *Polym. Eng. Sci.* **1983**, *23*, 697-703.

(42) Strobl, G. *The Physics of Polymers*; Springer-Verlag: Berlin Heidelberg, 1996.

(43) Ward, I. M.; Hadley, D. W. *An introduction to the mechanical properties of solid polymers*; John Wiley & Sons: West Sussex, 1993.

(44) Termonia, Y. *Macromolecules* **1996**, *29*, 4891-4894.

(45) Saraf, R. F.; Porter, R. S. *J. Polym. Sci.: Part B: Polym. Phys.* **1988**, *26*, 1049-1057.

(46) Gerrits, N. S. J. A.; Young, R. J. *J. Mater. Sci.* **1991**, *26*, 2137-2142.

(47) Lin, L.; Argon, A. S. *J. Mater. Sci.* **1994**, *29*, 294-323.

(48) Young, R. J. *Polymer* **1975**, *16*, 450-458.

(49) Aharoni, S. M.; Sibilia, J. P. *Polym. Eng. Sci.* **1979**, *19*, 450-455.

(50) Aharoni, S. M.; Sibilia, J. P. *J. Appl. Polym. Sci.* **1979**, *23*, 133-140.

(51) Bigg, D. M. *Polym. Eng. Sci.* **1988**, *28*, 830-841.

(52) Gedde, U. W. *Polymer Physics*; Chapman & Hall: London, 1995.

(53) Garrett, P. D.; Grubb, D. T. *J. Polym. Sci.: Polym. Phys.* **1988**, *26*, 2509-2523.

(54) Govaert, L. E.; Lemstra, P. J. *Coll. Poly. Sci.* **1992**, *270*, 455-464.

(55) Ward, I. M. *Plastics, Rubber and Composites Processing and Applications* **1993**, *19*, 7-13.

(56) Boyd, R. H. *Polymer* **1985**, *26*, 323,1123.

(57) Sadler, D. M.; Barham, P. J. *Polymer* **1990**, *31*, 36, 43, 46.

(58) Takayanagi, M.; Nitta, K.-H. *Macromol. Theory Simul.* **1997**, *6*, 181-195.

(59) Plummer, C. J. G.; Cudre-Mauroux, N.; Kausch, H.-H. *Polym. Eng. Sci.* **1994**, *34*, 318-329.

(60) Ginzburg, B. M.; Tuichiev, S. *J. Macromol. Sci.-Phys.* **1992**, *B31*, 291-317.

(61) McCrum, N. G.; Read, B. E.; Williams, G. *Anelastic and Dielectric Effects in Polymeric Solids*; Dover Publications, Inc.: New York, 1991.

(62) Schmidt-Rohr, K.; Spiess, H. W. *Multidimensional Solid-State NMR and Polymers*; Academic Press: London, 1994.

(63) Olf, H. G.; Peterlin, A. *J. Polym. Sci. Part A-2* **1970**, *8*, 753.

(64) Hentschel, D.; Sillescu, H.; Spiess, H. W. *Polymer* **1984**, *25*, 1078-1086.

(65) McCall, D. W.; Douglass, D. C. *Appl. Phys. Lett.* **1965**, *7*, 12-14.

(66) McCall, D. W. *Accounts Chem. Res.* **1971**, *4*, 223-232.

(67) Kentgens, A. P. M.; de Boer, E.; Veeman, W. S. *J. Chem. Phys.* **1987**, *87*, 6859-6866.

(68) Hagemeyer, A.; Schmidt-Rohr, K.; Spiess, H. W. *Adv. Magn. Reson.* **1989**, *13*, 85-130.

(69) Schmidt-Rohr, K.; Spiess, H. W. *Macromolecules* **1991**, *24*, 5288-5293.

(70) Klein, P. G.; Robertson, M. B.; Driver, M. A. N.; Ward, I. M.; Packer, K. J. *Polym. Int'l* **1998**, *47*, 76-83.

(71) Robertson, M. B.; Ward, I. M.; Klein, P. G.; Packer, K. J. *Macromolecules* **1997**, *30*, 6893-6898.

(72) Schaefer, D.; Spiess, H. W.; Suter, U. W.; Fleming, W. W. *Macromolecules* **1990**, *23*, 3431-3439.

(73) Johansson, A.; Tegenfeldt, J. *Macromolecules* **1992**, *25*, 4712-4715.

(74) Reneker, D. H. *J. Polym. Sci.* **1962**, *59*, S39-S42.

(75) Mansfield, M.; Boyd, R. H. *J. Polym. Sci.: Polym. Phys. Ed.* **1978**, *16*, 1227-1252.

(76) Hoffman, J. D.; Williams, G.; Passaglia, E. *J. Polym. Sci.: Part C* **1966**, *14*, 173-235.

(77) Hu, W.-G.; Boeffel, C.; Schmidt-Rohr, K. *Macromolecules* **1999**, *32*, 1611-1619.

(78) Axelson, D. E.; Mandelkern, L.; Popli, R.; Mathieu, P. *J. Polym. Sci.: Polym. Phys. Ed.* **1983**, *21*, 2319-2335.

(79) Vega, A. J.; English, A. D. *Macromolecules* **1980**, *13*, 1635-1647.

(80) Kimmig, M.; Strobl, G.; Stuhn, B. *Macromolecules* **1994**, *27*, 2481-2495.

(81) Hirschinger, J.; Schaefer, D.; Spiess, H. W.; Lovinger, A. J. *Macromolecules* **1991**, *24*, 2428-2433.

(82) Grobelny, J.; Tekely, P.; Turska, E. *Polymer* **1981**, *22*, 1649-1654.

(83) Thomsen, T.; Zachmann, H. G.; Korte, S. *Macromolecules* **1992**, *25*, 6934-6937.

(84) Iwayanagi, S.; Miura, I. *Rep. Progr. Polym. Phys. Japan* **1965**, *8*, 303.

(85) Schilling, F. C.; Gomez, M. A.; Tonelli, A. E.; Bovey, F. A.; Woodward, A. E. *Macromolecules* **1987**, *20*, 2954-2957.

(86) Lyerla, J. R.; Economy, J.; Maresch, G. G.; Muhlebach, A.; Yannoni, C. S.; Fyfe, C. A. In *Liquid-Crystalline Polymers*, Weiss, R. A.; Ober, C. K., Ed.; American Chemical Society, 1990; Vol. 435, pp 359-368.

(87) Wunderlich, B. In *Integration of Fundamental Polymer Science and Technology-2*, Lemstra, P. J.; Kleintjens, L. A., Ed.; Elsevier Applied Science, 1987, pp 329-333.

(88) Syi, J.-L.; Mansfield, M. L. *Polymer* **1988**, *29*, 987-997.

(89) Shadrake, L. G.; Guiu, F. *Philosophical Magazine* **1976**, *34*, 565-581.

(90) Kiho, H.; Peterlin, A.; Geil, P. H. *Polym. Lett.* **1965**, *3*, 257-262.

(91) Young, R. J.; Bowden, P. B.; Ritchie, J. M.; Rider, J. G. *J. Mater. Sci.* **1973**, *8*, 23-26.

(92) Ohde, Y.; Miyaji, H.; Asai, K. *Jap. J. Appl. Phys.* **1971**, *10*, 178.

(93) Rault, J. *J. Polym. Sci.: Rev. Macromol. Chem. Phys.* **1997**, *C37*, 335-387.

(94) Burmester, A. F.; Dreyfuss, P.; Geil, P.; Keller, A. *J. Polym. Sci.: Polym. Lett. Ed.* **1972**, *10*, 769-775.

(95) Hirschinger, J.; Miura, H.; Gardner, K. H.; English, A. D. *Macromolecules* **1990**, *23*, 2153-2169.

(96) Kanamoto, T.; Ohama, T.; Tanaka, K.; Takeda, M.; Porter, R. S. *Polymer* **1987**, *28*, 1517-1520.

(97) Adams, W. W.; Yang, D.; Thomas, E. L. *J. Mater. Sci.* **1986**, *21*, 2239-2253.

(98) Petermann, J.; Kluge, W.; Gleiter, H. *J. Polym. Sci.: Polym. Phys. Ed.* **1979**, *17*, 1043-1051.

(99) Chuah, H. H.; Lin, J. S.; Porter, R. S. *Macromolecules* **1986**, *19*, 2732-2736.

(100) van Aerle, N. A. J. M.; Braam, A. W. M. *J. Mater. Sci.* **1988**, *23*, 4429.

(101) Kanamoto, T.; Porter, R. S. *J. Polym. Sci.: Polym. Lett. Ed.* **1983**, *21*, 1005-1010.

(102) Smith, P.; Lemstra, P. J.; Booij, H. C. *J. Polym. Sci., Polym. Phys. Ed.* **1981**, *19*, 877-888.

(103) Furuhata, K.; Yokokawa, T.; Seoul, C.; Miyasaka, K. *J. Polym. Sci.: Polym. Phys. Ed.* **1986**, *24*, 59-67.

(104) Brady, J. M.; Thomas, E. L. *Polymer* **1989**, *30*, 1615-1622.

(105) Kim, B. S.; Porter, R. S. *Macromolecules* **1985**, *18*, 1214-1217.

(106) Mitchell, D. J.; Porter, R. S. *Macromolecules* **1985**, *18*, 1218-1221.

(107) Owen, A. J. In *Developments in Oriented Polymers-2*, Ward, I. M., Ed.; Elsevier Applied Science: London and New York, 1987, pp 237-268.

(108) Davis, G. W.; Talbot, J. R. In *Encyclopedia of Polymer Science and Engineering*, Mark, H. F.; Bikales, N. M.; Overberger, C. G.; Menges, G., Ed.; John Wiley & Sons, 1988; Vol. 12, pp 151.

(109) Klement, J. J.; Geil, P. H. *J. Macromol. Sci.-Phys.* **1972**, *B6*, 31-56.

(110) Appelt, B.; Porter, R. S. *J. Appl. Polym. Sci.* **1981**, *26*, 2841-2851.

(111) Bensason, S.; Minick, J.; Moet, A.; Chum, S.; Hiltner, A.; Baer, E. *J. Polym. Sci.: Part B: Polym. Phys.* **1996**, *34*, 1301-1315.

(112) Mead, W. T.; Porter, R. S. *J. Polym. Sci.: Polym. Symp.* **1978**, *63*, 289-312.

(113) Eyring, H. *J. Chem. Phys.* **1936**, *4*, 283-291.

(114) Truss, R. W.; Clarke, P. L.; Duckett, R. A.; Ward, I. M. *J. Polym. Sci.: Polym. Phys. Ed.* **1984**, *22*, 191-209.

(115) Ohta, Y.; Yasuda, H. *J. Polym. Sci.: Part B: Polym. Phys.* **1994**, *32*, 2241-2249.

(116) Ohta, Y.; Sugiyama, H.; Yasuda, H. *J. Polym. Sci.: Part B: Polym. Phys.* **1994**, *32*, 261-269.

(117) Ward, I. M.; Wilding, M. A. *J. Polym. Sci.: Polym. Sci. Ed.* **1984**, *22*, 561-575.

(118) Peterlin, A. *J. Polym. Sci.:Part C* **1966**, *15*, 427-443.

(119) Attenburrow, G. E.; Bassett, D. C. *J. Mater. Sci.* **1977**, *12*, 192-200.

(120) Lovinger, A. J.; Lotz, B.; Davis, D. D.; Schumacher, M. *Macromolecules* **1994**, *27*, 6603-6611.

(121) Kausch, H. H.; Langbein, D. *J. Polym. Sci., Polym. Phys. Ed.* **1973**, *11*, 1201.

(122) Gohil, R. M.; Miles, M. J.; Petermann, J. *J. Macromol. Sci.-Phys.* **1982**, *B21*, 189-201.

(123) Jakeways, R.; Ward, I. M.; Wilding, M. A.; Hall, I. H.; Desborough, I. J.; Pass, M. G. *J. Polym. Sci., Polym. Phys. Ed.* **1975**, *13*, 799.

(124) Wilding, M. A.; Ward, I. M. *Polymer* **1981**, *22*, 870-876.

(125) Khanna, Y. P.; Sibilia, J. P.; Chandrasekaran, S. *Macromol.* **1986**, *19*, 2426-2431.

(126) Yamane, A.; Sawai, D.; Kameda, T.; Kanamoto, T.; Ito, M.; Porter, R. S. *Macromolecules* **1997**, *30*, 4170-4178.

(127) Beckham, H. W.; Schmidr-Rohr, K.; Spiess, H. W., unpublished result.

CHAPTER 5

MORPHOLOGY OF ULTRADRAWN POLYETHYLENE FIBERS

5.1 Introduetion

Ultradrawn, ultraoriented polyethylene fibers (UDF-PE)[1,2] are extremely strong yet lightweight and are used, for instanee, in bullet-proof vests. They can be produeed by gel spinning,[3] or solid-state extrusion and tensile drawing[4-6] of ultra-high moleeular weight polyethylene (UHMWPE). Investigation of the morphology is of both fundamental and praetieal signifieanee, providing an exeellent example of a unique mieroseopie strueture that produees outstanding maeroseopie properties.

The morphology of UDF-PE has been studied by various teehniques. However, even for the erystallinity, the results are not eonsistent. Transmission eleetron mieroseopy (TEM) elearly indieates that lamellar struetures are present at small draw ratios but are absent at large draw ratios (> 80).[7] Gauehe bands in the infrared (IR) speetrum and the peak in small-angle X-ray seattering (SAXS) disappear at draw ratios of > 80.[8] The density[9] and heat content of the amorphous eomponent of the fiber ean be different from the bulk material beeause the ehain mobility in the amorphous regions may be different. As a result, erystallinity measurements by IR and SAXS are problematie, and those by differential seanning calorimetry (DSC) and density method have to be used with eaution.[8] Crystallinity determination by wide-angle X-ray seattering (WAXS) is also diffieult due to the high orientation of the fibers. Traditional ^{13}C direet polarization

nuclear magnetic resonance (NMR) cannot give good crystallinity results since the crystalline ^{13}C T_1 relaxation time is extremely long and the amorphous band is broad and low. In Table 5.1 the problems of various methods to determine crystallinity in the fibers are summarized. We will present an approach to make this NMR technique applicable under these difficult circumstances and will compare the results with the crystallinity estimated based on the ^{1}H wideline shape, as well as the results obtained by other techniques in the literature.

Techniques	Problems
WAXS	Does not work well for highly oriented material
SAXS	No peak corresponding to crystalline region
Density	Amorphous region morphology is different from bulk PE case; possible presence of microvoids
DSC	Heat content of both crystalline and amorphous components are different from those in bulk PE
^{13}C NMR	too much measurement time required
IR	No gauche bands observed at high draw ratio

Table 5.1 Problems of various traditional methods to determine the crystallinity in ultradrawn, highly crystalline PE fibers.

Various structural models have been proposed to interpret the unusual morphology and the extraordinary mechanical properties of the fibers.[2,10-15] One of the contentious points is how the amorphous phase is distributed in the fiber. In the "continuous crystal" model, [2,11] the amorphous segments are dispersed defects within the crystalline phase. This would lead to a structure very different from that of bulk HDPE material, where amorphous segments are aggregated and form extensive layers. To

elarify this issue, it is neeessary to determine the sizes of, and mobilities in, the erystalline and amorphous regions in the fibers. In the following, the domain sizes will be determined by ^{1}H spin diffusion and mobilities by ^{1}H and ^{13}C NMR speetra. Based on the NMR data and a eomparison with other experimental faets, a struetural model of UDF-PE will be proposed.

There are several other important morphologieal features of the fibers whieh have not been charaeterized eonelusively. For example, based on NMR experiments, it has been elaimed that a large (>25%) mobile but oriented interphase component is present in the fibers.[16] Also, it is not elear if there are any trapped entanglements (rigid gauehe eonformers) within the erystallites of ultradrawn PE. Finally, strong small angle X-ray seattering (SAXS) equatorial intensity (perpendieular to the fiber axis) in fibers with high draw ratio has been observed[5,17] and assigned to voids.[17] We will address these issues in this paper.

In addition to the intermediately mobile amorphous regions, a highly mobile fraetion in drawn polyethylenes has been deteeted by ^{1}H wideline NMR.[18,19] But sueh a eomponent was not observed in extruded PE by Porter and eoworkers.[20] We will confirm the presenee of a highly mobile phase in the drawn UDF-PE, whieh does not exist either in the extruded preeursor material or after the fibers have been melted and re-erystallized. The size, ehemieal eomposition and physieal origin of the highly mobile eomponent will be diseussed.

5.2 Experimental

A sample of ultradrawn UHMWPE fibers (cross section 0.1 mm × 1.8 mm, referred to as UDF-PE in the following) was kindly provided by the late Prof. R. S. Porter. The molecular weight (viscosity average) is about 3×10^6. To produce the fibers, films of compacted Himont Hifax 1900 reactor powder were solid-state extruded at 110°C to a draw ratio of 5, followed by tensile drawing at 135°C. The final draw ratio achieved is 82-85, with tensile moduli of up to 130 GPa. No isotopic labeling was used. A commercial gel-spun UHMWPE fiber Spectra® 900 (gel-spun UDF-PE) was also studied for comparison.

The following samples were used in the various NMR experiments: (1) UDF-PE, placed in a 7-mm rotor for the MAS experiments, with the fiber axes along the rotor axis. (2) A uniaxially oriented UDF-PE sample for static NMR experiments: The fibers were aligned parallel to each other and wrapped with Teflon® tape. Two sections of 6-mm length were cut out and aligned parallel to each other in the NMR radio-frequency coil of 8-mm diameter. (3) Extruded UHMWPE (precursor of UDF-PE fiber) with extrusion ratio of 5 (E-PE). The dimensions of the sample are 5 mm × 6 mm × 15 mm. (4) A bulk UHMWPE sample which was prepared by melting the UDF-PE fibers and cooling them in air (UDF-PE_{melted}). (5) Randomly oriented gel-spun UDF-PE fibers in a 7-mm rotor.

The dimensional density of UDF-PE and E-PE was determined by measuring the mass and the dimensions of the materials. The dimensions of E-PE were taken directly

by a caliper. The width and length of UDF-PE were measured directly and the thickness was calculated by stacking many layers of the tapes together and measuring the total thickness. The dimensional density measured this way is (1.00±0.03) g/cm^3 for E-PE, and (0.85±0.03) g/cm^3 for UDF-PE, which agrees with the reduced dimensional density measured in highly drawn HDPE by Ward et al.[21]

The NMR experiments were performed on Bruker MSL 300 and DSX 300 spectrometers (B_0= 7 T). Several different NMR pulse sequences were used in this study, as shown in Fig. 5.1: (1) Direct polarization (DP). ^{13}C magnetization is exited by a single 90° pulse, see Fig. 5.1(a). (2) A CP (cross polarization)/^{13}C T_1 ($T_{1,C}$) filter experiment[22], see Fig. 5.1(b). The $T_{1,C}$ filter is created by storing the ^{13}C magnetization alternatively along the ±z direction after CP. The ^{13}C magnetization with shorter T_1 will survive the filter to a lesser extent. (3) Goldman-Shen experiment with ^{1}H detection using a dephasing time of 100 μs, see Fig. 5.1(c). The highly mobile phase was selected. (4) Goldman-Shen experiment with ^{13}C detection, see Fig. 5.1(d). The cross polarization time was 1 ms. The dephasing time was 29.3 μs so that after the dephasing the crystalline signal vanishes but most of the amorphous signal is retained. In all experiments, the ^{1}H 90°-pulse lengths were 4.0 μs and the decoupling power was 80 kHz. The chemical shift calibration is based on a crystalline PE chemical shift of 32.8 ppm. One 90° pulse was used to obtain the ^{1}H signals, with a short dead-time delay of 3 μs before detection. The recycle delays used in the CP and proton experiments were 10 s. With such a recycle

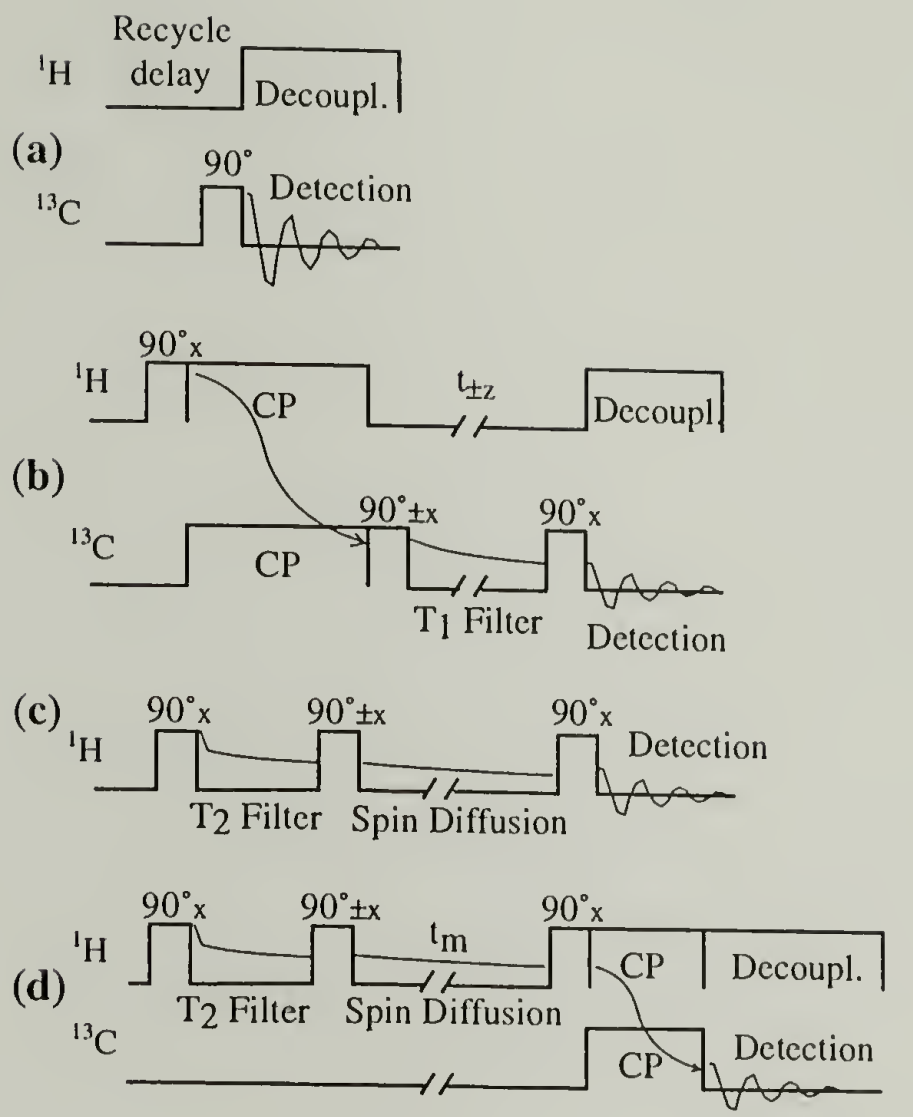

Fig. 5.1: Solid-state NMR pulse sequences used in Chapter 5. Except for minor modifications, they have been described in the literature. (a) Direct-polarization (DP) ^{13}C NMR experiment. (b) CP/$T_{1,C}$ experiment. Cross-polarization excites rigid regions efficiently. A +z/-z phase cycle in alternate scans is introduced so that the final ($t_{\pm z}$ -> ∞) signal is zero. (c) ^{1}H spin diffusion Goldman-Shen experiment (without sample rotation). (d) ^{1}H spin diffusion Goldman-Shen experiment with ^{13}C detection under magic-angle spinning.

delay, the ^{1}H lineshape is the same as with an infinitely long recycle delay since during this period spin diffusion is efficient enough to equilibrate the magnetization.

5.3 Results

5.3.1 Crystallinity Measurement

In the DP/MAS spectrum the amorphous and crystalline peaks appear at 31.3 and 32.8 ppm, respectively, as seen in Figures 5.2(a) and (b). In order to calculate the crystallinity from the spectra, two problems have to be overcome: (1) Full relaxation of both components is required, but in UDF-PE the crystalline regions have an extremely long ^{13}C T_1 (~ 5000 s), see Discussion. In addition, the amorphous component makes up only a small portion of the fibers. Therefore, the measurement time necessary to acquire a fully relaxed ^{13}C spectrum with good amorphous signal is intolerable (>10 days). (2) Crystalline and amorphous signals partially overlap.

The problems can be solved by a combination of four ^{13}C NMR experiments: (1) A DP experiment with a relatively short recycle delay and a large number of scans to measure the amorphous signal with good sensitivity. (2) A DP experiment with a long recycle delay and a small number of scans to measure the almost fully relaxed crystal signal. (3) A CP/$T_{1,C}$ filter experiment (Figure 5.1) with the $T_{1,C}$-filter length equal to the recycle delay in experiment (2) to determine the correction factor for incomplete relaxation of the crystal signal. (4) An experiment to determine the pure amorphous signal line shape.

Since the amorphous regions have a short $T_{1,C}$, in experiment (1) we can observe the fully relaxed amorphous signal. To avoid the heteronuclear Overhauser enhancement of the ^{13}C signal, the recycle delay must be much longer than $T_{1,H}$. Recycle delays of 20 s and 50 s were used, giving very similar amorphous signal heights per scan, see Fig. 5.2(a) and (b). However, in this spectrum the crystalline signal is incompletely relaxed. In experiment (2) where the recycle delay was long (10,000 s), a sufficiently strong crystalline signal is obtained but the amorphous signal is poor because of the low crystallinity and the small number of scans, see Fig. 5.2(c) and (d). So by combining two experiments (1) and (2), the relative intensity of the signals of the crystalline and amorphous regions can be obtained.

To determine the correction factor for incomplete relaxation after a recycle delay t_{RD} = 10,000 s, we performed the CP/$T_{1,C}$ filter experiment (3). Due to the phase cycling that stores the magnetization along +z and -z in alternate scans, the total intensity decays towards zero as a function of the $T_{1,C}$ filter time. The decay constant is the same as that in the signal increasing from zero towards the full equilibrium magnetization in the direct polarization experiment. The data in Figure 5.3 (a) and (b) show that at ambient temperature, the signal at t_{fil} =10,000 s decays to 10 % of the original signal, which was obtained with a short filter time of 1 s. This means that in the DP experiment with a recycle delay of 10,000 s the crystalline signal shows 90% of the fully relaxed intensity.

To separate out the amorphous component in the partially crystalline signal, we obtained pure amorphous line shapes in two different ways using (i) a DP/MAS experiment with very short recycle delay (1 s), and (ii) CP/$T_{2,H}$ filter experiment, where a

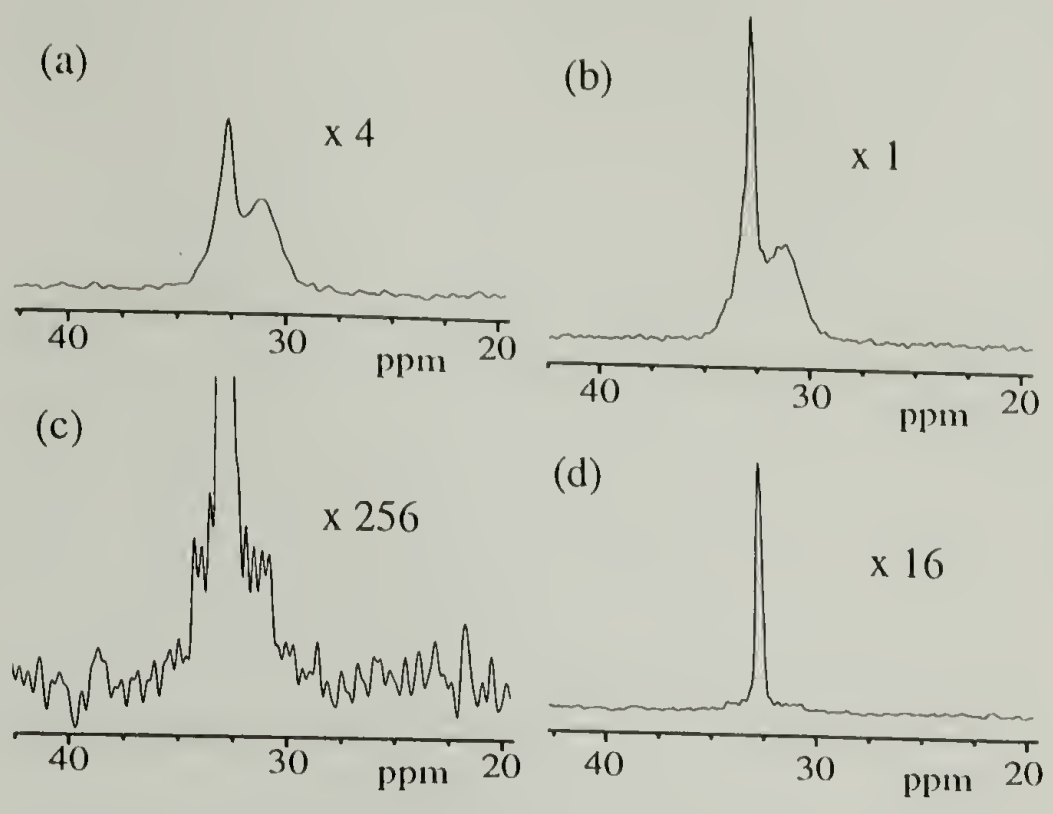

Fig. 5.2: ^{13}C direct-polarization spectra of UDF-PE demonstrating the procedure for crystallinity measurement. The spectra in (a) - (c) are rescaled to compensate for the different numbers of scans. (a) Recycle delay of 20 seconds, 512 scans. (b) Recycle delay of 50 seconds, 2048 scans. (c) Recycle delay of 10,000 seconds, 8 scans. (d) Same as (c), but scaled by 1/16 to show the crystalline peak fully. The small signal to the left of the peak of the predominant orthorhombic crystallites is due to the monoclinic crystal modification.

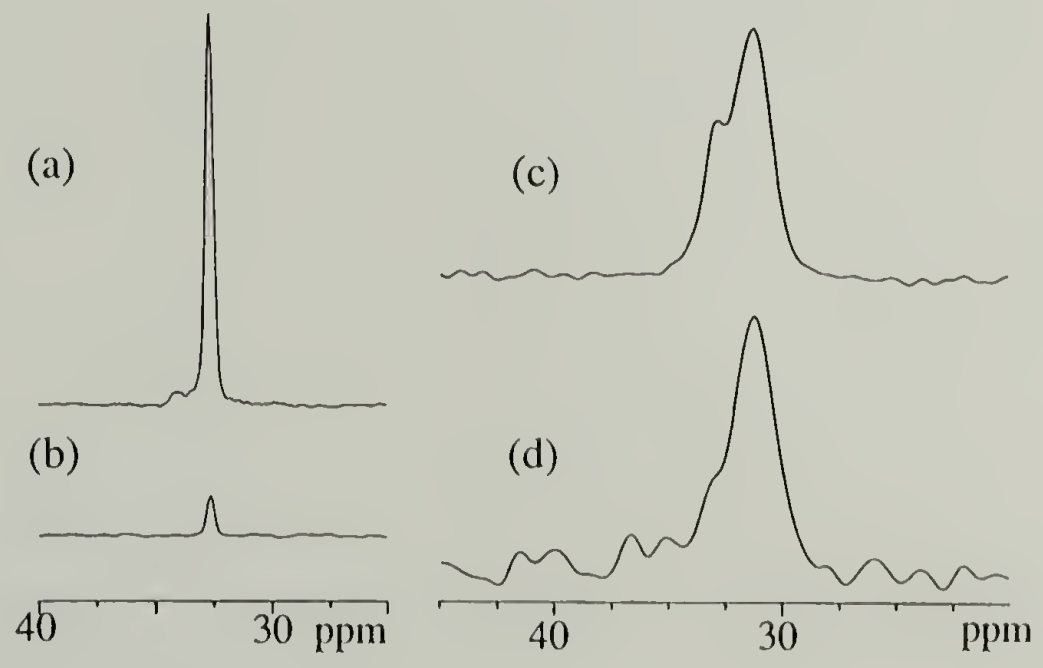

Fig. 5.3: $CP/T_{1,C}$ filter spectra and pure amorphous line shapes of UDF-PE. (a) and (b): $CP/T_{1,C}$ filter spectra of UDF-PE with filter length of (a) 1 s and (b) 10,000 s. (c) and (d): Pure amorphous line shapes of UDF-PE obtained by (c) DP (recycle delay = 1 s) and (d) CP/T_2 filter (filter time =16 ms).

free ^1H evolution (16 μs) before CP is applied and the crystalline-phase magnetization is destroyed as a result of the strong ^1H-^1H dipolar couplings. The spectra are shown in Fig. 5.3(c) and (d). The area/height ratios for the two line shapes are equal within an error margin of 3%.

With the information obtained in the above experiments, the crystallinity can be calculated from the following formula:

$$f_{crystal} = \frac{A_c^{\infty}/NS_c}{\frac{A_c^{\infty}}{NS_c} + \frac{A_{ac}}{NS_{ac}}} = \frac{1}{1 + \frac{NS_c}{NS_{ac}}\frac{A_{ac}}{A_c^{\infty}}} \qquad (5.1)$$

where A_c^{∞} is the area of the completely relaxed crystalline magnetization after NS_c scans, and A_{ac} is the fully relaxed amorphous component after a recycle delay of 20 or 50 s, with NS_{ac} scans.

The CP/T_1 correction leads to:

$$A_c^{\infty} = A_c/(1 - \frac{I_{cpfil}}{I_{cp}}) \qquad (5.2)$$

where A_c is the area of crystalline signal at long recycle time (10,000 s), I_{cpfil} and I_{cp} are crystalline signal height in CP spectra with long (10,000 s) and short (1 s) $T_{1,C}$ filter, respectively.

From simple peak-shape considerations,

$$\frac{A_{ac}}{A_a} = \frac{I_{ac}}{I_a} \qquad (5.3)$$

with the area A_a and height I_a of the pure amorphous line shape spectrum.

Thus, we obtain

$$f_{Crystal} = \frac{1}{1 + \frac{NS_c}{NS_{ac}} \frac{A_a}{A_c} \frac{I_{ac}}{I_a} (1 - \frac{I_{cpfil}}{I_{cp}})} \qquad (5.4)$$

The ratio of the numbers of scans, NS_c/NS_{ac}, is exactly known. Thus, the crucial factor is the ratio of the pure amorphous and crystalline peak areas, each of which is available with good signal-to-noise ratio. The signal heights I_a and I_{ac} can be read off with high precision. Note that $(1-I_{cpfil}/I_{cp})$ is a minor correction factor that deviates from unity typically by less than 10%.

The crystallinity result obtained based on Eq. (5.4) is (87.5±1)%. Taking into account possible uncertainties from spectrometer instability which may lead to signal amplitude fluctuation, the crystallinity from our method is (88±2)%. This value agrees with the ~ 90% crystallinity reported in the literature[5,8] based on density measurements for similar fibers with a draw ratio of ~ 100. It is higher than the simple DSC crystallinity of ~ 80% obtained for similar fibers.[8] Considering the uncertainties of the DSC method mentioned in the Introduction, we believe that our result is more reliable.

^{1}H spectra are often useful to obtain mobility information in materials. Fig. 5.4 (pg. 117) shows the ^{1}H spectra of three samples: the extruded precursor (E-PE), the drawn fibers(UDF-PE), and the fiber material after melting (UDF-PE_{melted}). The chain axes of the first two samples were aligned along the magnetic field while the last sample is isotropic. In all the three spectra broad and narrow components are observed, associated with relatively rigid crystalline and mobile amorphous regions, respectively. The linewidth of the amorphous signal is narrower (i.e., the ^{1}H T_2 is longer) because the

mobility of the segments in the amorphous regions partially averages out the strong ^{1}H-^{1}H dipolar couplings. Based on the linewidth difference, the crystallinity of the fibers can be estimated from the ^{1}H spectrum. In Fig. 5.4(b), the crystalline and amorphous signals are quite clearly distinguished. In a wideline-separation experiment,[23] the ^{1}H lineshape of the crystalline regions was determined. The crystallinity from the area ratio is (88±2)%, which agrees very well with the ^{13}C NMR result. The ^{1}H result may be complicated by dead time and finite pulse-length problems; therefore, ^{13}C NMR is a more accurate way to determine the crystallinity in these materials.

5.3.2 A Second, Highly Mobile Amorphous Phase in the Fibers

In Fig. 5.4, the ^{1}H spectra of E-PE and UDF-PE$_{melted}$ show the typical two-phase feature of PE materials: a broad crystalline part and a narrower amorphous part. However, in the UDF-PE spectrum, besides these two phases, there is an additional sharper component with much higher mobility, as indicated by a ^{1}H line width of (1.8±0.2) kHz. This highly mobile phase makes up (0.8±0.2)% of the total sample.

The ^{1}H chemical shift of the component is (1.5±0.1) ppm, which is the typical methylene proton value. To examine if it is a small-molecule impurity, a DP/MAS ^{13}C spectrum was measured with short recycle delay of 1 s, which is long enough for the $T_{1,C}$ relaxation of the highly mobile components, see Fig. 5.5. From the chemical shift values, the small peaks at 14 and 23 ppm can be assigned to end groups (CH_3) and next-to-end CH_2 units. With the reasonable approximation that all the peaks in the spectrum are relaxed to the same extent and have a similar nuclear Overhauser enhancement, each small

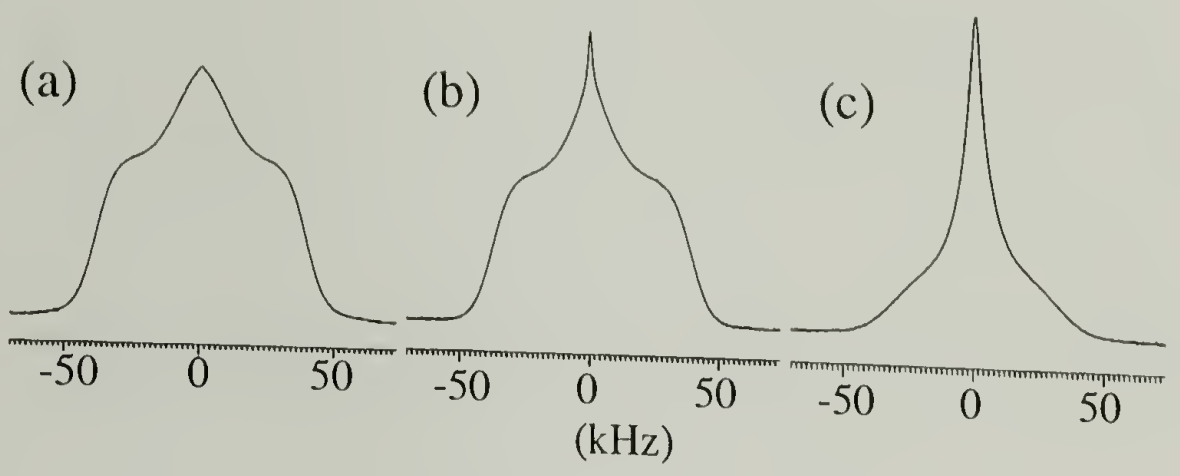

Fig. 5.4: ^{1}H wideline spectra of UHMWPE. (a) Extruded precursor, draw ratio $\lambda = 5$ (E-PE); (b) Ultradrawn fiber, draw ratio $\lambda = 82\text{-}85$ (UDF-PE). (c) Fiber material after melting and recrystallization ($UDF\text{-}PE_{melted}$). The ultradrawn fiber shows a narrow (i.e. highly mobile) component that is absent in the other spectra.

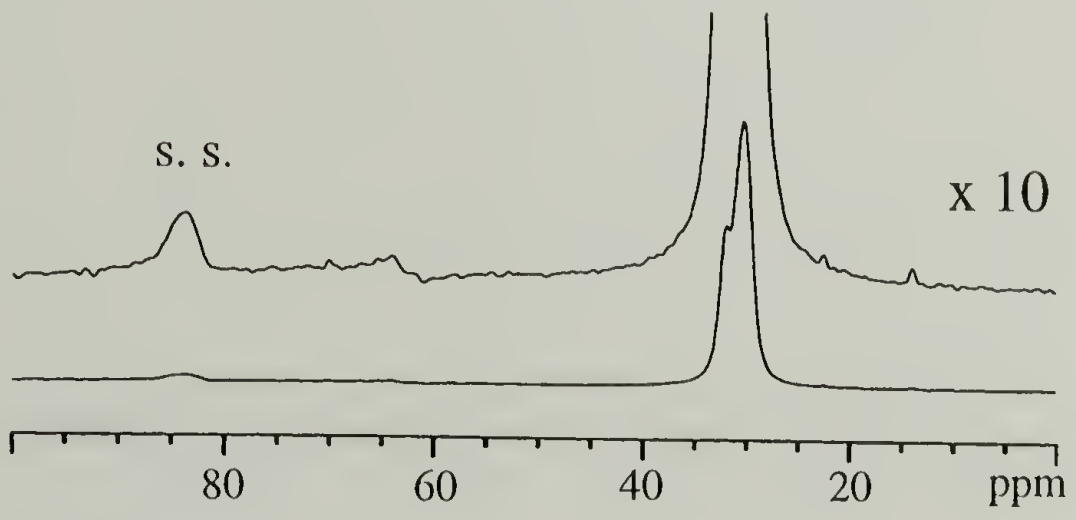

Fig. 5.5: ^{13}C direct polarization spectra of UDF-PE to detect impurities. The signal at 84 ppm is a spinning sideband (indicated by s.s.) of the major CH_2 peak. The dispersive signal at 63 ppm is background from outside the sample.

peak makes up 0.01% of the total ^{13}C signal (including crystalline). Assuming that the end groups are methyl groups and the chains are relatively free of long branches, these concentrations agree with those expected for end groups of polymers with a number-average molecular weight of ~300,000. If the highly mobile chains were short-chain paraffins, the end-group signal would be much higher. Therefore, the major component of the highly mobile phase must be polyethylene chains. A similar narrow ^{1}H signal was also found in the gel-spun Spectra® 900 fibers (gel-spun UDF-PE), with a similar concentration. Another mobile component which is separate from the highly mobile CH_2 units was found in this gel-spun material, with ^{13}C and ^{1}H chemical shifts of 4.0 and 71 ppm, respectively. It is assigned to ethylene oxide oligomers used as an additive to assist the gel-spinning process. Considering the different processing involved in the production of the two kinds of fibers, the presence of the highly mobile phase seems to be a universal feature of ultradrawn PE fibers.

Among the three spectral components, the narrow line of the highly mobile phase is least sensitive to dead time problems and other spectrometer limitations, and the isolated sharp line observed after ^{1}H T_2 selection (see Figure 5.6, pg. 120) confirms its presence unequivocally. As regards the quantification, even if the area of the rigid components were underrepresented by 20% in Fig. 5.4, the fraction of highly mobile CH_2 groups would be reduced by only 0.2%, to 0.6%.

There is further strong evidence that this component is not a small-molecule impurity: i) GPC of the fiber material shows no small MW products.[24] ii) The UDF-PE fibers were produced by solid-state deformation, so no solvent was introduced; no other

additives were put into the material either. iii) The component is found neither in the precursor (E-PE) nor after recrystallization (UDF-PE_{melted}). A similar sharp component was also observed by other groups and ourselves in HDPE[18,19] that had been highly drawn without any use of additives (see Section 5.4.4).

To show that the small sharp signal indeed is due to very highly mobile segments and not just the narrowest part of the general amorphous signal, we selected it by a ^1H T_2 filter. By a very long $T_{2,H}$ filter time of 100 μs, the magnetization in both crystalline and normal amorphous regions were destroyed by dephasing and only that in the highly mobile phase survived, see Fig. 5.6 (a), which was taken with a negligible spin diffusion time of 0.5 ms. This means that the highly mobile component has a much longer $T_{2,H}$ than the normal amorphous phase and the former is not a part of the latter, but a distinct phase. By contrast, in a $T_{2,H}$ dephasing experiment of UDF-PE_{melted}, all of the amorphous signal was uniformly suppressed by the filter. It was impossible to separate a component with longer $T_{2,H}$. This shows that the highly mobile component has vanished after melting and recrystallization.

A Goldman-Shen ^1H spin diffusion experiment was performed to obtain the information about the size of the highly mobile phase. First, a $T_{2,H}$ filter of 100 μs was applied to select the magnetization in the highly mobile phase while the magnetization in the crystalline and normal amorphous regions was destroyed by dephasing. Then the magnetization was flipped back to the z-direction and ^1H spin diffusion proceeded. Very little diffusion from the highly mobile phase to the other two phases was observed even

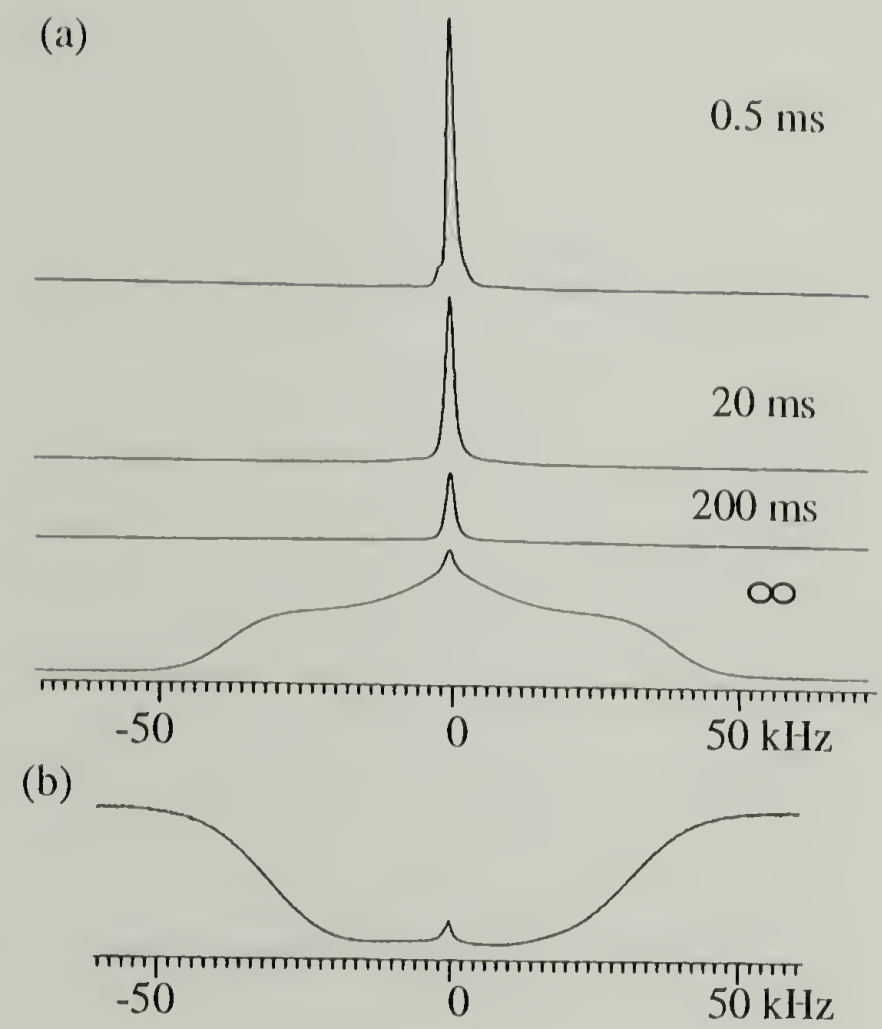

Fig. 5.6: ^{1}H spin diffusion and inversion recovery spectrum of UDF-PE. (a) ^{1}H spin diffusion of UDF-PE from the highly mobile amorphous phase, after a T_2 filter of 100 μs duration with mixing times as indicated. At the bottom, the unfiltered spectrum (corresponding to infinite diffusion time) is shown for reference. Equilibrium is not achieved even after 200 μs of spin diffusion. (b) ^{1}H inversion recovery spectrum of UDF-PE, with a recovery time of 500 ms. The short $T_{1,H}$ and distinct nature of the highly mobile phase are apparent in its faster inversion recovery behavior.

after 200 ms of spin diffusion (Fig. 5.6(a)). Equilibrium was not achieved at very long diffusion time (>1 s) even if accelerated by the $T_{1,H}$ relaxation. In comparison, spin diffusion from >5-nm thick rubbery domains[25,26] or from 3-nm thick water layers between lipid bilayers[27] with even narrower protons lines proceeds much faster. Based on these references, the diameter of the highly mobile domains is estimated very conservatively as > 3 nm. In fact, as discussed below, it is well possible that the highly mobile components do not form compact domains, but loose loops and isolated chains in voids of > 100 nm diameter. Inversion recovery, Fig. 5.6(b), shows that $T_{1,H}$ of the highly mobile component is less than 0.5 s, which is much shorter than for the other protons (> 2 s for both amorphous and crystalline protons). This is further proof that the spin diffusion between the highly mobile components and the other regions is very slow.

5.3.3 Sizes of Crystalline and Amorphous Regions

The crystalline and amorphous domain sizes can be characterized by ^1H spin diffusion.[28,29] The ^1H magnetization in the amorphous regions can be selected based on the longer ^1H T_2, and diffusion into the crystallites can be observed. A Goldman-Shen experiment with ^{13}C detection was performed to determine the domain sizes in the UDF-PE. The dephasing time was chosen so that the crystalline magnetization was exactly zero while the major part of the amorphous region magnetization was preserved. Equilibrium of magnetization across the two phases appears to be reached after 100 ms (Figure 5.7).

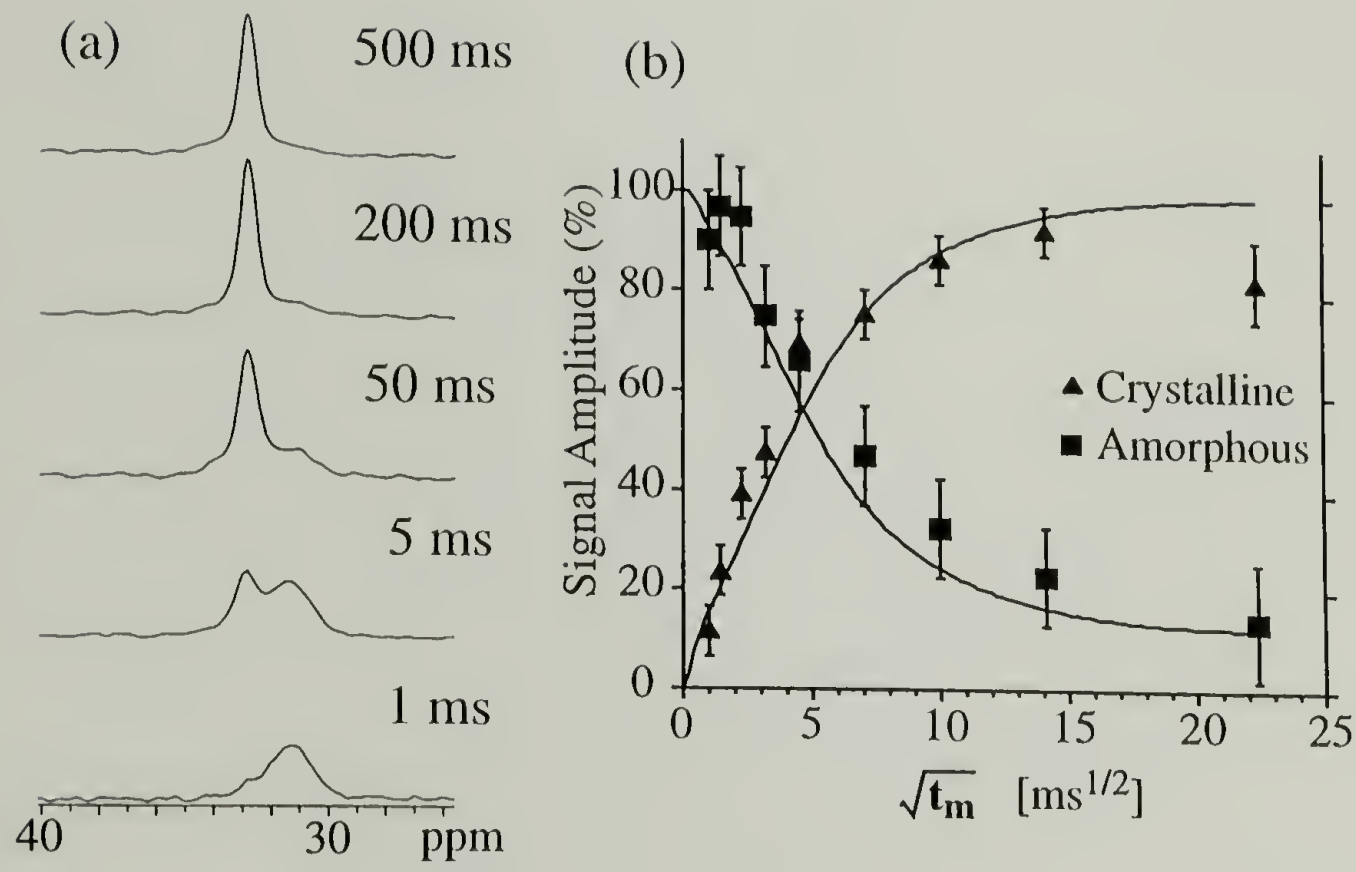

Fig. 5.7: ^{13}C-detected ^{1}H spin diffusion from amorphous to crystalline regions. (a) Series of spectra with diffusion times of 1 ms to 500 ms as indicated. (b) Spin-diffusion plot of crystalline and amorphous signal intensities with fits. For fit parameters see text.

While the final value in the increasing crystalline-phase magnetization may be vaguely defined, the amorphous-phase magnetization will decrease to an asymptotic value of 1 - f_c, where f_c is the crystallinity. The data show that this final value is nearly reached within the accessible mixing times.

A simulation based on a 1-D spin diffusion model was performed (see Fig. 5.7). The input information was: a crystallinity of 88% and lamellar morphology; spin diffusion coefficients in crystalline and amorphous regions of 0.8 and 0.15 nm^2/ms, respectively. The data were corrected for T_1 relaxation to first order[28,29], but otherwise T_1 relaxation was not taken into account in the simulation. The best fit corresponds to an amorphous region size of 5.5 nm and crystallite diameter of 50 nm. These values should be understood as the smallest diameter rather than the average size of the domains. The true smallest thickness of the domains will be larger, since the fibers do not have a lamellar morphology. The simulation was based on a simple diffusion model appropriate for a lamellar morphology, where only one dimension (perpendicular to the lamellae) is relevant for the diffusion process. If more dimensions participate in the spin diffusion, e.g. two for cylindrical or three for spherical domains, the smallest domain size found from the initial slope in the spin diffusion plot increases proportional to this dimensionality.[30] Given that the amorphous regions are more likely to be dispersed in the crystalline matrix, a dimensionality of two is a reasonable estimate. The smallest diameter of the amorphous regions is thus estimated as 10 ± 5 nm, and the crystallite diameter as 100 ± 50 nm, with

large error bars to account for the uncertainties in the shape and diffusion coefficient of the amorphous regions.

5.3.4 Search for Immobile Defects

In some models of the ultradrawn fibers, gauche conformers are considered to be embedded in the crystalline phase.[11] Based on the γ-gauche effect, ^{13}C NMR can distinguish between segments in all-trans conformation, which appear at > 32.5 ppm, and in gauche-containing environments, with chemical shifts < 32.5 ppm. Whereas the domain size of the amorphous phase detected above has shown that the majority of the gauche conformers form distinct amorphous regions instead of being dispersed in the crystalline phase, it is still interesting to investigate whether there are any dispersed "locked in" gauche defects. Rigid gauche segments would not undergo fast large amplitude motions (including trans-gauche or gauche$^+$/gauche$^-$ isomerizations); therefore, these segments should have a $T_{1,C}$ relaxation time comparable to that of the crystalline components. Since the rigid gauche segments should have both a long $T_{1,C}$ relaxation time and a high CP efficiency (comparable to that of the crystalline regions), a comparison of a simple CP and a CP/$T_{1,C}$ filter experiment can give information about the possible existence of these immobile defects. The spectra are shown in Fig. 5.8 (pg. 129). In Fig. 5.8(b), the signals at 34 and 32.8 ppm are from the monoclinic[31,32] and the orthorhombic crystalline phase, respectively, with an area ratio of 1:23. The shoulder on the up-field side of the 32.8 ppm signal is from gauche-containing segments. In Fig. 5.8(a),

the filter length was 10 s so that the mobile-amorphous components were screened out but the contribution of the rigid gauche segments would remain ($T_{1,C} \geq 10$ s). They would appear at the up-field side of the crystalline signal. In the spectrum of Fig. 5.8(a), no such gauche signal with long $T_{1,C}$ was found, which suggests that the rigid gauche component makes up less than 1% of the total rigid population.

5.4 Discussion

5.4.1 Sizes of Crystalline and Amorphous Regions

At room temperature, the UDF-PE fiber has a long-time $T_{1,C}$ of 5,000 s. The $T_{1,C}$ of crystalline PE has been studied with various samples and it was found that it depends mainly on the crystallite thickness.[33] If we assume that this conclusion can be extended to ultradrawn fibers, the $T_{1,C}$ of 5,000 s corresponds to a crystal thickness of ~ 60 nm in UDF-PE.[33] This is in agreement with the result obtained by our spin diffusion experiment.

According to the domain size obtained from spin diffusion and the mobility of the amorphous regions reflected in the ^1H line shape, the amorphous regions are neither large separate pockets outside of huge continuous crystals, nor very small defects embedded in them. The size of the amorphous regions more likely resembles that in bulk HDPE.

Knowing the domain sizes, we are able to interpret the ^1H T_1 relaxation behavior. In the UDF-PE studied here, $T_{1,H}$ is about 3.2 s at room temperature, which is at least twice as long as in melt-crystallized high density polyethylenes. It increases slightly with

temperature, to ~ 4.5 s at 360 K. Since the intrinsic $T_{1,H}$ in the crystalline regions expected on the basis of the ^{13}C T_1 is much longer, the measured $T_{1,H}$ values must reflect ^1H spin diffusion from the amorphous regions, where $T_{1,H}$ relaxation is relatively fast. Due to the high crystallinity, it takes the small amorphous fraction a longer time to relax the magnetization in the crystallites than it does in HDPE. The increase of $T_{1,H}$ in the crystallites with temperature reflects the increase of $T_{1,H}$ in the amorphous regions, which are in the fast-motion limit. There are two facts indicating that spin-diffusion is not the rate-limiting step: First, the Goldman-Shen experiment shows that equilibrium can be reached in 0.1 s, which is much shorter than $T_{1,H}$. Secondly, $T_{1,H}$ is mono-exponential to a good approximation.

In the absence of spin diffusion, the equation for $T_{1,H}$ relaxation can be written as

$$\frac{\Delta M_a^{T_1}}{\Delta t} = -\frac{1}{T_{1a}}(M_a^{T_1} - M_a^{\infty}) \qquad (5.5)$$

where M_a^{T1} is the magnetization in the amorphous regions if there is no spin diffusion, T_{1a} is intrinsic relaxation time of the amorphous regions, and M_a^{∞} is the equilibrium magnetization of the amorphous regions. If spin diffusion is much faster than relaxation, then the increase ΔM_a of the magnetization in the amorphous regions is only a fraction f_a (=1-f_c, where f_c is the crystallinity) of what it would be without spin diffusion:

$$\frac{\Delta M_a}{\Delta t} = \frac{\Delta M_a^{T_1}}{\Delta t}(1 - f_c)$$

Therefore, we have

$$T_1 = \frac{T_{1a}}{1 - f_c} \tag{5.6}$$

Where T_1 is the ^1H relaxation time of the amorphous regions in the presence of fast spin diffusion. It is also the T_1 of the total sample. This suggests that erystallinity ean be estimated from $T_{1,H}$ of the sample. On the other hand, knowing the erystallinity and the T_1 relaxation time of the whole sample, the intrinsie T_1 relaxation time of the amorphous regions ean be obtained. For UDF-PE, with a erystallinity of 88% and T_1 of 3.2 s, T_{1a} is approximately 0.4 s.

Equation (5.6) also suggests that for semierystalline polymer samples of different erystallinity, even if the intrinsie T_1 of the amorphous regions T_{1a} may be similar, the overall $T_{1,H}$ ean be quite different. For example, with the same T_{1a} of 0.4 s, a PE sample with erystallinity of 88% has a $T_{1,H}$ of 3.2 s, while it is only 1.3 s when the erystallinity is 70%.

5.4.2 Mobility of Amorphous Regions

In Fig. 5.4 the ^1H line widths at half height of amorphous PE in E-PE, UDF-PE and UDF-PE_{melted} are (19±1) kHz, (15±1) kHz, and (8±1) kHz, respeetively. For referenee, the amorphous-eomponent linewidth of a eommereial HDPE with 70% erystallinity is (11±1) kHz. This means that there are different mobilities in amorphous regions of various PE materials. Correspondingly, the density of the amorphous regions may be different for different materials, whieh must be taken as a preeaution when using the density method for crystallinity measurements.

5.4.3 A Large Interphase?

Recently, NMR data of ultradrawn PE fibers very similar to the UDF-PE investigated here were interpreted in terms of a 30 % mobile and oriented interfacial fraction which has a ^{13}C T_1 of 1.8 s.[16] Our measurements show that this conclusion is incorrect. In the spectrum shown in Fig. 5.2(a), the interfacial fraction is nearly fully relaxed in the 20 s of recycle delay, yet makes up a much smaller area than the amorphous signal, which corresponds to about 10% of the total material. Actually, the same conclusion can be drawn from the first spectrum (with recycle delay of 10 s) in Fig. 2 of reference 7, which shows that the mobile oriented fraction is comparable to the amorphous fraction. Both observations show that the mobile and oriented interfacial fraction is less than 10%.

It is also important to note that the $T_{1,C}$ relaxation in the crystallites is mostly not due to an intrinsic mechanism but results from chain (or spin) diffusion from the amorphous regions.[34-36] So it has a $\sqrt{t}$ rather than an exponential time dependence. Therefore, the exponential fits to $T_{1,C}$ decay data to extract multiple components lack experimental support.

Still, the fast-relaxing crystalline component can be assigned to the interfacial regions, since the $T_{1,C}$ relaxation is mostly due to chain diffusion from the fast-relaxing amorphous regions.[34-36] ^{13}C direct-polarization spectra after recycle delays of 20 s and 10,000 s, Figures 5.9(a) and (b), show that the fast-relaxing all-trans fraction has a

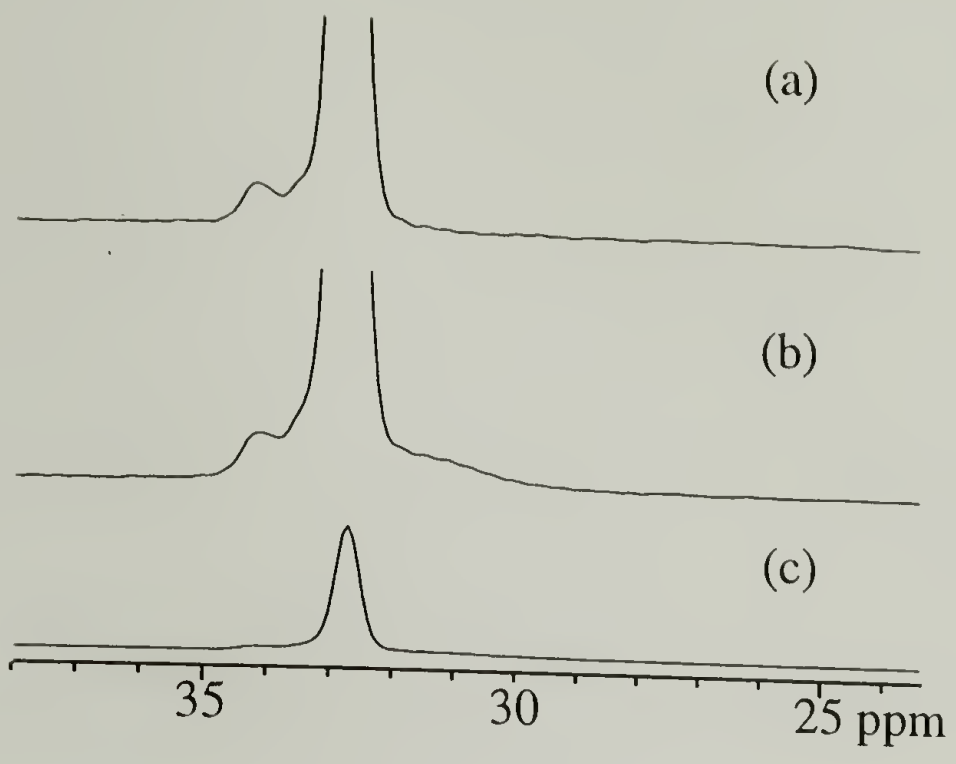

Fig. 5.8: CP and CP/$T_{1,C}$ filtered spectra of UDF-PE. (a) CP/$T_{1,C}$ filtered spectrum, filter length = 10 s selecting relatively immobile segments. No signal is observed in the 25 ~ 30 ppm range (gauche information). The signal at 34 ppm is from the monoclinic modification. (b) Regular CP spectrum for reference. The shoulder at 30 ~ 32 ppm is from the amorphous phase. (c) CP spectrum scaled by 1/10 to show the whole signal.

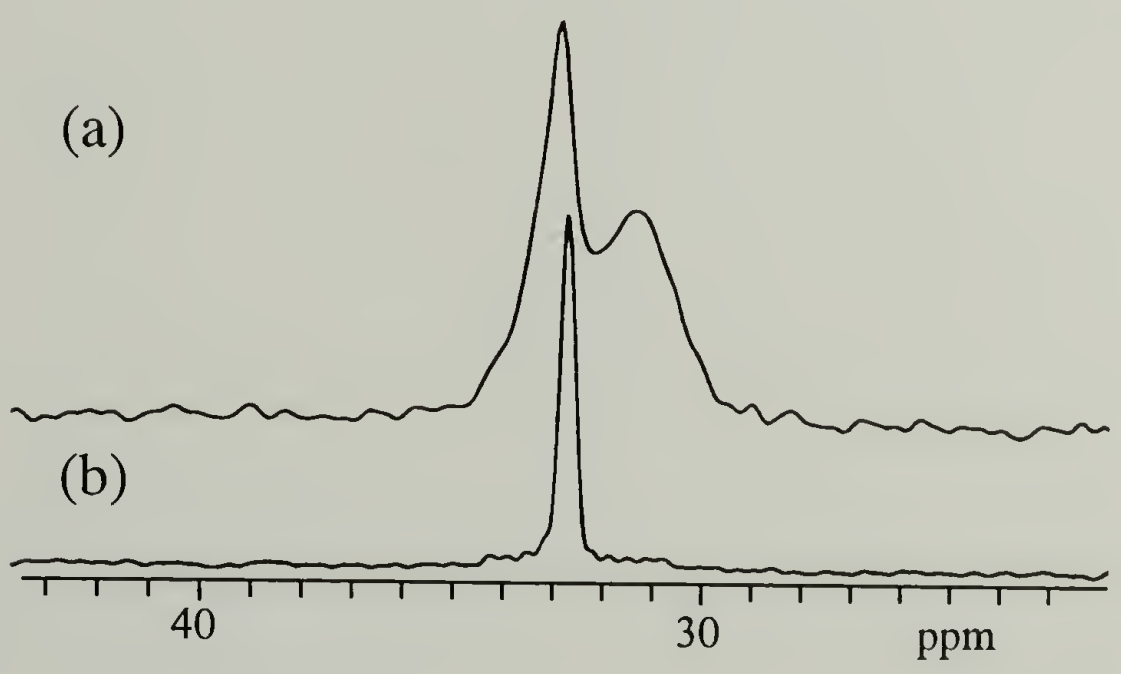

Fig. 5.9: ^{13}C direct-polarization spectra at recycle delays of (a) 20 s and (b) 10,000 s, respectively, taken from Fig. 5.2(a) and (d) to show the lineshape difference of the all-trans signals at different relaxation times.

distinctly larger ^{13}C MAS linewidth. Its full width at half maximum is 70 Hz, compared to 25 Hz for the crystalline core. The increased linewidth indicates that the segments near the interface have some limited mobility and disorder, while their chemical shift shows that they are still mostly all-trans. The all-trans signal after a recycle delay of 50 s (Fig. 5.2b) has a composite line shape which can be decomposed into 70-Hz and 25-Hz components to a good approximation, indicating that a relatively clear boundary exists between the two components. In the total material, the fast relaxing, broadened all-trans component accounts for ~ 5%. In addition to the interface, taut tie molecules[37,38] may also contribute to this signal.

5.4.4 The Highly Mobile Phase

The series of spectra in Fig. 5.4 and Fig. 5.6 clearly show the presence of 0.8% of a highly mobile phase in UDF-PE, apparently induced by tensile drawing. A similar mobile fraction was also observed by other groups and ourselves in drawn high-density polyethylenes ($M_w \sim 10^5$).[18,19] Smith et al.[18] and Kitamaru et al.[19] suggested that it was due to a low-molecular-weight fraction and to the segments which are close to the chain ends, respectively. However, there was no experimental proof for these arguments and it is not clear why these fractions should become observable only upon drawing.

By measuring the mass and dimension of the fibers, Ward et al. obtained a fiber density of ~ 0.8 g/cm^3, while by the floatation method, the density was close to 1.00 g/cm^3.[21] They reasonably attributed this discrepancy to the existence of voids in the

fibers. By SEM, they observed that the voids are long thin cavities between the fibrils, with widths greater than 100 nm.[21] The density of UDF-PE which we determined by measuring the mass and dimensions was (0.85±0.03) g/cm^3, which is close to the result by Ward et al. In contrast, the density of the extruded precursor (E-PE) measured in the same way is (1.00±0.03) g/cm^3. This suggests that the drawing process introduces a considerable volume of voids, while extrusion does not. An interesting fact is that the highly mobile phase was not observed in extruded PE (Fig. 6a, also see ref. [20]). These observations strongly suggest that voids may lead to the highly mobile phase.

A reasonable speculation to explain such a relationship is the following: The segments on the void surface and traversing the voids to connect different crystallites are highly mobile. Due to their mobility and limited contact with the crystallites and regular amorphous regions, spin diffusion from and to the highly mobile segments is slow. Since a material with many voids has a big surface area, the fibers will have a considerable amount of such a mobile component, as observed in the ^{1}H spectra. A rough estimate of the void size from the highly mobile fraction of 0.8 %, the void volume fraction of 20%, and a hypothetical thickness of the mobile surface-layer component of 3 nm yields a diameter of ~ 300 nm, assuming the voids have a cylindrical shape. This is consistent with the widths of the voids observed by SEM.[21]

Pennings and coworkers observed excess SAXS intensity in gel-spun PE fibers and ascribed it to the existence of voids.[17] Assuming that the voids are empty, they calculated a void volume fraction of 1% in hot-drawn gel-spun fibers. The discrepancy

with the void volume fraction of ~ 15% obtained by the density measurements must be due to the fact that only the voids which are small enough (< 100 nm) produce detectable SAXS intensity.

A highly mobile, liquid-like component on the surface of the fibrils will have properties of a lubricant. Indeed, it is well known that ultradrawn PE fibers have a very low friction coefficient and exceptionally good abrasion resistance compared, for instance, to carbon or Kevlar® fibers.[1] We suggest that this could be due to the highly mobile component on the surface of the PE fibrils.

With the above hypothesis, we need to understand why these surface segments should have a higher mobility than their regular amorphous counterparts. Actually, HDPE has an unusually low mobility in the amorphous regions considering its low glass transition temperature (mobility sets in at -130°C or possibly even lower, as indicated by the fact that PE is drawable at 77K [39]). This is probably because the strong crystallization tendency of HDPE chains shortens the amorphous segments connecting the crystallites and thus lowers their mobility. This becomes more obvious if we compare with the amorphous segment mobility in LDPE, which has a ^{1}H width of several kHz, similar to the highly mobile component in the fiber and much narrower than for amorphous HDPE. Therefore, the mobility of the "highly mobile" component is not unusually high, but rather normal.

5.4.5 A Structural Model for Ultradrawn UHMWPE

The tensile modulus of ultradrawn PE fibers which is close to the theoretical value suggests that in the fibers there are continuous crystals along the fiber direction.[2] In fact, long crystalline blocks (~ 3 μm) were found by transmission electron microscopy (TEM).[7] On the other hand, our study shows that the material studied has a considerable amorphous component (~12%) with an average diameter of ~ 10 nm. A study of the same material has shown that the chain undergo 180° flips with rates of 1000/s at 360 K[40]. This mobility strongly suggests that most chains have alternate crystalline and amorphous portions. The fact that in hot drawing, a single molecule is drawn to a ratio significantly smaller than that of the whole material[41] and less than necessary for stretching the chain out completely[6,42] also requires that chains will have many folds which form amorphous regions. The seemingly contradictory observations of continuous crystals and small amorphous domains are accommodated by the following structural model: In every fibril the crystalline phase is continuous but an individual chain is not in a continuous crystal. The amorphous phase is dispersed in the crystal and most of the chains are alternately crystalline and amorphous. This is similar to the picture described in ref. [43] where the high modulus is provided by the continuous crystalline phase, except that in our model there are few if any fully extended crystalline chains. The sizes of amorphous regions are roughly comparable to those in melt-crystallized linear high-density polyethylene. There are voids between the fibrils and the segments on the surfaces are highly mobile. A schematic of this phase structure is shown in Fig. 5.10.

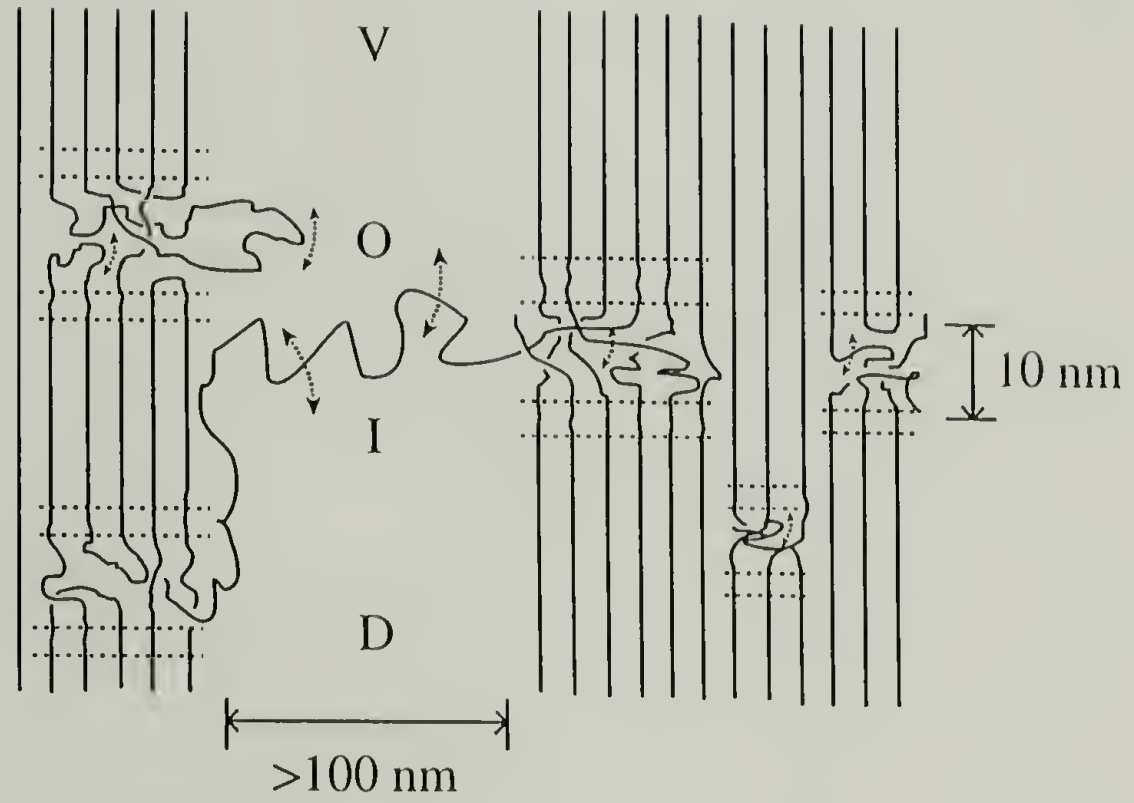

Figure 5.10: Proposed phase structure of ultradrawn UHMWPE fibers, consisting of five components: 80 % orthorhombic crystal, 3 % monoclinic crystal, 5 % crystal-amorphous interface (delineated by dashed lines), 11 % amorphous region, and 0.8 % highly-mobile component. The monoclinic and orthorhombic crystallites are indicated by different spacings. The crystalline phase is continuous but the chains alternately traverse crystalline and amorphous regions. The interfacial segments are all-trans but have partial dynamical disorder. There are voids between the fibrils. The segments on the surface of the voids or traversing them are highly mobile (dashed arrows).

Altogether, five morphological components have been identified: 83% crystal core, of which 80% is orthorhombic and 3% monoclinic, with a thickness of ~100 nm; 5% disordered all-trans interfacial and/or tie molecules; 11% mobile amorphous regions, with diameters of ~ 10 nm; and 1% highly mobile segments, probably at void surfaces or traversing voids.

5.5 Summary

The structure of ultradrawn ultra-high molecular weight polyethylene fibers has been investigated by solid-state NMR. A crystallinity of (88±2)% was determined by traditional ^{1}H NMR lineshape decomposition, and by a new adaptation of ^{13}C NMR crystallinity determination for polyethylenes with extremely long crystalline T_1 relaxation times. ^{1}H spin diffusion yields amorphous domain sizes of 10 ± 5 nm, and crystalline regions of 100 ± 50 nm diameters. A second, highly mobile, amorphous phase, making up (0.8±0.2)% of the sample, was detected by ^{1}H NMR. In spite of its 1.8 kHz ^{1}H line width, it shows little spin diffusion to the other phases, even on a 500-ms time scale; this suggests domains of more than 3 nm thickness or chains extending into voids. Being undetectable in the extruded precursor material and in the fibers after melting, this highly mobile phase must have been induced by the drawing process. ^{13}C NMR confirms that no low-molecular-weight additives are present on a level above 0.01%. %. A similar highly mobile component has also been detected in drawn medium-molecular-weight polyethylenes. The fraction of partially mobile, oriented interfacial material or tie-molecules in the fiber was found to be ~ 5%, while rigid gauche conformers could not be

detected (concentration < 1%). Altogether, five morphological components have been identified: 83% crystal core, of which 80% is orthorhombic and 3% monoclinic, with thickness of ~100 nm; 5% disordered all-trans interfacial and/or tie molecules; 11% mobile amorphous regions, with diameters of ~10 nm; and 1% highly mobile segments, probably at void surfaces. On this basis, a structural model for ultradrawn PE fibers is proposed.

5.6 References

(1) Lemstra, P. J.; Kirschbaum, R.; Ohta, T.; Yasuda, H. In *Developments in Oriented Polymers-2*, Ward, I. M., Ed.; Elsevier Applied Science: London and New York, 1987, pp 39-77.

(2) Porter, R. S.; Wang, L.-H. *J. Macromol. Sci.-Rev. Macromol. Chem. Phys., C* **1995**, *35*, 63-115.

(3) Smith, P.; Lemstra, P. J. *J. Mater. Sci.* **1980**, *15*, 505-514.

(4) Capaccio, G.; Ward, I. M. *Nature Phys. Sci.* **1973**, *243*, 143.

(5) Kanamoto, T.; Tsuruta, A.; Tanaka, K.; Takeda, M.; Porter, R. S. *Macromolecules* **1988**, *21*, 470-477.

(6) Hu, W.-G.; Schmidt-Rohr, K. *Acta Polymer.* **1999**, in press.

(7) Brady, J. M.; Thomas, E. L. *Polymer* **1989**, *30*, 1615-1622.

(8) Furuhata, K.; Yokokawa, T.; Seoul, C.; Miyasaka, K. *J. Polym. Sci.: Polym. Phys. Ed.* **1986**, *24*, 59-67.

(9) Adams, W. W.; Briber, R. M.; Sherman, E. S.; Porter, R. S.; Thomas, E. L. *Polymer* **1985**, *26*, 17.

(10) Fischer, E. W.; Goddar, H. *J. Polym. Sci., PT. C* **1969**, *16*, 4405-4427.

(11) Clark, E. S.; Scott, L. S. *Polym. Eng. Sci.* **1974**, *14*, 682-686.

(12) Peterlin, A. *Coll. Polym. Sci.* **1975**, *253*, 809-823.

(13) Barham, P. J.; Arridge, R. G. C. *J. Polym. Sci., Polym. Phys. Ed.* **1977**, *15*, 1177-1188.

(14) Arridge, R. G. C.; Barham, P. J.; Keller, A. *J. Polym. Sci., Polym. Phys. Ed.* **1977**, *15*, 389-401.

(15) Gibson, A. G.; Davies, G. R.; Ward, I. M. *Polymer* **1978**, *19*, 683-693.

(16) Chen, W.; Fu, Y.; Wunderlich, B.; Cheng, J. *J. Polym. Sci. Part B: Polym. Phys.* **1994**, *32*, 2661-2666.

(17) Hoogsteen, W.; Brinke, G. T.; Pennings, A. J. *J. Mater. Sci.* **1990**, *25*, 1551-1556.

(18) Smith, J. B.; Manuel, A. J.; Ward, I. M. *Polymer* **1975**, *16*, 57-65.

(19) Kitamaru, R.; Horii, F. *Adv. Polym. Sci.* **1978**, *26*, 137-178.

(20) Ito, M.; Kanamoto, T.; Tanaka, K.; Porter, R. S. *Macromolecules* **1981**, *14*, 1779-1784.

(21) Smith, J. B.; Davies, G. R.; Capaccio, G.; Ward, I. M. *J. Polym. Sci.: Polym. Phys. Ed.* **1975**, *13*, 2331-2343.

(22) Torchia, D. A. *J. Magn. Reson.* **1978**, *30*, 613-616.

(23) Schmidt-Rohr, K.; Clauss, J.; Spiess, H. W. *Macromolecules* **1992**, *25*, 3273-3277.

(24) Porter, R. S. *Private discussions* .

(25) Spiegel, S.; Schmidt-Rohr, K.; Boeffel, C.; Spiess, H. W. *Polymer* **1993**, *34*, 4566-4569.

(26) Cai, W. Z.; Schmidt-Rohr, K.; Egger, N.; Gerharz, B.; Spiess, H. W. *Polymer* **1993**, *32*, 267-276.

(27) Kumashiro, K. K.; Schmidt-Rohr, K.; Murphy, O. J.; Ouellette, K. L.; Cramer, W. A.; Thompson, L. K. *J. Am. Chem. Soc.* **1998**, *120*, 5043-5051.

(28) Packer, K. J.; Pope, J. M.; Yeung, R. R.; Cudby, M. E. A. *J. Polym. Sci.: Polym. Phys. Ed.* **1984**, *22*, 589-616.

(29) Schmidt-Rohr, K.; Spiess, H. W. *Multidimensional Solid-State NMR and Polymers*; Academic Press: London, 1994.

(30) Clauss, J.; Schmidt-Rohr, K.; Spiess, H. W. *Acta Polymer.* **1993**, *44*, 1.

(31) VanderHart, D. L.; Khoury, F. *Polymer* **1984**, *25*, 1589-1599.

(32) Tzou, D. L.; Schmidt-Rohr, K.; Spiess, H. W. *Polymer* **1994**, *35*, 4728-4733.

(33) Axelson, D. E.; Mandelkern, L.; Popli, R.; Mathieu, P. *J. Polym. Sci.: Polym. Phys. Ed.* **1983**, *21*, 2319-2335.

(34) Schmidt-Rohr, K.; Spiess, H. W. *Macromolecules* **1991**, *24*, 5288-5293.

(35) Robertson, M. B.; Ward, I. M.; Klein, P. G.; Packer, K. J. *Macromolecules* **1997**, *30*, 6893-6898.

(36) Klein, P. G.; Robertson, M. B.; Driver, M. A. N.; Ward, I. M.; Packer, K. J. *Polym. Int'l* **1998**, *47*, 76-83.

(37) Peterlin, A. *Polym. Eng. Sci.* **1978**, *18*, 488-495.

(38) Peterlin, A. *Coll. Polym. Sci.* **1987**, *265*, 357-382.

(39) Peterman, J.; Gleiter, H. *J. Polym. Sci.: Polym. Phys. Ed.* **1973**, *11*, 359-368.

(40) Hu, W.-G.; Boeffel, C.; Schmidt-Rohr, K. *Macromolecules* **1999**, *32*, 1611-1619.

(41) Sadler, D. M.; Barham, P. J. *Polymer* **1990**, *31*, 36,43,46.

(42) Kanamoto, T.; Porter, R. S. *J. Polym. Sci.: Polym. Lett. Ed.* **1983**, *21*, 1005-1010.

(43) Taylor, W. N.; Clark, E. S. *Polym. Eng. Sci.* **1978**, *18*, 518-526.

CHAPTER 6

POLYETHYLENE-LIKE CRYSTALLITES IN HUMIC SUBSTANCES

6.1 Introduction

Soil organic matter (SOM) represents a major component of the world surface carbon reserves. It exerts a profound influence on many aspects of the nature of soil and on many environmental processes, such as fertility, ion exchange capacity, water holding capacity and sorption of metals and organics. The structures of individual SOM fractions regulate their reactivity, property, and functions, but are poorly understood. A better understanding of SOM structures, particularly humic substances, would help to determine their origin and genesis, reactivity, and roles in environmental processes.

Significant fractions of SOM are poorly soluble or insoluble, being mainly constituted of macromolecules with molecular weight of $> 10^3$. Therefore, solid-state nuclear magnetic resonance (NMR) is the method of choice for investigating their chemical and physicochemical structure. Modern solid-state NMR can provide information on composition, segmental dynamics, domain sizes, and local ordering of macromolecules.[1,2] However, because of the highly diverse and irregular chemical structure of SOM, the application of solid-state NMR to SOM has been mainly limited to composition characterization.[3-7]

So far, SOM was considered to be amorphous. In this chapter, we describe the identification and characterization of poly(methylene) crystallites in various humic

substances by variable-temperature magic-angle spinning, wide-line separation, and spin diffusion NMR experiments, and by wide-angle X-ray scattering. Implications of these crystallites for soil properties are briefly discussed.

6.2 Experimental

To represent a range of different origins and processing procedures of SOM, the following samples were chosen: 1. a commercial humic acid purchased from Aldrich®, which was extracted from brown coal (ALD-HA); 2. a humic acid and a humin which were extracted from a peat at Amherst, Massachusetts, USA (AMH-HA and AMH-humin); 3. An International Humic Substance Society reference material, Florida Pahokee peat (FLA-peat), and a humin extracted from it (FLA-humin).

As references to the SOM samples, high density polyethylene (HDPE), $[\text{-}CH_2\text{-}]_n$ (~ 70% crystalline) and an ethylene/vinyl acetate copolymer with 9% vinyl acetate by weight (35% crystalline) were also measured.

The NMR experiments were performed on a Bruker MSL-300 spectrometer, at a ^1H frequency of 300.13 MHz and a ^{13}C frequency of 75.47 MHz. Four kinds of experiments were conducted: 1. Cross-polarization (CP) from ^1H to ^{13}C; 2. Direct-polarization (DP) by a ^{13}C 90° pulse; 3. A Goldman-Shen spin-diffusion experiment[8] with ^{13}C detection; 4. A two-dimensional (2D) wideline separation (WISE)[9] experiment with total suppression of sidebands (TOSS[10]) before detection. All the experiments were performed under magic angle spinning (MAS), with proton decoupling during

deteetion. The spinning speed used in the WISE experiment was 4.5 kHz, while it was 3 kHz in the variable-temperature experiments. In all other experiments, it was 4 kHz. At these spinning speeds, the sideband intensity of $(CH_2)_n$ carbons is less than 5% of the eenterband, and sidebands of other major eomponents are much less than the $(CH_2)_n$ signal in the vicinity of 30 ppm. The CP time was 0.8 ms, the reeycle delay 1 s. The ^1H decoupling power was 70 kHz. The measuring time for a simple CP spectrum was typieally 2 - 4 hours. The DP speetrum of ALD-HA took 4 hours, that of AMH-HA 12 hours. The WISE experiment was acquired with 16 t_1 inerements of 4 μs, in a total measuring time of 48 hours.

The wide angle X-ray seattering (WAXS) experiments were eondueted on a Siemens D500 diffractometer. The souree of the radiation is the Cu K_α line, with a wavelength of 1.5418 Å. For AMH-humin, the intensity was averaged for 51 hours, for ALD-HA for 22 hours.

6.3 Results and Discussion

6.3.1 NMR Identifieation of Poly(methylene) Crystallites

Fig. 6.1(a) shows the CP ^{13}C NMR sspectrum of ALD-HA. The signal spreads over a wide range (10 - 210 ppm), and ean be assigned to aliphatie, aromatic, earbonyl, and other chemical groups.[11] There is a striking sharp peak at 32.9 ppm. In the DP speetrum in Fig. 6.1(b), the 32.9-ppm peak is relatively lower and the 31-ppm peak beeomes prominent. The 32.9-ppm and 31-ppm peaks are assigned to erystalline and

amorphous $(CH_2)_n$ units ("poly(m)ethylene-like" chains), respectively. For comparison, the CP and DP spectra of a high density polyethylene (HDPE) sample are shown in Fig. 6.1(c) and (d). The sharp crystalline signal at 32.8 ppm and the broad amorphous signal at 31 ppm can be clearly distinguished. Even though the amorphous and crystalline regions have the same chemical structure, they exhibit slightly different chemical shifts due to their different conformations: In the crystalline state, $(CH_2)_n$ chains are all-trans, while in the amorphous state, the chains have both trans and gauche conformations. Due to the γ-gauche effect[12], the crystalline and amorphous signals appear at different chemical shifts. The DP spectrum in Fig. 6.1(d) was acquired with a recycle delay of 10 s, which is short compared to ^{13}C T_1 relaxation time of the crystalline component (>100 s). The crystalline signal is underrepresented due to the incomplete relaxation, while the amorphous signal is shown much better since its ^{13}C T_1 is much shorter than 10 s as a result of the chain mobility.

The CP and DP spectra of ALD-HA (Fig. 6.1a and b) display a similar feature: in the DP spectrum the crystalline signal is suppressed while the amorphous signal is better represented. This confirms the crystalline nature of the 32.9 ppm signal.

We have also found the crystalline and amorphous poly(methylene) components in surface-soil humin and humic acid samples. Fig. 6.2 shows the CP spectra of FLA-humin and AMH-humin. The sharp peak at 32.9 ppm and the shoulder centered at 31 ppm is remarkable. Fig. 6.3(a) and (b) show the CP and DP spectra of AMH-HA. Similar as in Fig. 6.1(a) and (c), in the DP spectrum of AMH-HA the crystalline signal at

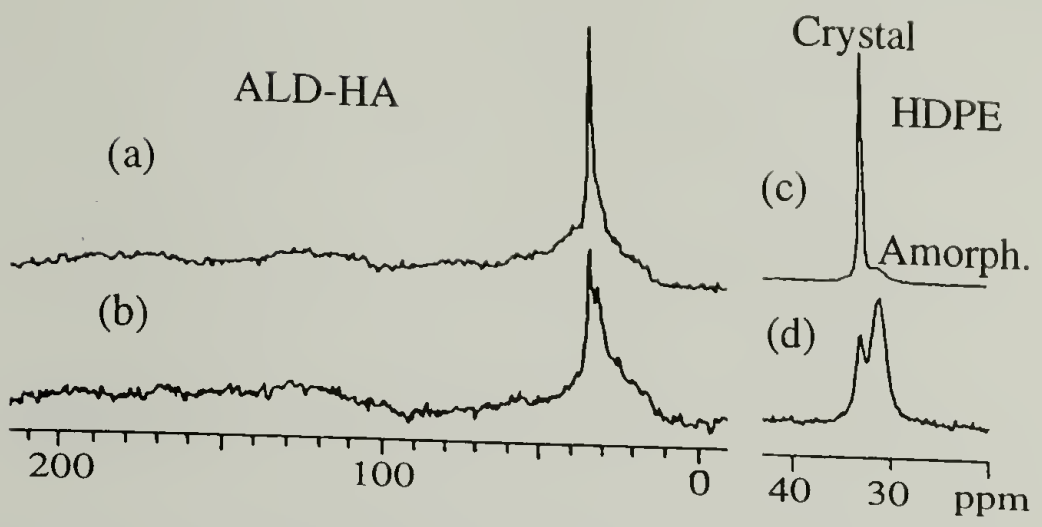

Fig. 6.1. MAS spectra of ALD-HA and HDPE. (a) CP ^{13}C spectrum and (b) DP ^{13}C spectrum (recycle delay = 2 s) of ALD-HA. (c) and (d): CP and DP (recycle delay = 10 s) ^{13}C spectra of HDPE. Note that the scale in (c) and (d) is expanded by a factor of three.

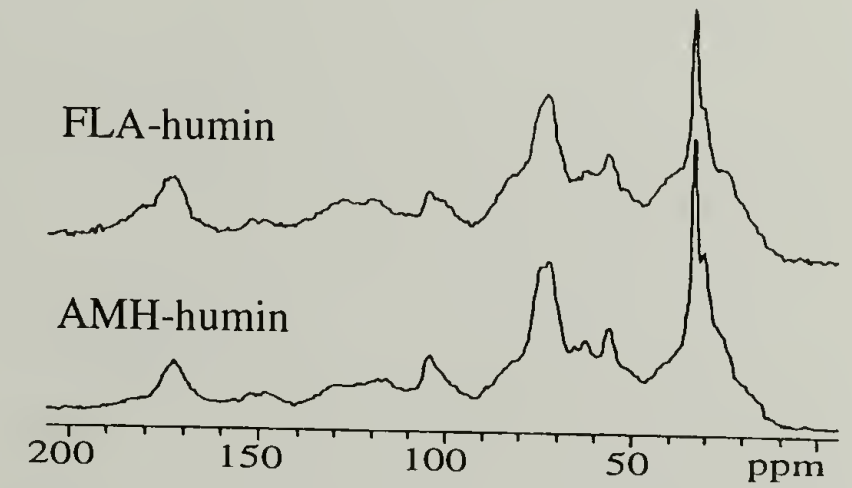

Fig. 6.2: CP ^{13}C spectra of FLA-humin and AMH-humin, showing the characteristic peak-and-shoulder pattern of semicrystalline $(CH_2)_n$ near 32 ppm.

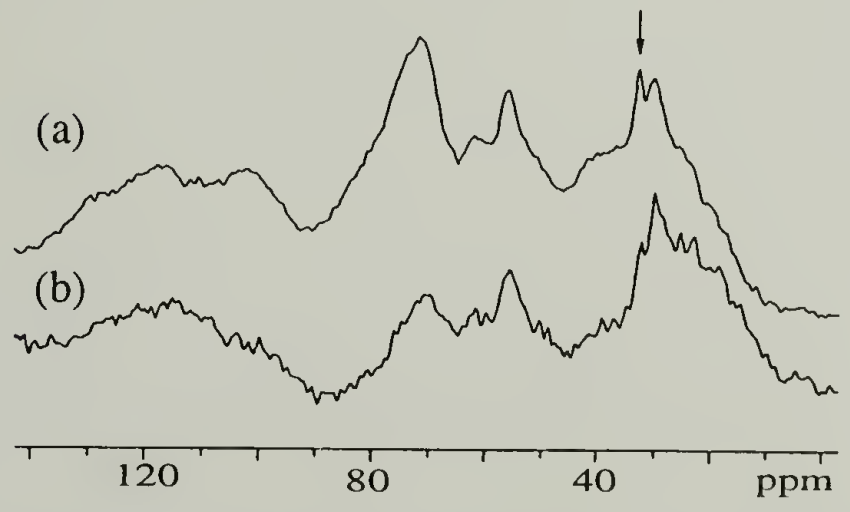

Fig. 6.3: CP and DP spectra of AMH-HA. (a) CP; (b) DP (recycle delay = 2 s). In the CP spectrum the crystalline signal at 33 ppm is clearly seen (indicated by the arrow). In the DP spectrum, the crystalline signal is suppressed because of incomplete ^{13}C T_1-relaxation during the short recycle delay.

32.9 ppm is suppressed. It is clear that the fraction of the crystalline component in AMH-HA is much smaller than in AMH-humin.

It should be noted that in CP spectra the crystalline signal is over-emphasized due to its high CP efficiency which results from the rigidity and the abundance of hydrogens in the crystallites. A quantification of the percentage is achieved through DP with fully relaxed crystalline signal, which yields that at 20°C, the crystalline and amorphous $(CH_2)_n$ in ALD-HA together make up (9±2)% of the total material, with (4±1)% being crystalline. The percentage of $(CH_2)_n$ in AMH-humin is about (7±2)%, (3±1)% being crystalline. In FLA-humin, the total $(CH_2)_n$ fraction is (6±2)%, and (2.5±1)% are crystalline. In the peat humic acid samples, the $(CH_2)_n$ fractions are smaller.

The 2D wideline-separation (WISE) spectrum of AMH-humin (Fig. 6.4, pg. 148) shows differences in the ^{1}H-linewidths in ω_1. The crystalline signal is appreciably wider than that of the amorphous $(CH_2)_n$ region, indicating higher mobility in the amorphous regions. Still, with a halfwidth of 50 kHz, the crystalline signal is narrower than that in HDPE, which suggests fast anisotropic chain dynamics in the crystallites in AMH-humin.

Signal intensity at 30-33 ppm in various SOM samples and its assignment to $(CH_2)_n$ groups has been documented in the literature.[6,13] It has also been reported that part of it has a short ^{1}H-^{1}H dipolar dephasing time and long ^{13}C T_1.[13,14] However, the characteristic two-peak crystalline-amorphous structure was never resolved in the spectra, due to line-broadening introduced by weak decoupling, short acquisition times,

and data smoothing. Therefore, the semicrystalline nature of this component was not recognized.

It has been found that the $(CH_2)_n$ segments persist to a late stage in decomposition of soil and aquatic organic matter[6,15-17] and this is likely the mechanism of kerogen formation[18]. It is well known that synthetic HDPE is extremely difficult to degrade in the natural environment.[19] All these facts suggest that the PE-like component is long-lasting in soil. We propose that this is at least partly due to the semicrystalline nature of the poly(methylene) component. Being inaccessible to chemicals[20] or enzymes, crystalline domains in polymers are much harder to biodegrade than their amorphous counterparts. For example, in poly(ε-caprolactone) (PCL), $[-(CH_2)_5\text{-}COO-]_n$, the amorphous regions are degraded prior to the degradation of the crystalline regions.[21] Therefore, we believe that in addition to the chemical stability of the $(CH_2)_n$ molecules, the highly compact structure of the $(CH_2)_n$ crystal contributes to making the residence time of the $(CH_2)_n$ component longer than that of other components in humic substances.

Investigating forest soil organic matter by solid-state NMR, Kögel-Knabner et al. found that the $(CH_2)_n$ signal in the neighborhood of 30 ppm can be decomposed into more rigid and more mobile parts and the rigid fraction increases with depth from which the humic acid was extracted.[13] Since the most likely reason for the mobility difference of $(CH_2)_n$ segments is a difference in packing order (crystalline vs. amorphous), in view of our results it must be expected that the more rigid part described in ref. [13] is crystalline, and since it is more resistant to permeation by small molecules, it has a longer residence

time than the amorphous chains. The high concentration of the $(CH_2)_n$ crystallites in humic acids from young coal (ALD-HA) found here supports this view.

6.3.2 Wide-Angle X-ray Scattering

To further prove the crystalline nature of the 32.9 ppm peak, wide-angle X-ray scattering (WAXS) was performed. Fig. 6.5 shows the WAXS patterns of ALD-HA, AMH-humin, and HDPE (as a reference). The unit cell of orthorhombic PE is a = 7.417 Å, b = 4.945 Å, and c = 2.547 Å.[22] The strongest Bragg reflections are (110) (lattice spacing of 4.11 Å) and (200) (3.71 Å), which appear at $2\theta = 21.6^\circ$ and 24.0°, respectively, for Cu K_α radiation. AMH-humin shows a small but clear (110) reflection at $2\theta = 21.6^\circ$, and ALD-HA shows a more intense (110) reflection, as well as a (200) reflection at $2\theta = 24.0^\circ$. Due to the small quantity and finite size (see below) of the crystallites and the possible presence of defects, some reflections will be too wide to be distinguished from the background. Therefore, the reflection intensities do not necessarily reflect the quantity shown by NMR. These scattering experiments further prove that crystalline PE-like domains exist in the samples studied, and have the common orthorhombic crystal modification.

Contrary to the common speculation that rigid chains would be easier to crystallize in humic substances, the crystallites that we have observed are composed of highly flexible chains. Having the simplest chemical structure and the widest application, polyethylene (PE) is by far the most thoroughly studied synthetic polymer. Despite the

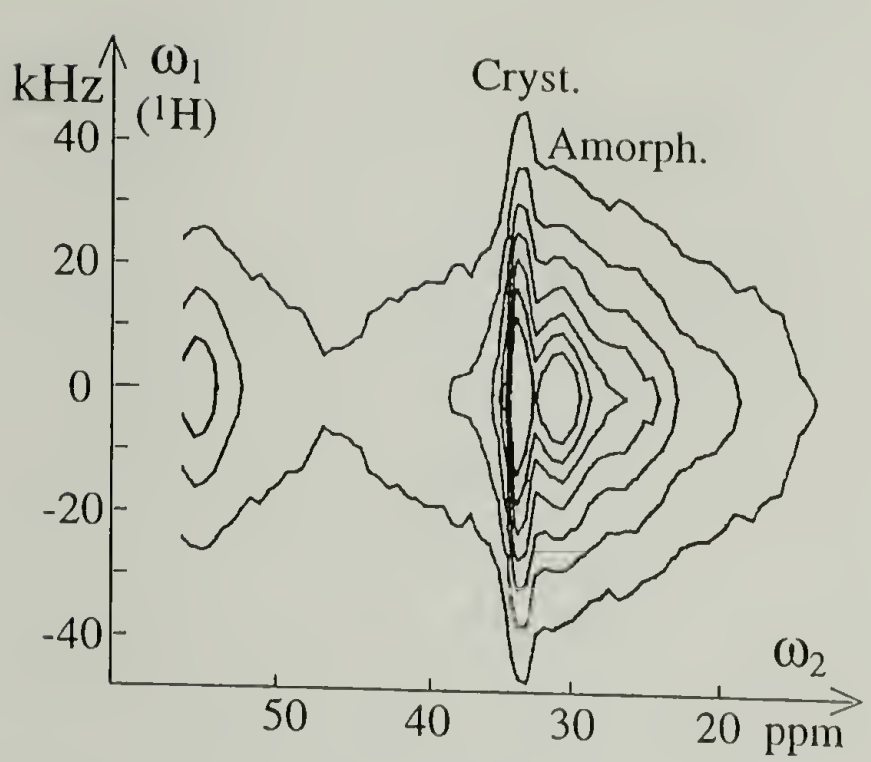

Fig. 6.4: 2D wideline separation (WISE) spectrum of AMH-humin. The first dimension, ω_1, displays the ^1H wideline shape, which indicates mobility (rigid: broad; mobile: narrow), while the ω_2 dimension identifies the structure in terms of the ^{13}C chemical shift.

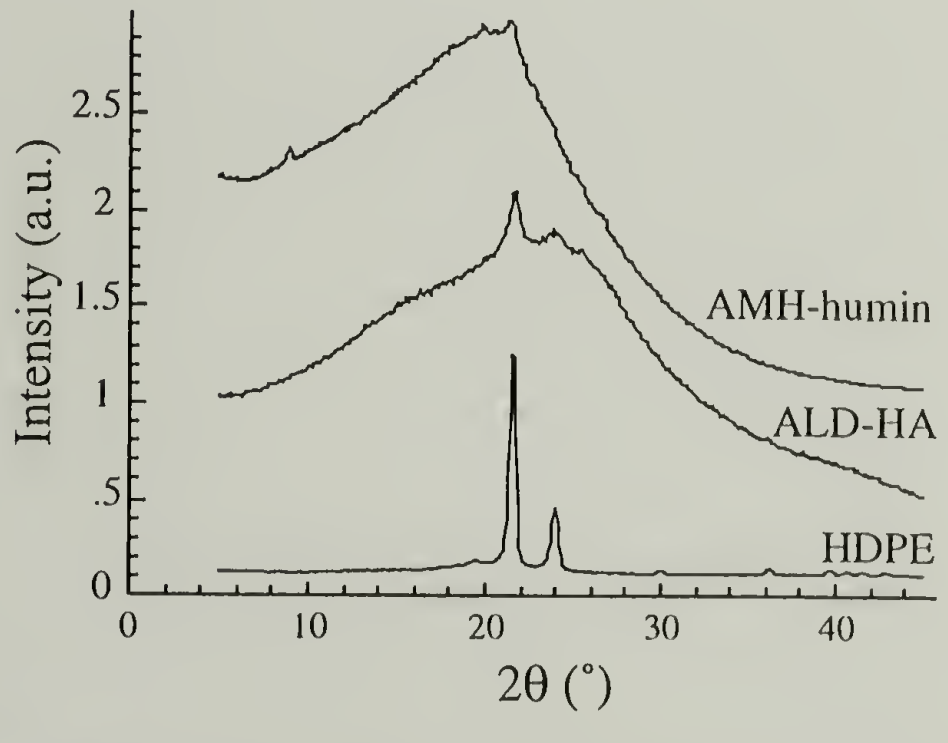

Fig. 6.5: Wide-angle X-ray scattering pattern of AMH-humin, ALD-HA and HDPE. The small peaks at $2\theta = 9^\circ$ and 19.7° in AMH-humin scattering are from unidentified crystals.

flexibility of the polyethylene chains, the crystal formed by them are very rigid as manifested by the fact that highly crystalline PE fibers have tensile moduli higher than steel and are used to make bullet-proof vests[23,24]. Thus, it is expected that the $(CH_2)_n$ crystallites will exhibit very different properties compared to other non-crystallizable aliphatic components in SOM.

Visser et al. have found the evidence of hexagonal crystalline domains in microbial humic acids.[25] These domains are different from the orthorhombic crystallites that we discuss here, and their chemical structure is not clear.

Schnitzer et al. [26] performed systematic x-ray studies of various humic acids. They found that one of three broad bands observed correlates with the aliphatic content. This, however, is not the signal of poly(methylene) crystallites reported here. The band under consideration is nearly an order of magnitude wider than the Bragg peaks that we have observed. The broad band actually corresponds to the "amorphous halo" observed for non-crystalline polyethylene and other hydrocarbons, which reflects the "liquid-like" short-range order of the segments. Comparison with our x-ray scattering patterns, Fig. 6.5, shows that the signal-to-noise ratio in the diffractograms of ref. [26] is insufficient to detect the small Bragg reflections of the poly(methylene) crystallites in humic acids.

6.3.3 Size of the Crystallites

The melting point T_m of a polyethylene crystallite is a function of its thickness d, $(T_m - T_m^0) \sim 1/d$, where T_m^0 ($\sim 145^\circ C$) is the melting point for infinitely thick crystals.

For example, the melting point is ~ 135°C for common HDPE (thickness ~ 20 nm). Therefore, the thickness of a crystallite can be estimated by its melting point. Fig. 6.6 shows the temperature dependence of the $(CH_2)_n$ NMR signals in ALD-HA, compared with those of the ethylene/vinyl acetate copolymer. As the temperature increases, the crystalline peak in both samples becomes smaller and the amorphous signal larger and sharper, indicating melting of the crystallites. In the copolymer, the side groups disrupt crystallization of $(CH_2)_n$ units so the crystallites are only ~ 4 nm thick, as determined by small-angle X-ray scattering. They are thinner than in HDPE and thus have a lower melting point, as seen in Fig. 6.6(b). In Fig. 6.6(a) the crystallites in ALD-HA are foudn to have an average melting point of 70°C. From comparison with long-chain paraffins (Table VIII.4 in ref.[27]) and the melting point depression equation (Gibbs-Thomson equation) in Fig. VIII.10[27], this corresponds to a thickness of ~ 3 nm, or ~ 25 CH_2 units.

The crystallites in AMH-humin show a similar melting behavior, see Fig. 6.7, where again the crystalline signal decreases and the non-crystalline band increases at high temperatures. The melting of the crystallites in both SOM samples is another proof of the crystalline nature of the 32.9-ppm peak. Note also that the signal of the amorphous regions sharpens in a similar way in both series of spectra Fig. 6.6(a) and (b), indicating increased thermal mobility of the amorphous $(CH_2)_n$ regions.

The actual crystallite thickness may deviate from the above estimate since various end groups may shift the melting point. To estimate the crystal size in a less model-dependent way, a Goldman-Shen experiment was performed on ALD-HA, see Fig. 6.8.

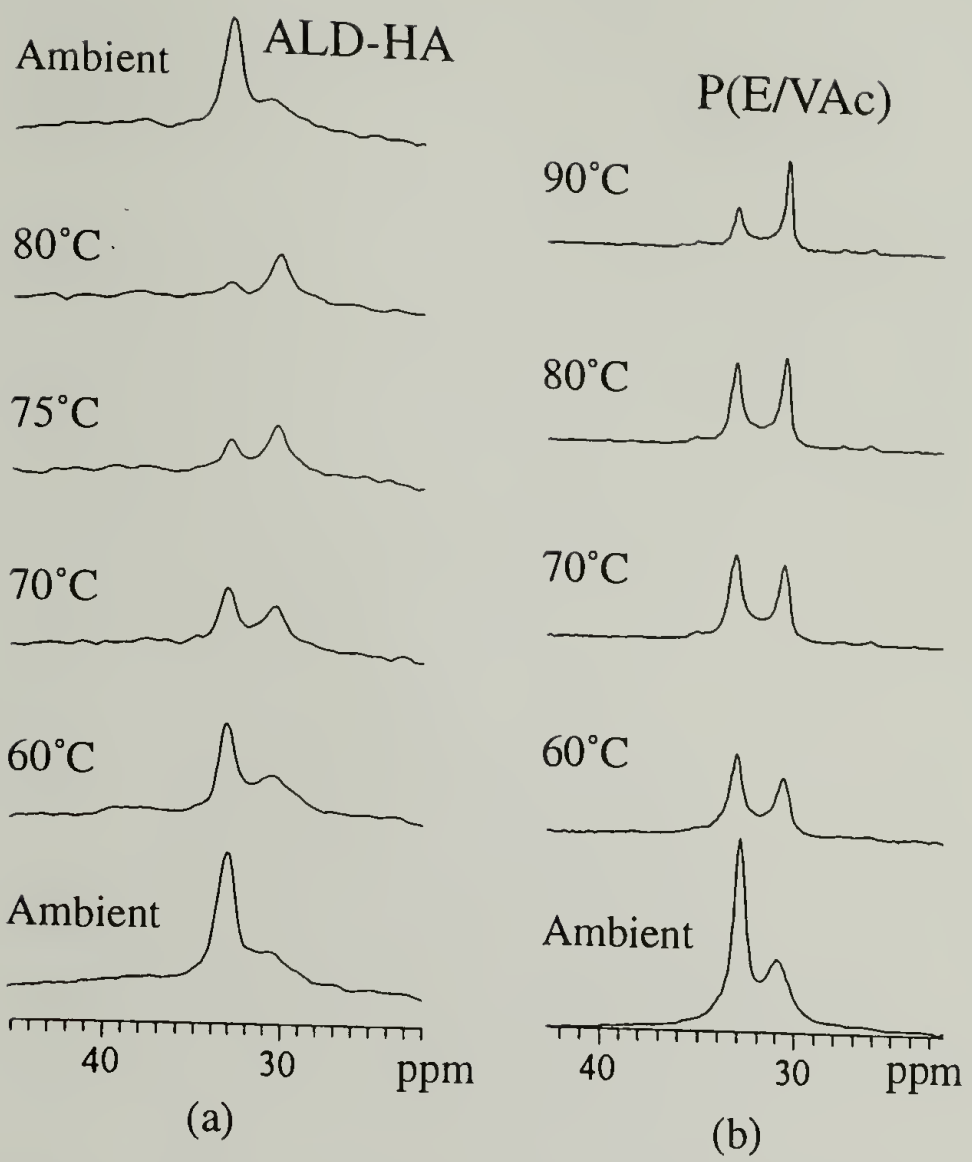

Fig. 6.6: Variable temperature spectra of ALD-HA and P(E/VAc) copolymer. The spectra in (a) were taken at temperatures of 20°C, 60°C, 70°C, 75°C, 80°C, and 20°C (after cooling down from 80°C). The spectra in (b) were taken at 20°C, 60°C,70°C, 80°C, and 90°C.

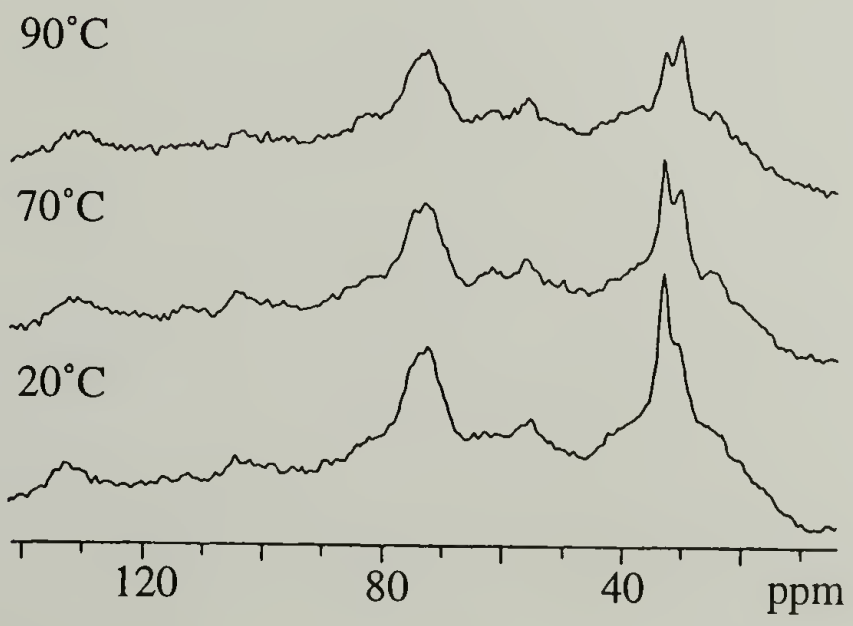

Fig. 6.7: Variable temperature cross polarization spectra of FLA-peat. Melting of the crystallites is clearly observed.

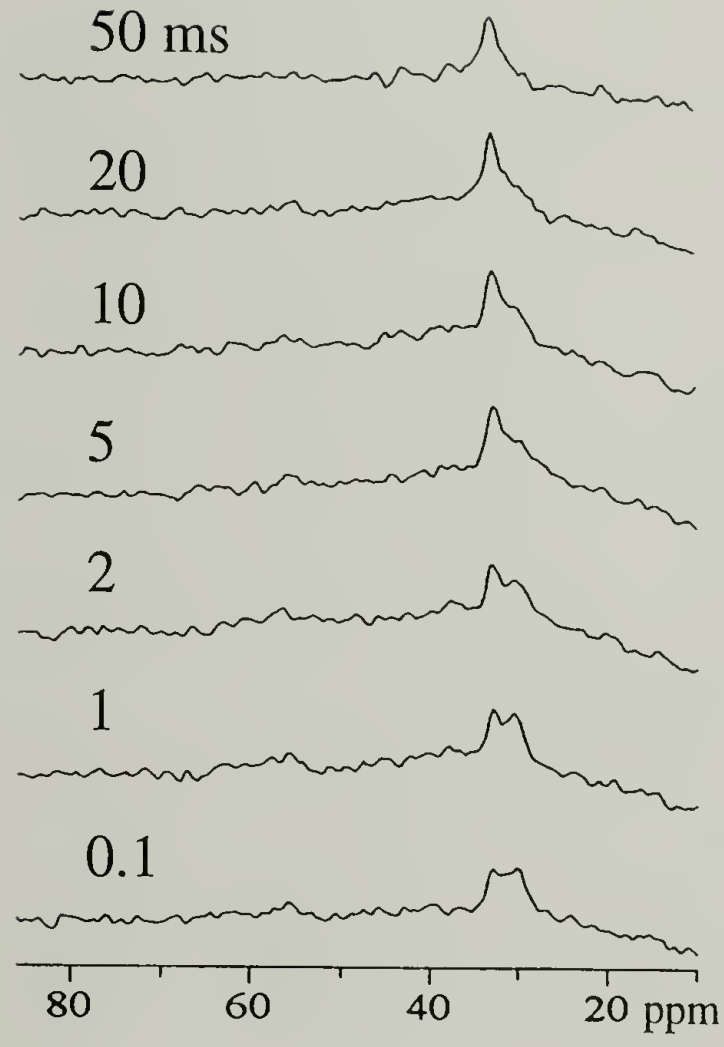

Fig. 6.8: Spin diffusion spectra of ALD-HA. A 20-μs ^1H T_2 filter was used for selecting the mobile components. The diffusion times were 0.1, 1, 2, 5, 10, 20, 50 ms. The rising crystalline signal with diffusion time is clearly seen.

After selection of ^{1}H-magnetization in the most mobile regions using a 20-μs ^{1}H T_2 filter, diffusion of the magnetization into the surrounding regions occurs during a variable mixing time t_m and is observed by the reappearanec of the signal of the rigid regions. The smaller the domain sizes, the faster the reequilibration process. For better struetural resolution, the ^{1}H magnetization distribution is detected indirectly on ^{13}C, after ^{1}H-^{13}C cross polarization. With longer spin diffusion time, the increase of the crystalline peak height and the decrease of the amorphous signal are evident in Fig. 6.8. The equilibrium is reaehed within 5~10 ms, which eorresponds to a thickness of ~ 3 nm.[28] This agrees with the result obtained from the melting point depression.

In thin PE erystallites, fast ehain flips occur[29,30] which produce an increased MAS line width, decreased ^{1}H line width[31-33] and shorter ^{13}C T_1 and ^{1}H $T_{1\rho}$ relaxation times.[34,35] In addition, dynamie disorder may be present, whieh has similar speetral effeets.[28] In Figs. 6.1 and 6.2, the erystalline signal ($\Delta\nu$ ~ 130 Hz) is not as sharp as that of HDPE ($\Delta\nu$ ~ 30 Hz). The ^{13}C T_1 of the ALD-HA erystalline peak (32.8 ppm) is ~ 5 s (defined by the time when the signal deeays to 1/e of its initial height in a CP/T_1 experiment[36]), whieh is mueh shorter than in HDPE samples[35]. The $T_{1\rho,H}$ of 5 ms is also shorter than that of HDPE[30]. These short relaxation times support the notion of thin $(CH_2)_n$ erystallites in SOM. Paramagnetie species eould also reduce the relaxation times. However, sinee they are most likely outside the crystallites, their influence on the relaxations will be limited.

6.3.4 Relation between Crystallites and Soil Properties

The characteristic all-trans CH_2 ^{13}C chemical shift of 32.9 ppm, the melting behavior, and the X-ray reflections together show unambiguously that there is a crystalline component composed of $(CH_2)_n$ chains in humic substances. The melting range, chain dynamics, and spin diffusion experiment indicate that the domains have a thickness of ~ 3 nm. The presence of these crystallites may contribute specific properties to soil. Since crystalline regions are much less permissive to small molecules than the amorphous regions, they must have very different sorption capacities. The crystallites may act as physical cross-links and influence the swelling and solubility properties. This is consistent with the enrichment of the $(CH_2)_n$ components in the insoluble humin fraction of the AMH peat material. In an environment where the soil temperature is high, the physical properties of the soil may change because part of the crystallites have already melted at 60°C.

The $(CH_2)_n$ fraction in AMH-HA is smaller than in AMH-humin, which indicates that only a small portion of the $(CH_2)_n$ chains in SOM has polar end groups that make them soluble in basic solution. The amorphous $(CH_2)_n$ segments are likely to be shorter than their crystalline counterparts.

The $(CH_2)_n$ component may derive from aliphatic biopolymers in algal cell walls and the protective layers of higher terrestrial plants.[16,37,38] Despite their initial low concentrations in organisms, the high preservation potential of such structures will result

in their selective enrichment during diagenesis.[18] This process was found to be related to the formation of kerogen.[18]

The formation of humic substances is not well understood. This is largely due to the diversity of their chemical structures. Because of the chemical regularity of the polyethylene-like component, further investigations to isolate and thoroughly characterize it, regarding chain length, end groups, and its reactions since the beginning of the decomposition of plant residue, may be more straightforward than for the other components. Due to its chemical stability, the crystalline component remains unchanged over long times. Therefore, it could serve as an "internal standard" of the evolution of SOM. In short, the semicrystalline PE-like component could bring a new perspective to the understanding of soil organic matter.

6.4 Summary

Crystalline domains composed of poly(methylene) chains have been unambiguously detected by solid-state NMR and wide angle X-ray scattering (WAXS) in several samples of soil organic matter, including surface soil (peat), humic acids from surface soil and young coal, and humins. From the melting range of 60°C to >80°C and ^1H spin diffusion experiments, a crystallite thickness of > 3 nm or 25 CH_2 units is deduced. The overall fraction of $(CH_2)_n$ carbons in these materials is up to 9%, increasing with soil age and insolubility. About half of this poly(methylene) is crystalline, the other half non-crystalline and more isotropically mobile. The crystalline chains undergo fast dynamics

around their axes at ambient temperature, as manifested by a smaller ^{1}H line width in WISE spectra, shorter relaxation times, and larger ^{13}C line widths than found for synthetic polyethylene. The crystallites are expected to be resistant to environmental attack and thus inert in the soil and have long residence time. Their presence may affect many physical and chemical properties of soil organic matter.

6.5 References

(1) Schmidt-Rohr, K.; Spiess, H. W. *Multidimensional Solid-State NMR and Polymers*; Academic Press: London, 1994.

(2) Schmidt-Rohr, K.; Hu, W.; Zumbulyadis, N. *Science* **1998**, *280*, 714-717.

(3) Hatcher, P. A.; VanderHart, D. L.; Earl, W. *Org. Geochem.* **1980**, *2*, 87-92.

(4) Barron, P. F.; Wilson, M. A. *Nature* **1981**, *289*, 275-276.

(5) Preston, C. M.; Schnitzer, M.; Ripmeester, J. A. *Soil Sci. Soc. Am. J.* **1989**, *53*, 1442-1447.

(6) Baldock, J. A.; Oades, J. M.; Waters, A. G.; Peng, X.; Vassallo, A. M.; Wilson, M. A. *Biogeochemistry* **1992**, *16*, 1-42.

(7) Mao, J.; Hu, W.-G.; Schmidt-Rohr, K.; Davies, G.; Ghabbour, E. A.; Xing, B. *submitted to Soil Sci. Soc. Am. J.* .

(8) Goldman, M.; Shen, L. *Phys. Rev.* **1966**, *144*, 321.

(9) Schmidt-Rohr, K.; Clauss, J.; Spiess, H. W. *Macromolecules* **1992**, *25*, 3273-3277.

(10) Dixon, W. T. *J. Chem. Phys.* **1982**, *77*, 1800.

(11) Wilson, M. A. *J. Soil Sci.* **1981**, *32*, 167-186.

(12) Tonelli, A. E. *NMR Spectroscopy and Polymer Microstructure: the Conformational Connection*; VCH: New York, 1989.

(13) Kogel-Knabner, I.; Hatcher, P. G.; Tegelaar, E. W.; de Leeuw, J. W. *Sci. Tot. Environ.* **1992**, *113*, 89-106.

(14) Newman, R. H.; Condron, L. M. *Solid State Nucl. Magn. Reson.* **1995**, *4*, 259-266.

(15) Hatcher, P. G.; Spiker, E. C.; Szeverenyi, N. M.; Maciel, G. E. *Nature* **1983**, *305*, 498-501.

(16) Tegelaar, E. W.; de Leeuw, J. W.; Saiz-Jimenez, C. *Sci. Tot. Environ.* **1989**, *81/82*, 1-17.

(17) Tegelaar, E. W.; Kerp, H.; Visscher, H.; Schenck, P. A.; de Leeuw, J. W. *Paleobiology* **1991**, *17*, 133-144.

(18) Tegelaar, E. W.; De Leeuw, J. W.; Derenne, S.; Largeau, C. *Geochim. Cosmochim. Acta* **1989**, *53*, 3103-3106.

(19) Potts, J. E. In *Aspects of Degradation and Stabilization of Polymers*, Jellinek, H. H. G., Ed.; Elsevier: New York, 1978, pp 617-658.

(20) Blundell, D. J.; Keller, A.; Ward, I. M.; Grant, I. J. *J. Polym. Sci., Polym. Lett. Ed.* **1966**, *4*, 781-786.

(21) Huang, S. J. In *Encyclopedia of Polymer Science and Engineering*, Mark, H. F.; Bikales, N. M.; Overberger, C. G.; Menges, G., Ed.; John Wiley & Sons: New York, 1985; Vol. 2, pp 220-242.

(22) Brandrup, J.; Immergut, E. H.*Polymer Handbook*; 3rd ed.; John Wiley & Sons, 1989.

(23) Lemstra, P. J.; Kirschbaum, R.; Ohta, T.; Yasuda, H. In *Developments in Oriented Polymers-2*, Ward, I. M., Ed.; Elsevier Applied Science: London and New York, 1987, pp 39-77.

(24) Porter, R. S.; Wang, L.-H. *J. Macromol. Sci.-Rev. Macromol. Chem. Phys., C* **1995**, *35*, 63-115.

(25) Visser, S. A.; Mendel, H. *Soil Biol. Biochem.* **1971**, *3*, 259-265.

(26) Schnitzer, M.; Kodama, H.; Ripmeester, J. A. *Soil Sci. Soc. Am. J.* **1991**, *55*, 745-750.

(27) Wunderlich, B. *Macromolecular Physics*; Academic Press: New York, 1980; Vol. 3.

(28) Clauss, J.; Schmidt-Rohr, K.; Adam, A.; Boeffel, C.; Spiess, H. W. *Macromolecules* **1992**, *25*, 5208-5214.

(29) Mansfield, M.; Boyd, R. H. *J. Polym. Sci.: Polym. Phys. Ed.* **1978**, *16*, 1227-1252.

(30) Hu, W.-G.; Boeffel, C.; Schmidt-Rohr, K. *Macromolecules* **1999**, *32*, 1611-1619.

(31) Olf, H. G.; Peterlin, A. *J. Polym. Sci. Part A-2* **1970**, *8*, 753-770.

(32) Olf, H. G.; Peterlin, A. *J. Polym. Sci.: A-2* **1970**, *8*, 771-790.

(33) Olf, H. G.; Peterlin, A. *J. Polym. Sci.: A-2* **1970**, *8*, 791-797.

(34) McCall, D. W. *Accounts Chem. Res.* **1971**, *4*, 223-232.

(35) Axelson, D. E.; Mandelkern, L.; Popli, R.; Mathieu, P. *J. Polym. Sci.: Polym. Phys. Ed.* **1983**, *21*, 2319-2335.

(36) Torchia, D. A. *J. Magn. Reson.* **1978**, *30*, 613-616.

(37) Baker, E. A. In *The Plant Cuticle*, Cutler, D. F.; Alvin, K. L.; Price, C. E., Ed.; Academic Press: New York, 1982, pp 139-165.

(38) Pacchiano, R. A. J.; Sohn, W.; Chlanda, V. L.; Garbow, J. R.; Stark, R. E. *J. Agric. Food Chem.* **1993**, *41*, 78-83.

BIBLIOGRAPHY

Abe, A.; Jernigan, R. L.; Flory, P. J. (1966). "Conformational Energies of n-alkanes and the Random Configuration of Higher Homologs Including Polymethylene." *J. Am. Chem. Soc.* **88**(4): 631-639.

Abragam, A. (1961). *Principles of Nuclear Magnetism*. Oxford University Press: Oxford.

Adams, W. W.; Briber, R. M.; Sherman, E. S.; Porter, R. S.; Thomas, E. L. (1985). "Microstructure of High Modulus Solid State Extruded Polyethylene: 2. X-Ray Scattering Study of 12, 24 and 36 Extrusion Draw Ratio." *Polymer* **26**: 17.

Adams, W. W.; Yang, D.; Thomas, E. L. (1986). "Direct visualization of microstructural deformation processes in polyethylene." *J. Mater. Sci.* **21**: 2239-2253.

Aharoni, S. M.; Sibilia, J. P. (1979). "Crystalline Transitions and the Solid-State Extrusion of Polymers." *J. Appl. Polym. Sci.* **23**: 133-140.

Aharoni, S. M.; Sibilia, J. P. (1979). "On the Conformational Behavior and Solid-state Extrudability of Crystalline Polymers." *Polym. Eng. Sci.* **19**(6): 450-455.

Albrecht, T.; Strobl, G. (1995). "Temperature-Dependent Crystalline-Amorphous Structures in Linear Polyethylene: Surface Melting and the Thickness of the Amorphous Layers." *Macromolecules* **28**: 5827-5833.

Andrew, E. R. (1950). "Molecular Motion in Certain Solid Hydrocarbons." *J. Chem. Phys.* **18**(5): 607-618.

Appelt, B.; Porter, R. S. (1981). "Ultradrawing of Polystyrene by Solid-State Coextrusion: Shear-Induced Crystallization in Isotactic Polystyrene." *J. Appl. Polym. Sci.* **26**: 2841-2851.

Arridge, R. G. C.; Barham, P. J.; Keller, A. (1977). "Self-Hardening of Highly Oriented Polyethylene." *J. Polym. Sci., Polym. Phys. Ed.* **15**: 389-401.

Ashcraft, C. R.; Boyd, R. H. (1976). "A Dielectric Study of Molecular Relaxation in Oxidized and Chlorinated Polyethylenes." *J. Polym. Sci.: Polym. Phys. Ed.* **14**: 2153-2193.

Attenburrow, G. E.; Bassett, D. C. (1977). "On the plastic deformation of chain-extended polyethylene." *J. Mater. Sci.* **12**: 192-200.

Axelson, D. E.; Mandelkern, L.; Popli, R.; Mathieu, P. (1983). "Carbon-13 NMR of Polyethylenes: Correlation of the Crystalline Component T_1 with Structure." *J. Polym. Sci.: Polym. Phys. Ed.* **21**: 2319-2335.

Baker, E. A. (1982). "Chemistry and morphology of plant epicuticular waxes." In *The Plant Cuticle*. Cutler, D. F.; Alvin, K. L. et al., Ed. Academic Press: New York, 139-165.

Baldock, J. A.; Oades, J. M.; Waters, A. G.; Peng, X.; Vassallo, A. M.; Wilson, M. A. (1992). "Aspects of the chemical structure of soil organic materials as revealed by solid-state ^{13}C NMR spectroscopy." *Biogeochemistry* **16**: 1-42.

Ball, R.; Porter, R. S. (1977). "Solid-State Extrusion of Poly(1-butene)." *J. Polym. Sci.: Polym. Lett. Ed.* **15**: 519-526.

Balta-Calleja, F. J.; Peterlin, A. (1970). "Plastic Deformation of Polypropylene. VI. Mechanism and Properties." *J. Macromol. Sci.-Phys.* **B4**(3): 519-540.

Barham, P. J.; Arridge, R. G. C. (1977). "A Fiber Composite Model of Highly Oriented Polyethylene." *J. Polym. Sci., Polym. Phys. Ed.* **15**: 1177-1188.

Barron, P. F.; Wilson, M. A. (1981). "Humic soil and coal structure study with magic-angle spinning ^{13}C CP-NMR." *Nature* **289**: 275-276.

Beckham, H. W.; Schmidt-Rohr, K.; Spiess, H. W. (1995). "Conformational Disorder and Its Dynamics Within the Crystalline Phase of the Form II Polymorph of Isotactic Poly(1-butene)." In *Multidimensional Spectroscopy of Polymers*. Urban, M. W.; Provder, T., Ed. American Chemical Society: Washington DC, **598:** 243-253.

Benner, R.; Pakulski, J. D.; McCarthy, M.; Hedges, J. I.; Hatcher, P. G. (1992). "Bulk Chemical Characteristics of Dissolved Organic Matter in the Ocean." *Science* **255**: 1561-1564.

Bensason, S.; Minick, J.; Moet, A.; Chum, S.; Hiltner, A.; Baer, E. (1996). "Classification of Homogeneous Ethylene-Octene Copolymers Based on Comonomer Content." *J. Polym. Sci.: Part B: Polym. Phys.* **34**: 1301-1315.

Bigg, D. M. (1988). "Mechanical Property Enhancement of Semicrystalline Polymers-A Review." *Polym. Eng. Sci.* **28**(13): 830-841.

Blundell, D. J.; Keller, A.; Ward, I. M.; Grant, I. J. (1966). "Examination of Degraded Polyethylene Single Crystals by Gel Permeation Chromatography." *J. Polym. Sci., Polym. Lett. Ed.* **4**: 781-786.

Bovey, F. A.; Jelinski, L.; Mirau, P. A. (1988). *Nuclear Magnetic Resonance Spectroscopy.* Academic Press: San Diego.

Boyd, R. H. (1984). "Strengths of the Mechanical alpha-, beta-, and gamma-Relaxation Processes in Linear Polyethylene." *Macromolecules* **17**: 903-911.

Boyd, R. H. (1985). "Relaxation processes in crystalline polymers." *Polymer* **26**: 323,1123.

Boyd, R. H.; Yemni, T. (1979). "A Dielectric Study of the Crystal and Amorphous Fractions in Oriented Polyethylenes." *Polym. Eng. Sci.* **19**(14): 1023-1028.

Brady, J. M.; Thomas, E. L. (1989). "Conversion of single crystal mats to ultrahigh modulus polyethylene: the formation of a continuous crystalline phase." *Polymer* **30**: 1615-1622.

Brandrup, J.; Immergut, E. H., Eds. (1989). *Polymer Handbook*, John Wiley & Sons.

Brew, B.; Ward, I. M. (1978). "Study of the Production of Ultra-High Modulus Polyoxymethylene by Tensile Drawing at High Temperatures." *Polymer* **19**: 1338.

Burmester, A. F.; Dreyfuss, P.; Geil, P.; Keller, A. (1972). "On the Annealing of Polyamide Crystal Mats." *J. Polym. Sci.: Polym. Lett. Ed.* **10**: 769-775.

Cai, W. Z.; Schmidt-Rohr, K.; Egger, N.; Gerharz, B.; Spiess, H. W. (1993). "A solid-state n.m.r. study of microphase structure and segmental dynamics of poly(styrene-b-methylphenylsiloxane) diblock copolymers." *Polymer* **32**: 267-276.

Cansfield, D. L. M.; Capaccio, G.; Ward, I. M. (1976). "The Preparation of Ultra-High Modulus Polypropylene Films and Fibres." *Polym. Eng. Sci.* **16**(11): 721.

Capaccio, G.; Ward, I. M. (1973). "Properties of Ultra-high Modulus Linear Polyethylenes." *Nature Phys. Sci.* **243**: 143.

Capaccio, G.; Ward, I. M. (1974). "Preparation of ultra-high modulus linear polyethylenes; effect of molecular weight and molecular weight distribution on drawing behaviour and mechanical properties." *Polymer* **15**: 233-238.

Chen, Q.; Yamada, T.; Kurosu, H.; Ando, I.; Shiono, T.; Doi, Y. (1991). "Structural Characterization of solution-crystallized ^{13}C-labeled polyethylene over a wide range of temperatures by means of high-resolution ^{13}C-NMR spectroscopy." *J. Mol. Struct.* **263**: 319-327.

Chen, W.; Fu, Y.; Wunderlich, B.; Cheng, J. (1994). "The Morphology of Gel-Spun Polyethylene Fibers, Investigated by Solid-State ^{13}C NMR." *J. Polym. Sci. Part B: Polym. Phys.* **32**: 2661-2666.

Chuah, H. H.; Lin, J. S.; Porter, R. S. (1986). "On Deformation of Polyethylene: The Question of Melting and Recrystallization." *Macromolecules* **19**: 2732-2736.

Clark, E. S.; Scott, L. S. (1974). "Superdrawn Crystalline Polymers: A New Class of High-Strength Fiber." *Polym. Eng. Sci.* **14**(10): 682-686.

Clauss, J.; Schmidt-Rohr, K.; Adam, A.; Boeffel, C.; Spiess, H. W. (1992). "Stiff Macromolecules with Aliphatic Side Chains: Side Chain Mobility, Conformation, and Organization from 2D Solid-State NMR Spectroscopy." *Macromolecules* **25**(20): 5208-5214.

Clauss, J.; Schmidt-Rohr, K.; Spiess, H. W. (1993). "Determination of Domain Sizes in Polymers." *Acta Polymer.* **44**: 1.

Cruz, H. B.; Goncalves, L. L. (1981). "Time-dependent correlations of the one-dimensional isotropic XY model." *J. Phys. C: Solid State Phys.* **14**: 2785-2791.

Davis, G. W.; Talbot, J. R. (1988). "Polyesters, Fibers." In *Encyclopedia of Polymer Science and Engineering*. Mark, H. F.; Bikales, N. M. et al., Ed. John Wiley & Sons **12:** 151.

Desper, C. R. (1973). "Structural Characterization of Isotactic Polypropylene Films of Ultrahigh Orientation. I. Determination of Crystalline and Amorphous Orientations." *J. Macromol. Sci., Phys. Ed.* **B7**(1): 105-119.

Dixon, W. T. (1982). "NMR Spectra in Spinning Samples (TOSS)." *J. Chem. Phys.* **77**: 1800.

Edzes, H. T.; Bernards, J. P. C. (1984). "2D NMR in Static Powders: Interchain ^{13}C Spin Exchange in PE." *J. Am. Chem. Soc.* **106**: 1515.

Egorov, E. A.; Zhizhenkov, V. V. (1982). "NMR Studies of Molecular Mobility in Uniaxially Stretched Oriented Polymers." *J. Polym. Sci., Polym. Phys. Ed.* **20**: 1089-1106.

Ewen, B.; Fischer, E. W.; Piesczek, W.; Strobl, G. (1974). "Defect structure and molecular motion in the four modifications of n-tritriacontane. II. Study of molecular motion using infrared spectroscopy and wide-line nuclear magnetic resonance measurements." *J. Chem. Phys.* **61**(12): 5265-5272.

Ewen, B.; Strobl, G. R.; Richter, D. (1980). "Phase Transitions in Crystals of Chain Molecules: Relation between Defect Structures and Molecular Motion in the Four Modifications of n-$C_{33}H_{68}$." *Faraday Dis. Chem. Soc.* **69**: 19-31.

Eyring, H. (1936). "Viscosity, Plasticity, and Diffusion as Examples of Absolute Reaction Rates." *J. Chem. Phys.* **4**: 283-291.

Fischer, E. W.; Goddar, H. (1969). "Elektronenmikroskopische Untersuchungen an verstrecktem Polyathylen." *J. Polym. Sci., PT. C* **16**: 4405-4427.

Flory, P. J.; Yoon, D. Y. (1978). "Molecular morphology in semicrystalline polymers." *Nature* **272**(16 March): 226-229.

Furuhata, K.; Yokokawa, T.; Seoul, C.; Miyasaka, K. (1986). "Drawing of Ultrahigh-Molecular-Weight Polyethylene Single-Crystal Mats: The Crystallinity." *J. Polym. Sci.: Polym. Phys. Ed.* **24**: 59-67.

Gao, P.; Cheung, M. K.; Leung, T. Y. (1996). "Effects of Compaction pressure on cohesive strength and chain mobility of low-temperature compacted nascent UHMWPE." *Polymer* **37**(15): 3265-3272.

Garrett, P. D.; Grubb, D. T. (1988). "Effect of Drawing on the alpha Relaxation of Poly(vinyl alcohol)." *J. Polym. Sci.: Polym. Phys.* **26**: 2509-2523.

Gedde, U. W. (1995). *Polymer Physics*. Chapman & Hall: London.

Gerrits, N. S. J. A.; Young, R. J. (1991). "Texture development in uniaxially drawn polyethylene tape." *J. Mater. Sci.* **26**: 2137-2142.

Gibson, A. G.; Davies, G. R.; Ward, I. M. (1978). "Dynamic mechanical behaviour and longitudinal crystal thickness measurements on ultra-high modulus linear polyethylene: a quantitative model for the elastic modulus." *Polymer* **19**: 683-693.

Ginzburg, B. M.; Tuichiev, S. (1992). "Microdeformational Behavior of Oriented Semicrystalline Polymers." *J. Macromol. Sci.-Phys.* **B31**(3): 291-317.

Gogolewski, S.; Pennings, A. J. (1985). "High-modulus fibres of nylon-6 prepared by a dry-spinning method." *Polymer* **26**: 1394-1400.

Gohil, R. M.; Miles, M. J.; Petermann, J. (1982). "On the Molecular Mechanism of the Crystal Transformation (Tetragonal-Hexagonal) in Polybutene-1." *J. Macromol. Sci.-Phys.* **B21**(2): 189-201.

Goldman, M.; Shen, L. (1966). "Spin-Spin Relaxation in LaF_3." *Phys. Rev.* **144**: 321.

Govaert, L. E.; Lemstra, P. J. (1992). "Deformation behavior of oriented UHMW-PE fibers." *Coll. Poly. Sci.* **270**: 455-464.

Grobelny, J.; Tekely, P.; Turska, E. (1981). "A broad-line nuclear magnetic resonance investigation of polyacrylonitrile phase structure and chain conformation." *Polymer* **22**: 1649-1654.

Haeberlen, U. (1976). *High Resolution NMR of Solids*. Academic Press: San Diego.

Haeberlen, U.; Waugh, J. S. (1968). "Coherent Averaging Effects in Magnetic Resonance." *Phys. Rev.* **175**: 453.

Hagemeyer, A.; Schmidt-Rohr, K.; Spiess, H. W. (1989). "Two-Dimensional Nuclear Magnetic Resonance Experiments for Studying Molecular Order and Dynamics in Static and in Rotating Solids." *Adv. Magn. Reson.* **13**: 85-130.

Hatcher, P. A.; VanderHart, D. L.; Earl, W. (1980). "Use of solid-state ^{13}C NMR in structural studies of humic acids and humin from Holocene sediments." *Org. Geochem.* **2**: 87-92.

Hatcher, P. G.; Spiker, E. C.; Szeverenyi, N. M.; Maciel, G. E. (1983). "Selective preservation and origin of petroleum-forming aquatic kerogen." *Nature* **305**: 498-501.

He, T.; Porter, R. S. (1987). "Uniaxial draw of poly(4-methyl-pentene-1) by solid-state coextrusion." *Polymer* **28**: 946-950.

Hedvig, P. (1977). *Dielectric Spectroscopy of Polymers*. Wiley: New York.

Henrichs, P. M.; Linder, M. (1984). "^{13}C Spin Diffusion: Intermolecular Structure in Solids." *J. Magn. Reson.* **58**: 458.

Henry, E. R.; Szabo, A. (1985). "Influence of Vibrational Motion on Solid State Line Shapes and NMR Relaxation." *J. Chem. Phys.* **82**(11): 4753-4761.

Hentschel, D.; Sillescu, H.; Spiess, H. W. (1979). "Molecular Motion in Solid Polyethylene as Studied by 2D Wide Line NMR Spectroscopy." *Makromol. Chem.* **180**: 241-249.

Hentschel, D.; Sillescu, H.; Spiess, H. W. (1984). "Deuteron n.m.r. study of chain motion in solid polyethylene." *Polymer* **25**: 1078-1086.

Heuer, A.; Wilhelm, M.; Zimmermann, H.; Spiess, H. W. (1995). "Rate Memory of Structural Relaxation in Glasses and Its Detection by Multidimensional NMR." *Phys. Rev. Lett.* **75**(15): 2851-2854.

Hillebrand, L.; Schmidt, A.; Bolz, A.; Hess, M.; Veeman, W. (1998). "The NMR detection of two distinctly different chains in the orthorhombic crystalline phase of polyethylenes." *Macromolecules* **31**: 5010-5021.

Hirschinger, J.; Miura, H.; Gardner, K. H.; English, A. D. (1990). "Segmental Dynamics in the Crystalline Phase of Nylon 66: Solid-State ^{2}H NMR." *Macromolecules* **23**: 2153-2169.

Hirschinger, J.; Schaefer, D.; Spiess, H. W.; Lovinger, A. J. (1991). "Chain Dynamics in the Crystalline α-Phase of Poly(vinylidene fluoride) by Two-Dimensional Exchange 2H NMR." *Macromolecules* **24**: 2428-2433.

Hoffman, J. D.; Williams, G.; Passaglia, E. (1966). "Analysis of the α, β, and γ Relaxations in Polychlorotrifluoroethylene and Polyethylene: Dielectric and Mcchanical Properties." *J. Polym. Sci.: Part C* **14**: 173-235.

Hong, M.; Gross, J. D.; Hu, W.; Griffin, R. G. (1998). "Determination of the Peptide Torsion Angle ϕ by ^{15}N Chemical Shift and $^{13}C_{\alpha}$-$^{1}H_{\alpha}$ Dipolar Tensor Correlation in Solid-State MAS NMR." *J. Magn. Reson.* **135**: 169-177.

Hoogsteen, W.; Brinke, G. T.; Pennings, A. J. (1990). "SAXS experiments on voids in gel-spun polyethylene fibres." *J. Mater. Sci.* **25**: 1551-1556.

Hope, P. S.; Richardson, A.; Ward, I. M. (1981). "Manufacture of Ultrahigh-Modulus Poly(oxymethylene) by Die Drawing." *J. Appl. Polym. Sci.* **26**: 2879-2896.

Hu, W.-G.; Boeffel, C.; Schmidt-Rohr, K. (1999). "Chain Flips in Polyethylene Crystallites and Fibers Characterized by Dipolar ^{13}C NMR." *Macromolecules* **32**(5): 1611-1619.

Hu, W.-G.; Mao, J.; Xing, B.; Schmidt-Rohr, K. "Poly(methylene) Crystallites in Humic Substances Detected by Nuclear Magnetic Resonance." *submitted to Environ. Sci. Tech.*

Hu, W.-G.; Schmidt-Rohr, K. (1999). "Characterization of Ultradrawn UHMWPE Fibers by NMR: Crystallinity, Domain Size and a Highly Mobile Second Amorphous Phase." *Polymer*: in press.

Hu, W.-G.; Schmidt-Rohr, K. (1999). "Explanation of Polymer Drawability in Terms of alpha-Relaxation Chain Mobility in the Crystallites." *Acta Polymer.*: in press.

Huang, B.; Ito, M.; Kanamoto, T. (1994). "Deformation mcchanism of amorphous poly(ethylene terephthalate) as a function of molecular weight and entanglemcnts." *Polymer* **35**(6): 1210-1215.

Huang, B.; Ito, M.; Kanamoto, T. (1994). "Effects of draw conditions on deformability and draw efficiency of high molecular weight poly(ethylene terephthalate) fibres." *Polymer* **35**(6): 1329-1331.

Huang, S. J. (1985). "Biodegradable Polymers." In *Encyclopedia of Polymer Science and Engineering*. Mark, H. F.; Bikales, N. M. et al., Ed. John Wiley & Sons: New York, **2:** 220-242.

Humphreys, J.; Ward, I. M.; Nix, E. L.; Mcgrath, J. C.; Emi, T. (1985). "A Study of the Drawing Behavior of Polyvinylidene Fluoride." *J. Appl. Polym. Sci.* **30**: 4069-4079.

Ichida, T.; Tsuji, M.; Murakami, S.; Kawaguchi, A.; Katayama, K. (1985). "Thickening process of polyethylene single crystals at an early stage of annealing. II. Computer simulation of lamellar thickening." *Coll. Polym. Sci.* **263**: 293-300.

Ishikawa, K.; Miyasaka, K.; Maeda, M. (1968). *Rept. Progr. Polym. Phys. Japan* **11**: 185.

Ishikawa, S.; Ando, I. (1993). "Structural studies of n-octadecanol by variable-temperature solid-state high-resolution ^{13}C NMR spectroscopy." *J. Mol. Struct.* **291**: 183-190.

Ishikawa, S.; Kurosu, H.; Ando, I. (1991). "Structural studies of n-alkanes by variable-temperature solid-state high-resolution ^{13}C NMR spectroscopy." *J. Mol. Struct.* **248**: 361-372.

Ito, M.; Kanamoto, T.; Tanaka, K.; Porter, R. S. (1981). "Pulsed NMR Studies of Crystalline State Extrusion of High-Density Polyethylene." *Macromolecules* **14**(6): 1779-1784.

Ito, M.; Morishita, Y.; Mizuochi, K.; Kanamoto, T. (1997). "Deformation Behavior of Nylon 6 Solution-Grown Crystals." *J. Macromol. Sci. -Phys.* **B36**(3): 367-380.

Ito, M.; Takahashi, K.; Kanamoto, T. (1990). "Preparation of High-Modulus and High-Strength Fibers from High Molecular Weight Poly(ethylene Terephthalate)." *J. Appl. Polym. Sci.* **40**: 1257-1263.

Iwayanagi, S.; Miura, I. (1965). *Rep. Progr. Polym. Phys. Japan* **8**: 303.

Jakeways, R.; Ward, I. M.; Wilding, M. A.; Hall, I. H.; Desborough, I. J.; Pass, M. G. (1975). "Crystal Deformation in Aromatic Polyesters." *J. Polym. Sci., Polym. Phys. Ed.* **13**: 799-813.

Johansson, A.; Tegenfeldt, J. (1992). "NMR Study of Crystalline and Amorphous Poly(ethylene oxide)." *Macromolecules* **25**: 4712-4715.

Johansson, A.; Wendsjo, A.; Tegenfeldt, J. (1992). "NMR Spectroscopy of PEO-Based Polymer Electrolytes." *Electrochimica Acta* **37**(9): 1487-1489.

Kaji, A.; Yamanaka, A.; Murano, M. (1990). "Structural Analysis of Polyethylene Fibers by Solid State High Resolution NMR; the Distribution of ^{13}C Spin-Lattice Relaxation Times." *Polym. J.* **22**(10): 893-900.

Kanamoto, T.; Ohama, T.; Tanaka, K.; Takeda, M.; Porter, R. S. (1987). "Two-stage drawing of ultra-high molecular weight polyethylene reactor powder." *Polymer* **28**: 1517-1520.

Kanamoto, T.; Porter, R. S. (1983). "On the Minimum Draw Ratio Necessary for Full Chain Extension: Illustrated with Polyethylene." *J. Polym. Sci.: Polym. Lett. Ed.* **21**: 1005-1010.

Kanamoto, T.; Tsuruta, A.; Tanaka, K.; Takeda, M. (1984). "Ultra-High Modulus and Strength Films of High Molecular Weight Polypropylene Obtained by Drawing of Single Crystal Mats." *Polym. J.* **16**(1): 75-79.

Kanamoto, T.; Tsuruta, A.; Tanaka, K.; Takeda, M.; Porter, R. S. (1988). "Superdrawing of Ultrahigh Molecular Weight Polyethylene. 1. Effect of Techniques on Drawing of Single Crystal Mats." *Macromolecules* **21**: 470-477.

Kanamoto, T.; Zachariades, A. E.; Porter, R. S. (1982). "The Effect of Anhydrous Ammonia on the Crystalline-State Deformation of Nylon 6 and 6,6." *J. Polym. Sci., Polym. Phys. Ed.* **20**: 1485-1496.

Kausch, H. H.; Langbein, D. (1973). "Elastic Interaction between Linear Polymeric Chains and Periodic Potentials." *J. Polym. Sci., Polym. Phys. Ed.* **11**: 1201-1218.

Kentgens, A. P. M.; de Boer, E.; Veeman, W. S. (1987). "Ultraslow Molecular Motions in Crystalline Polyoxymethylene. A Complete Elucidation Using Two-Dimensional Solid State NMR." *J. Chem. Phys.* **87**(12): 6859-6866.

Khanna, Y. P.; Sibilia, J. P.; Chandrasekaran, S. (1986). "Molecular Relaxations in Halar, an Alternating Copolymer of Ethylene and Chlorotrifluoroethylene." *Macromolecules* **19**: 2426-2431.

Kiho, H.; Peterlin, A.; Geil, P. H. (1965). "Polymer Deformation. IX. Deformation of Polyethylene crystals at large strain." *Polym. Lett.* **3**: 257-262.

Kim, B. S.; Porter, R. S. (1985). "Uniaxial Draw of Poly(ethylene oxide) by Solid-State Extrusion." *Macromolecules* **18**: 1214-1217.

Kimmig, M.; Strobl, G.; Stuhn, B. (1994). "Chain Reorientation in Poly(tetrafluoroethylene) by Mobile Twin-Helix Reversal Defects." *Macromolecules* **27**: 2481-2495.

Kitamaru, R.; Horii, F. (1978). "NMR approach to the phase structure of linear polyethylene." *Adv. Polym. Sci.* **26**: 137-178.

Klein, P. G.; Robertson, M. B.; Driver, M. A. N.; Ward, I. M.; Packer, K. J. (1998). "Chain diffusion in polyethylene and n-alkane crystals observed by carbon-13 NMR." *Polym. Int'l* **47**(1): 76-83.

Klement, J. J.; Geil, P. H. (1972). "Deformation and Annealing Behavior. III. Thin Films of Polycarbonate, Isotactic Polymethyl Methacrylate, and Isotactic Polystyrene." *J. Macromol. Sci.-Phys.* **B6**(1): 31-56.

Kogel-Knabner, I.; Hatcher, P. G.; Tegelaar, E. W.; de Leeuw, J. W. (1992). "Aliphatic components of forest soil organic matter as determined by solid-state ^{13}C NMR and analytical pyrolysis." *Sci. Tot. Environ.* **113**: 89-106.

Krentsel, B. A.; Kissin, Y. V.; Kleiner, V. I.; Stotskaya, L. L. (1997). *Polymers and Copolymers of Higher α-Olefins: Chemistry, Technology, Applications*. Hanser/Gardner: Munich.

Kuebler, S. C.; Heuer, A.; Spiess, H. W. (1997). "Glass transition of polymers: Memory effects in structural relaxation of polystyrene." *Phys. Rev. E* **56**(1): 741-749.

Kumashiro, K. K.; Schmidt-Rohr, K.; Murphy, O. J.; Ouellette, K. L.; Cramer, W. A.; Thompson, L. K. (1998). "A Novel Tool for Probing Membrane Protein Structure: Solid-State NMR with Proton Spin Diffusion and X-Nucleus Detection." *J. Am. Chem. Soc.* **120**: 5043-5051.

Kuwabara, K.; Kaji, H.; Horii, F.; Bassett, D. C.; Olley, R. H. (1997). "Solid-State ^{13}C NMR Analyses of the Crystalline-Noncrystalline Structure for Metallocene-Catalyzed Linear Low-Density Polyethylene." *Macromolecules* **30**: 7516-7521.

Lemstra, P. J.; Kirschbaum, R.; Ohta, T.; Yasuda, H. (1987). "High-Strength/High-Modulus Structures Based on Flexible Macromolecules: Gel-Spinning and Related Processes." In *Developments in Oriented Polymers-2*. Ward, I. M., Ed. Elsevier Applied Science: London and New York, 39-77.

Lesage, A.; Auger, C.; Caldarelli, S.; Emsley, L. (1997). "Determination of Through-Bond Carbon-Carbon Connectivities in Solid-State NMR Using the INADEQUATE Experiment." *J. Am. Chem. Soc.* **119**: 7867-7868.

Lin, L.; Argon, A. S. (1994). "Structure and plastic deformation of polyethylene." *J. Mater. Sci.* **29**: 294-323.

Lindsey, C. P.; Patterson, G. D. (1980). "Detailed comparison of the Williams-Watts and Cole-Davidson functions." *J. Chem. Phys.* **73**(7): 3348-3357.

Lovinger, A. J.; Lotz, B.; Davis, D. D.; Schumacher, M. (1994). "Morphology and Thermal Properties of Fully Syndiotactic Polypropylene." *Macromolecules* **27**: 6603-6611.

Lyerla, J. R.; Economy, J.; Maresch, G. G.; Muhlebach, A.; Yannoni, C. S.; Fyfe, C. A. (1990). "Molecular Motion in the Homopolyester of 4-Hydroxybenzoic Acid." In *Liquid-Crystalline Polymers*. Weiss, R. A.; Ober, C. K., Ed. American Chemical Society **435:** 359-368.

Madi, Z. L.; Brutscher, B.; Schulte-Herbruggen, T.; Bruschweiler, R.; Ernst, R. R. (1997). "Time Resolved Observation of Spin Waves in a Linear Chain of Nuclear Spins." *Chem. Phys. Lett.* **268**: 300-305.

Mansfield, M.; Boyd, R. H. (1978). "Molecular Motions, the alpha Relaxation and Chain Transport in Polyethylene Crystals." *J. Polym. Sci.: Polym. Phys. Ed.* **16**: 1227-1252.

Mansfield, M. L. (1980). "An Analysis of the Dielectric alpha-Relaxation of Crystalline Polyethylene in Terms of Solitons." *Chem. Phys. Lett.* **68**(2): 383-385.

Mao, J.; Hu, W.-G.; Schmidt-Rohr, K.; Davies, G.; Ghabbour, E. A.; Xing, B. "Characterization of Humic Acids Using DP-MAS Combined With CP T1/TOSS Correction ^{13}C Solid-State NMR." *submitted to Soil Sci. Soc. Am. J.*

McBrierty, V. J.; Packer, K. J. (1993). *Nuclear Magnetic Resonance in Solid Polymers*. Cambridge University Press: London.

McCall, D. W. (1971). "Nuclear Magnetic Resonance Studies of Molecular Relaxation Mechanisms in Polymers." *Accounts Chem. Res.* **4**: 223-232.

McCall, D. W.; Douglass, D. C. (1965). "Molecular Motion in Polyethylene. V." *Appl. Phys. Lett.* **7**(1): 12-14.

McCall, D. W.; Douglass, D. C.; Falcone, D. R. (1967). "Nuclear Magnetic Relaxation in Polytetrafluoroethylene." *J. Phys. Chem.* **71**(4): 998-1004.

McCrum, N. G.; Read, B. E.; Williams, G. (1991). *Anelastic and Dielectric Effects in Polymeric Solids*. Dover Publications, Inc.: New York.

Mead, W. T.; Porter, R. S. (1978). "Formation properties of solid-state extruded high density polyethylene fibers." *J. Polym. Sci.: Polym. Symp.* **63**: 289-312.

Mead, W. T.; Zachariades, A. E.; Shimada, T.; Porter, R. S. (1979). "Solid State Extrusion of Poly(vinylidene fluoride). 1. Ram and Hydrostatic Extrusion." *Macromolecules* **12**(3): 473-478.

Meinel, G.; Peterlin, A. (1967). "Changes in Noncrystalline Regions of Polyethylene During Annealing." *Polym. Lett.* **5**: 613-618.

Mitchell, D. J.; Porter, R. S. (1985). "Characterization of Poly(ethylene oxide) Drawn by Solid-State Extrusion." *Macromolecules* **18**: 1218-1221.

Miura, H.; Hirschinger, J.; English, A. D. (1990). "Segmental Dynamics in the Amorphous Phase of Nylon 66: Solid-State 2H NMR." *Macromolecules* **23**: 2169-2182.

Nakamae, K.; Nishino, T.; Shimizu, Y.; Hata, K. (1990). "Temperature dependence of the elastic modulus of crystalline regions of polyoxymethylene." *Polymer* **31**: 1909-1918.

Newman, R. H.; Condron, L. M. (1995). "Separating subspectra from cross polarization magic-angle spinning nuclear magnetic resonance spectra by proton spin relaxation editing." *Solid State Nucl. Magn. Reson.* **4**: 259-266.

Noid, D. W.; Sumpter, B. G.; Wunderlich, B. (1991). "Molecular Dynamics Simulation of Twist Motion in Polyethylene." *Macromolecules* **24**: 4148-4151.

Odajima, A.; Sauer, J. A.; Woodward, A. E. (1962). "Proton Magnetic Resonance of Some Normal Paraffins and Polyethylene." *J. Phys. Chem.* **66**: 718-724.

Ohde, Y.; Miyaji, H.; Asai, K. (1971). "Deformation of Sedimented Mats of Polyethylene Single Crystals." *Jap. J. Appl. Phys.* **10**(2): 178.

Ohta, T. (1983). "Review on Processing Ultra High Tenacity Fibers From Flexible Polymer." *Polym. Eng. Sci.* **23**(13): 697-703.

Ohta, Y.; Sugiyama, H.; Yasuda, H. (1994). "Short Branch Effects on the Creep Properties of the Ultra-High Strength Polyethylene Fibers." *J. Polym. Sci.: Part B: Polym. Phys.* **32**: 261-269.

Ohta, Y.; Yasuda, H. (1994). "The Influence of Short Branches on the alpha, beta and gamma-Relaxation Processes of Ultra-High Strength Polyethylene Fibers." *J. Polym. Sci.: Part B: Polym. Phys.* **32**: 2241-2249.

Olf, H. G.; Peterlin, A. (1970). "NMR Study of Molecular Motion in Oriented Long-Chain Alkanes. I. Theoretical Part." *J. Polym. Sci. Part A-2* **8**: 753-770.

Olf, H. G.; Peterlin, A. (1970). "NMR Study of Molecular Motion in Oriented Long-Chain Alkanes. II. Oriented Mats of Polyethylene Single Crystals." *J. Polym. Sci.: A-2* **8**: 771-790.

Olf, H. G.; Peterlin, A. (1970). "NMR Study of Molecular Motion in Oriented Long-Chain Alkanes. III. Oriented n-C32H66." *J. Polym. Sci.: A-2* **8**: 791-797.

Olley, R. H.; Bassett, D. C.; Hine, P. J.; Ward, I. M. (1993). "Morphology of compacted polyethylene fibres." *J. Mater. Sci.* **28**: 1107-1112.

Olmsted, P. D.; Poon, W. C. K.; McLeish, T. C. B.; Terrill, N. J.; Ryan, A. J. (1998). "Spinodal-assisted crystallization in polymer melts." *Phys. Rev. Lett.* **81**(2): 373-376.

Opella, S. J.; Waugh, J. S. (1977). "Two-dimensional ^{13}C NMR of highly oriented polyethylene." *J. Chem. Phys.* **66**(11): 4919-4924.

Owen, A. J. (1987). "Oriented Polyamides." In *Developments in Oriented Polymers-2*. Ward, I. M., Ed. Elsevier Applied Science: London and New York, 237-268.

Pacchiano, R. A. J.; Sohn, W.; Chlanda, V. L.; Garbow, J. R.; Stark, R. E. (1993). "Isolation and Spectral Characterization of Plant-Cuticle Polyesters." *J. Agric. Food Chem.* **41**: 78-83.

Packer, K. J.; Pope, J. M.; Yeung, R. R.; Cudby, M. E. A. (1984). "The Effects of Morphology on 1H NMR Spectra and Relaxation in Semicrystalline Polyolefins." *J. Polym. Sci.: Polym. Phys. Ed.* **22**: 589-616.

Pastawski, H. M.; Usaj, G.; Levstein, P. R. (1996). "Quantum interference phenomena in the local polarization dynamics of mesoscopic systems: an NMR obervation." *Chem. Phys. Lett.* **261**: 329-334.

Patel, G. N.; Keller, A. (1975). "Crystallinity and the Effect of Ionizing Radiation in Polyethylene. II. Crosslinking in Chain-Folded Single Crystals." *J. Polym. Sci., Polym. Phys. Ed.* **13**: 323-331.

Peguy, A.; Manley, R. S. J. (1984). "Ultra-drawing of high molecular weight polypropylene." *Polym. Commun.* **25**: 39-42.

Pennings, A. J. (1979). "Lamellar and Fibrillar Crystallization of Polymers." *Makromol. Chem. Suppl.* **2**: 99-142.

Peterlin, A. (1966). "Plastic Deformation of Polyethylene. Mechanism and Properties." *J. Polym. Sci.:Part C* **15**: 427-443.

Peterlin, A. (1971). "Molecular Model of Drawing Polyethylene and Polypropylene." *J. Mater. Sci.* **6**: 490-508.

Peterlin, A. (1974). "Plastic Deformation and Structure of Extruded Polymer Solids." *Polym. Eng. Sci.* **14**(9): 627-632.

Peterlin, A. (1975). "Plastic deformation of polymers with fibrous structure." *Coll. Polym. Sci.* **253**(10): 809-823.

Peterlin, A. (1977). "Drawing and annealing of fibrous material." *J. Appl. Phys.* **48**(10): 4099-4108.

Peterlin, A. (1978). "Annealing of Drawn Crystalline Polymers." *Polym. Eng. Sci.* **18**(6): 488-495.

Peterlin, A. (1987). "Drawing and extrusion of semi-crystalline polymers." *Coll. Polym. Sci.* **265**: 357-382.

Peterman, J.; Gleiter, H. (1973). "Drawing of Fibers from Irradiated Polyethylene Single Crystals." *J. Polym. Sci.: Polym. Phys. Ed.* **11**: 359-368.

Petermann, J.; Kluge, W.; Gleiter, H. (1979). "Electron Microscopic Investigation of the Molecular Mechanism of Plastic Deformation of Polyethylene and Isotactic Polystyrene Crystals." *J. Polym. Sci.: Polym. Phys. Ed.* **17**: 1043-1051.

Plummer, C. J. G.; Cudre-Mauroux, N.; Kausch, H.-H. (1994). "Deformation and Entanglement in Semicrystalline Polymers." *Polym. Eng. Sci.* **34**(4): 318-329.

Porter, R. S.; Wang, L.-H. (1995). "Uniaxial Extension and Order Development in Flexible Chain Polymers." *J. Macromol. Sci.-Rev. Macromol. Chem. Phys., C* **35**(1): 63-115.

Postema, A. R.; Smith, P.; English, A. D. (1990). "Ultra-drawing of polyamides: the hydrogen bond barrier." *Polym. Commun.* **31**: 444-447.

Potts, J. E. (1978). "Biodegradation." In *Aspects of Degradation and Stabilization of Polymers*. Jellinek, H. H. G., Ed. Elsevier: New York, 617-658.

Preston, C. M.; Newman, R. H. (1995). "A long-term effect of N fertilization on the ^{13}C CPMAS NMR of de-ashed soil humin in a second-growth Douglas-fir stand of coastal British Columbia." *Geoderma* **68**: 229-241.

Preston, C. M.; Schnitzer, M.; Ripmeester, J. A. (1989). "A Spectroscopic and Chemical Investigation on the De-ashing of a Humin." *Soil Sci. Soc. Am. J.* **53**: 1442-1447.

Rault, J. (1997). "The alpha-c Transition in Semicrystalline Polymers: A New Look at Crystallization Deformation and Aging Process." *J. Polym. Sci.: Rev. Macromol. Chem. Phys.* **C37**(2): 335-387.

Reddish, W.; Barrie, J. T. (1959). I.U.P.A.C. Symp. uber Macromol., Wiesbaden, Kurzmitteilung I.A.3.

Reneker, D. H. (1962). "Point Dislocations in Crystals of High Polymer Molecules." *J. Polym. Sci.* **59**(168): S39-S42.

Reneker, D. H.; Geil, P. H. (1960). "Morphology of Polymer Single Crystals." *J. Appl. Phys.* **31**(11): 1916-1925.

Richardson, A.; Ward, I. M. (1987). "Preparation of oriented poly(4-methyl pentene-1) rods by die drawing." *Polym. Commun.* **28**: 272-275.

Robertson, M. B.; Ward, I. M.; Klein, P. G.; Packer, K. J. (1997). "C-13 NMR investigation of molecular chain diffusion in semicrystalline polyethylene. 1. Effect of cross-linking." *Macromolecules* **30**(22): 6893-6898.

Robyr, P.; Gan, Z.; Suter, U. W. (1998). "Conformation of raceme and meso dyads in glassy polystyrenes from C-13 polarization transfer NMR." *Macromolecules* **31**(25): 8918-8923.

Robyr, P.; Meier, B. H.; Ernst, R. R. (1989). "Radio-Frequency-Driven Nuclear Spin Diffusion in Solids." *Chem. Phys. Lett.* **162**(6): 417-423.

Robyr, P.; Tomaselli, M.; Straka, J.; Grob-Pisano, C.; Suter, U. W.; Meier, B. H.; Ernst, R. R. (1995). "RF-driven and proton-driven NMR polarization transfer for investigating local order: An application to solid polymers." *Mol. Phys.* **84**(5): 995-1020.

Roessler, E. (1986). "Two-Dimensional Exchange NMR Analyzed in the Time Domain." *Chem. Phys. Lett.* **128**(3): 330-334.

Sadler, D. M.; Barham, P. J. (1990). "Structure of drawn fibres." *Polymer* **31**: 36,43,46.

Sakata, Y.; Unwin, A. P.; Ward, I. M. (1995). "The structure and mechanical properties of syndiotactic polypropylene." *J. Mater. Sci.* **30**: 5841-5849.

Saraf, R. F.; Porter, R. S. (1988). "Deformation of Semicrystalline Polymers via Crystal-Crystal Phase Transition." *J. Polym. Sci.: Part B: Polym. Phys.* **26**: 1049-1057.

Sawatari, C.; Matsuo, M. (1985). "Dynamic mechanical bahavior of ultradrawn polyethylene films produced by gelation/crystallization from solution." *Coll. Polym. Sci.* **263**: 783-790.

Schaefer, D.; Spiess, H. W.; Suter, U. W.; Fleming, W. W. (1990). "Two-Dimensional Solid-State NMR Studies of Ultraslow Chain Motion: Glass Transition in Atactic Poly(propylene) versus Helical Jumps in Isotactic Poly(propylene)." *Macromolecules* **23**: 3431-3439.

Schellekens, R.; Bastiaansen, C. (1991). "The Drawing Behavior of Polyvinylalcohol Fibers." *J. Appl. Polym. Sci.* **43**: 2311-2315.

Schilling, F. C.; Gomez, M. A.; Tonelli, A. E.; Bovey, F. A.; Woodward, A. E. (1987). "Variable-Temperature, High-Resolution Solid-State Carbon-13 NMR Study of 1,4-trans-Polybutadiene." *Macromolecules* **20**: 2954-2957.

Schilling, F. C.; Tonelli, A. E.; Cholli, A. L. (1992). "A ^{13}C NMR Study of the Effect of gamma-Irradiation on the Chain Dynamics of Poly(ethylene oxide)." *J. Polym. Sci.: Part B: Polym. Phys.* **30**: 91-96.

Schmidt, C.; Wefing, S.; Blumich, B.; Spiess, H. W. (1986). "Determination of Rotational Angles from 2D NMR of Powders." *Chem. Phys. Lett.* **130**: 84.

Schmidt-Rohr, K. (1998). "Complete Dipolar Decoupling of ^{13}C and Its Use in Two-Dimensional Double-Quantum Solid-State NMR for Determining Polymer Conformations." *J. Magn. Reson.* **131**: 209-217.

Schmidt-Rohr, K.; Clauss, J.; Spiess, H. W. (1992). "Correlation of Structure, Mobility, and Morphological Information in Heterogeneous Polymer Materials by Two-Dimensional Wideline-Separation NMR Spectroscopy." *Macromolecules* **25**(12): 3273-3277.

Schmidt-Rohr, K.; Hu, W.; Zumbulyadis, N. (1998). "Elucidation of the Chain Conformation in a Glassy Polyester, PET, by Two-Dimensional NMR." *Science* **280**: 714-717.

Schmidt-Rohr, K.; Spiess, H. W. (1991). "Chain Diffusion Between Crystalline and Amorphous Regions in Polyethylene Detected by 2D Exchange ^{13}C NMR." *Macromolecules* **24**(19): 5288-5293.

Schmidt-Rohr, K.; Spiess, H. W. (1994). *Multidimensional Solid-State NMR and Polymers.* Academic Press: London.

Schnitzer, M.; Kodama, H.; Ripmeester, J. A. (1991). "Determination of the Aromaticity of Humic Substances by X-Ray Diffraction Analysis." *Soil Sci. Soc. Am. J.* **55**: 745-750.

Schulte-Herbruggen, T.; Madi, Z. L.; Sorensen, O. W.; Ernst, R. R. (1991). "Reduction of multiplet complexity in COSY-type NMR spectra. The binlear and planar COSY experiments." *Mol. Phys.* **72**(4): 847-871.

Shadrake, L. G.; Guiu, F. (1976). "Dislocations in polyethylene crystals: Line energies and deformation modes." *Philosophical Magazine* **34**(4): 565-581.

Sheehan, W. C.; Cole, T. B. (1964). *J. Appl. Polym. Sci.* **8**: 2359.

Smith, J. B.; Davies, G. R.; Capaccio, G.; Ward, I. M. (1975). "The Dynamic Mechanical Behavior of Ultra-High Modulus Linear Polyethylenes." *J. Polym. Sci.: Polym. Phys. Ed.* **13**: 2331-2343.

Smith, J. B.; Manuel, A. J.; Ward, I. M. (1975). "Broadline n.m.r. studies of ultra-high modulus polyethylenes." *Polymer* **16**: 57-65.

Smith, P.; Lemstra, P. J. (1980). "Ultra-high-strength polyethylene filaments by solution spinning/drawing." *J. Mater. Sci.* **15**: 505-514.

Smith, P.; Lemstra, P. J.; Booij, H. C. (1981). "Ultradrawing of High-Molecular-Weight Polyethylene Cast from Solution. II. Influence of Initial Polymer Concentration." *J. Polym. Sci., Polym. Phys. Ed.* **19**: 877-888.

Smith, P.; Lemstra, P. J.; Pijpers, J. P. L.; Kiel, A. M. (1981). "Ultra-drawing of high molecular weight polyethylene cast from solution." *Coll. Polym. Sci.* **259**: 1070-1080.

Spiegel, S.; Schmidt-Rohr, K.; Boeffel, C.; Spiess, H. W. (1993). "1H spin diffusion coefficient of highly mobile polymers." *Polymer* **34**: 4566-4569.

Spiess, H. W.; Schmidt-Rohr, K. (1992). "Multidimensional solid state NMR studies of chain motions in polymers." *Polym. Prepr.* **33**(1): 68-69.

Spiess, H. W.; Sillescu, H. (1981). "Solid Echoes in the Slow-Motion Region." *J. Magn. Reson.* **42**: 381-389.

Statton, W. O. (1967). "Coherence and Deformation of Lamellar Crystals after Annealing." *J. Appl. Phys.* **38**(11): 4149-4151.

Strobl, G. (1996). *The Physics of Polymers*. Springer-Verlag: Berlin Heidelberg.

Strobl, G.; Ewen, B.; Fischer, E. W.; Piesczek, W. (1974). "Defect structure and molecular motion in the four modifications of n-tritriacontane. I. Study of defect structure in the lamellar interfaces using small angle x-ray scattering." *J. Chem. Phys.* **61**(12): 5257-5264.

Syi, J.-L.; Mansfield, M. L. (1988). "Soliton model of the crystalline alpha relaxation." *Polymer* **29**: 987-997.

Takayanagi, M.; Nitta, K.-H. (1997). "Application of a tie molecule model to the postyielding deformation of crystalline polymers." *Macromol. Theory Simul.* **6**: 181-195.

Taylor, W. N.; Clark, E. S. (1978). "Superdrawn Filaments of Polypropylene." *Polym. Eng. Sci.* **18**(6): 518-526.

Tegelaar, E. W.; De Leeuw, J. W.; Derenne, S.; Largeau, C. (1989). "A reappraisal of kerogen formation." *Geochim. Cosmochim. Acta* **53**: 3103-3106.

Tegelaar, E. W.; de Leeuw, J. W.; Saiz-Jimenez, C. (1989). "Possible Origin of Aliphatic Moieties in Humic Substances." *Sci. Tot. Environ.* **81/82**: 1-17.

Tegelaar, E. W.; Kerp, H.; Visscher, H.; Schenck, P. A.; de Leeuw, J. W. (1991). "Bias of the paleobotanical record as a consequence of variations in the chemical composition of higher vascular plant cuticles." *Paleobiology* **17**(2): 133-144.

Termonia, Y. (1996). "Limits on Drawability of Semicrystalline Flexible Polymers." *Macromolecules* **29**: 4891-4894.

Thomsen, T.; Zachmann, H. G.; Korte, S. (1992). "Molecular Motion in Poly(acrylonitrile) As Determined by Deuteron NMR." *Macromolecules* **25**(25): 6934-6937.

Tonelli, A. E. (1989). *NMR Spectroscopy and Polymer Microstructure: the Conformational Connection*. VCH: New York.

Torchia, D. A. (1978). "The Measurement of Proton-Enhanced Carbon-13 T1 Values by a Method Which Suppresses Artifacts." *J. Magn. Reson.* **30**: 613-616.

Tracht, U.; Wilhelm, M.; Heuer, A.; Feng, H.; Schmidt-Rohr, K.; Spiess, H. W. (1998). "Length scale of dynamic heterogeneities at the glass transition determined by multidimensional nuclear magnetic resonance." *Phys. Rev. Lett.* **81**(13): 2727-2730.

Truss, R. W.; Clarke, P. L.; Duckett, R. A.; Ward, I. M. (1984). "The Dependence of Yield Behavior on Temperature, Pressure, and Strain Rate for Linear Polyethylenes of Different Molecular Weight and Morphology." *J. Polym. Sci.: Polym. Phys. Ed.* **22**: 191-209.

Tzou, D. L.; Schmidt-Rohr, K.; Spiess, H. W. (1994). "Solid-state n.m.r. studies of crystalline phases in gel-spun ultrahigh molecular weight polyethylene." *Polymer* **35**(22): 4728-4733.

Uehara, H.; Jounai, K.; Endo, R.; Okuyama, H.; Kanamoto, T.; Porter, R. S. (1997). "High Modulus Films of Polytetrafluoroethylene Prepared by Two-Stage Drawing of Reactor Powder." *Polym. J.* **29**(2): 198-200.

Uehara, H.; Kanamoto, T.; Kawaguchi, A.; Murakami, S. (1996). "Real-Time X-ray Diffraction Study on Two-Stage Drawing of Ultra-High Molecular Weight Polyethylene Reactor Powder above the Static Melting Temperature." *Macromol.* **29**: 1540-1547.

Uehara, H.; Yamazaki, Y.; Kanamoto, T. (1996). "Tensile properties of highly syndiotactic polypropylene." *Polymer* **37**(1): 57-64.

Ungar, G.; Keller, A. (1979). "Long Range Intermixing of Paraffin Molecules in the Crystalline State." *Colloid and Polymer Science* **257**(1): 90-94.

Utz, M.; Eisenegger, J.; Suter, U. W.; Ernst, R. R. (1997). "Determination of orientational anisotropy in glassy solids by 2D dipolar spectra with sample flipping." *J. Magn. Reson.* **128**(2): 217-227.

van Aerle, N. A. J. M.; Braam, A. W. M. (1988). "A Structural Study on Solid State Drawing of Solution-Crystallized Ultra-High Molecular Weight Polyethylene." *J. Mater. Sci.* **23**: 4429-4436.

van Aerle, N. A. J. M.; Lemstra, P. J.; Kanamoto, T.; Bastiaansen, C. W. M. (1991). "Solid-state deformation of trans-1,4-polybutadiene." *Polymer* **32**: 34-38.

Van Kampen, N. G. (1981). *Stochastic Processes in Physics and Chemistry*. North-Holland: Amsterdam.

VanderHart, D. L. (1976). "Characterization of the methylene ^{13}C chemical shift tensor in the normal alkane n-C20H42." *J. Chem. Phys.* **64**(2): 830-834.

VanderHart, D. L. (1976). "Observation of Natural-Abundance, ^{13}C-^{13}C Dipolar Satellites in Ultraoriented Polyethylene." *J. Magn. Reson.* **24**: 467-470.

VanderHart, D. L. (1981). "Influence of Molecular Packing on Solid-State ^{13}C Chemical Shifts: The n-Alkanes." *J. Magn. Reson.* **44**: 117-125.

VanderHart, D. L. (1987). "Natural-Abundance ^{13}C-^{13}C Spin Exchange in Rigid Crystalline Organic Solids." *J. Magn. Reson.* **72**: 13-47.

VanderHart, D. L.; Khoury, F. (1984). "Quantitative determination of the monoclinic crystalline phase content in polyethylene by ^{13}C n.m.r." *Polymer* **25**: 1589-1599.

Vega, A. J.; English, A. D. (1980). "Multiple-Pulse Nuclear Magnetic Resonance of Solid Polymers. Polymer Motions in Crystalline and Amorphous Poly(tetrafluoroethylene)." *Macromolecules* **13**: 1635-1647.

Visser, S. A.; Mendel, H. (1971). "X-Ray Diffraction Studies on the Crystallinity and Molecular Weight of Humic Acids." *Soil Biol. Biochem.* **3**: 259-265.

Ward, I. M. (1993). "A review of recent developments in the processing and propertics of oriented polyethylene." *Plastics, Rubber and Composites Processing and Applications* **19**(1): 7-13.

Ward, I. M.; Hadley, D. W. (1993). *An introduction to the mechanical properties of solid polymers*. John Wiley & Sons: West Sussex.

Ward, I. M.; Wilding, M. A. (1984). "Creep Behavior of Ultrahigh-Modulus Polyethylene: Influence of Draw Ratio and Polymer Composition." *J. Polym. Sci.: Polym. Sci. Ed.* **22**: 561-575.

Waugh, J. S.; Huber, L. M.; Haeberlen, U. (1968). "Approach to High-Resolution NMR in Solids." *Phys. Rev. Lett.* **20**(5): 180-182.

Weeks, N. E.; Porter, R. S. (1974). "Mechanical Properties of Ultra-Oriented Polyethylene." *J. Polym. Sci.: Poly. Phys. Ed.* **12**: 635.

Weynant, E.; Haudin, J. M.; G'Sell, C. (1980). "In situ observation of the spherulite deformation in polybutene-1 (Modification I)." *J. Mater. Sci.* **15**: 2677-2692.

Wignall, G. D.; Wu, W. (1983). "A SANS investigation into the role of melting and recrystallization during solid state deformation of polyethylene." *Polym. Commun.* **24**: 354-359.

Wilding, M. A.; Ward, I. M. (1978). "Tensile creep and recovery in ultra-high modulus linear polyethylenes." *Polymer* **19**: 969-976.

Wilding, M. A.; Ward, I. M. (1981). "Creep and recovery of Ultra high modulus polyethylene." *Polymer* **22**: 870-876.

Wilson, M. A. (1981). "Applications of Nuclear Magnetic Resonance Spectroscopy to the Study of the Structure of Soil Organic Matter." *J. Soil Sci.* **32**: 167-186.

Wu, W.; Wignall, G. D.; Mandelkern, L. (1992). "A SANS study of the plastic deformation mechanism in polyethylene." *Polymer* **33**(19): 4137-4140.

Wunderlich, B. (1980). *Macromolecular Physics*. Academic Press: New York.

Wunderlich, B. (1987). "Analysis of condis phase." In *Integration of Fundamental Polymer Science and Technology-2*. Lemstra, P. J.; Kleintjens, L. A., Ed. Elsevier Applied Science 329-333.

Yamamoto, T.; Nozaki, K. (1994). "Evidence of active chain diffusion in the rotator phase of n-alkanes: solid-state mixing of C21H44 and C23H48." *Polymer* **35**(15): 3340-3342.

Yamane, A.; Sawai, D.; Kameda, T.; Kanamoto, T.; Ito, M.; Porter, R. S. (1997). "Development of High Ductility and Tensile Properties upon Two-Stage Draw of Ultrahigh Molecular Weight Poly(acrylonitrile)." *Macromolecules* **30**: 4170-4178.

Young, R. J. (1975). "Deformation Mechanisms in Polytetrafluoroethylene." *Polymer* **16**: 450-458.

Young, R. J. (1987). "Polymer Single Crystal Fibers." In *Developments in Oriented Polymers-2*. Ward, I. M., Ed. Elsevier Applied Science: London and New York, 1-38.

Young, R. J.; Bowden, P. B.; Ritchie, J. M.; Rider, J. G. (1973). "Deformation Mechanisms in Oriented High-Density Polyethylene." *J. Mater. Sci.* **8**: 23-26.

Yu, Y.-F.; Ullman, R. (1962). "Microscope Investigations of Extension and Fracture in Crystalline Polymers." *J. Polym. Sci.* **60**: 55-64.

Zwijnenburg, A.; Pennings, A. J. (1976). "Longitudinal Growth of Polymer Crystals From Flowing Solutions. IV. The Mechanical Properties of Fibrillar Polyethylene Crystals." *J. Polym. Sci., Polym. Lett. Ed.* **14**: 339-346.